

**EFFECT OF CHLORIDE AND SULFATE IONS
ON DEACTIVATION OF TiO_2 ANATASE IN
PHOTOCATALYTIC TREATMENT OF
METHYLENE BLUE AND METHYL ORANGE**

HAMISU UMAR FAROUK

**FACULTY OF ENGINEERING
UNIVERSITY OF MALAYA
KUALA LUMPUR**

2019

**EFFECT OF CHLORIDE AND SULFATE IONS ON
DEACTIVATION OF TiO₂ ANATASE IN
PHOTOCATALYTIC TREATMENT OF METHYLENE
BLUE AND METHYL ORANGE**

HAMISU UMAR FAROUK

**THESIS SUBMITTED IN FULFILMENT OF THE
REQUIREMENTS FOR THE DEGREE OF DOCTOR OF
PHILOSOPHY**

**FACULTY OF ENGINEERING
UNIVERSITY OF MALAYA
KUALA LUMPUR**

2019

UNIVERSITY OF MALAYA
ORIGINAL LITERARY WORK DECLARATION

Name of Candidate: Hamisu Umar Farouk

Matric No.: KHA120142

Name of Degree: DOCTOR OF PHILOSOPHY

Title of Thesis ("this Work"):

EFFECT OF CHLORIDE AND SULFATE IONS ON DEACTIVATION
OF TiO₂ ANATASE IN PHOTOCATALYTIC TREATMENT OF METHYLENE
BLUE AND METHYL ORANGE

Field of Study: Health, Safety and Environment

I do solemnly and sincerely declare that:

- (1) I am the sole author/writer of this Work;
- (2) This Work is original;
- (3) Any use of any work in which copyright exists was done by way of fair dealing and for permitted purposes and any excerpt or extract from, or reference to or reproduction of any copyright work has been disclosed expressly and sufficiently and the title of the Work and its authorship have been acknowledged in this Work;
- (4) I do not have any actual knowledge nor do I ought reasonably to know that the making of this work constitutes an infringement of any copyright work;
- (5) I hereby assign all and every rights in the copyright to this Work to the University of Malaya ("UM"), who henceforth shall be owner of the copyright in this Work and that any reproduction or use in any form or by any means whatsoever is prohibited without the written consent of UM having been first had and obtained;
- (6) I am fully aware that if in the course of making this Work I have infringed any copyright whether intentionally or otherwise, I may be subject to legal action or any other action as may be determined by UM.

Candidate's Signature

Date:

Subscribed and solemnly declared before,

Witness's Signature

Date:

Name:

Designation:

**EFFECT OF CHLORIDE AND SULFATE IONS ON DEACTIVATION OF TiO₂
ANATASE IN PHOTOCATALYTIC TREATMENT OF METHYLENE BLUE
AND METHYL ORANGE**

ABSTRACT

Dye wastewaters contain dissolved organic compounds that are hazardous and very difficult to treat with conventional wastewater treatment methods. Photocatalytic treatment, an advanced oxidation process (AOP), of wastewater treatment, generators of hydroxyl radicals ($\bullet\text{OH}$), is capable of degrading most organic compounds. The most commonly used photocatalyst for this purpose is titanium dioxide (TiO₂) and its modified forms due to its stability and lower cost. However, the practical use of TiO₂ is limited due to possibility of deactivation. In textile wastewater, the presence of dye-enhancers such as sodium chloride (NaCl) and sodium sulfate (Na₂SO₄), releases Cl^- and SO_4^{2-} in the solution, reported to further deactivate TiO₂, but the interaction of these ions with TiO₂ surface is not comprehensively studied and reported. Therefore, in this work, the effect of Cl^- and SO_4^{2-} on photocatalytic degradation of methylene blue (MB), a cationic dye and methyl orange (MO), anionic dye as model contaminants was run with TiO₂ anatase, the experiments were conducted at different conditions. Fresh TiO₂ (T_F) and deactivated samples were compared for changes in elemental composition and how they affect the cumulative percent degradation (CPD). The CPD was used to measure the number of times, TiO₂ could be used repeatedly before deactivation over a 60h period divided into 10 hourly runs. A bulb with UV irradiation of wavelength 360-400 nm (UVA) was used. On the effect of SO_4^{2-} in MO, highest CPD 431.9% at pH4 was recorded. Sulfur (S) and Nitrogen (N) were not detected in any of MO samples. MB has highest CPD 294.5% at pH10 with added SO_4^{2-} . S and N species were detected due to their presence in MB structure and from added SO_4^{2-} ions and did not induce further deactivation. On the effect

of Cl^- , it was not detected in any of the MB or MO samples, Cl^- did not contribute to deactivation because of the high CPD values. There were changes in the composition of other elements, Oxygen (O), Sodium (Na), and Carbon (C). All deactivated samples show decrease in O, higher in MB than in MO samples. MO with higher amounts of O generally have high CPD. In some MO samples, on deconvolution of O, regeneration or increase in lattice oxygen (O^{2-}) was seen but did not increase the CPD. Na detected in some samples in MB and MO, due to added salts and higher values of Na in MO samples were due to the combined presence of Na^+ in the MO structure, presence of Na on deactivated samples did not affect the CPD. There was increase in carbon (C) in all deactivated samples, with more C species in MB samples than in MO. In conclusion, samples irradiated with UV yielded highest CPD values and the highest variety of new adsorbed elements in both MB and MO. The carbon species $\text{C}=\text{O}$, $\text{C}-\text{O}$ and $\text{C}-\text{C}$ were the predominant cause of deactivation, generated and adsorbed on the TiO_2 surface. It is feasible that these species were captured at the region of bridging O being the most probable source of $\bullet\text{OH}$ radical generation. Photocatalyst activity with reduced deactivation could be sustained with sufficient UV irradiation by generation of $\bullet\text{OH}$ continuously. The pH did not have a significant effect on the rate of deactivation.

Keywords: TiO_2 , deactivation, degradation, textile wastewater, photocatalyst

***KESAN Klorida DAN SULFAT PADA PENYAHAKTIFAN TiO₂ ANATASE
DALAM PEMANGKINFOTO RAWATAN AIR SISA METILENA BIRU DAN
METILENA OREN***

ABSTRAK

Air sisa tekstil mengandungi sebatian organik yang bersifat karsinogen sangat sukar dirawat dengan kaedah rawatan konvensional. Rawatan fotokatalik, ialah satu proses pengoksidaan lanjutan (AOP), daripada rawatan air sisa, penjana kepada hidroksil radikal (OH) mampu merendahkan sebatian organik. Pemangkinfoto yang paling biasa digunakan bagi tujuan ini adalah titanium dioksida (TiO₂) dan bentuknya pula mudah diubahsuai kerana kestabilan dan kos yang lebih rendah. Walau bagaimanapun, penggunaan TiO₂ secara praktikal adalah terhad disebabkan oleh penyahaktifan. Dalam sisa air tekstil, kehadiran pewarna seperti natrium klorida (NaCl) dan natrium sulfat (Na₂SO₄), menghasilkan Cl⁻ dan SO₄²⁻ dalam larutan dilaporkan menyahaktifkan TiO₂, tetapi interaksi antara ion-ion ini tidak dikaji secara mendalam dan dilaporkan secara komprehensif. Oleh itu, kesan Cl⁻ dan SO₄²⁻ pada degradasi pemangkinfoto metil biru (MB), pewarna kationik dan metil orange (MO), pewarna anionik sebagai model bahan pencemar dijalankan dengan anatase TiO₂, dilakukan secara berbeza. TiO₂ segar (T_F) dan sampel yang dinyahaktifkan telah dibandingkan dalam perubahan unsur komposisi dan bagaimana ia mempengaruhi penurunan nilai kumulatif (CPD). CPD telah digunakan untuk mengukur bilangan, TiO₂ juga boleh digunakan berulang kali sebelum penyahaktifan selama tempoh 60h dibahagikan kepada 10 jam. Satu mentol dengan UV penyinaran Panjang gelombang 360 – 400 nm digunakan. Kesan SO₄²⁻ dalam MO, CPD tertinggi sebanyak 431.9% telah direkodkan pada pH4. Manakala, Sulfur (S) dan Nitrogen (N) tidak dikesan dalam mana-mana sampel MO. MB mempunyai peratusan CPD tertinggi sebanyak 294.5% pada pH10 dengan tambahan SO₄²⁻. Kehadiran S dan N dikesan dalam struktur MB dari tambahan ion-ion SO₄²⁻ tetapi tidak mendorong kepada

penyahaktifan. Manakala, Cl^- , tidak dikesan dalam sampel MB atau MO, Cl^- tidak menyumbang kepada penyahaktifan kerana nilai CPD yang tinggi. Terdapat perubahan dalam unsur-unsur lain, iaitu Oksigen (O), Natrium (Na), dan Karbon (C). Semua sampel yang dinyahaktifkan menunjukkan penurunan dalam O, adalah lebih tinggi dalam MB berbanding MO. MO dengan nilai O yang lebih tinggi secara amnya mempunyai CPD tinggi. Dalam beberapa sampel MO, iaitu pada O, penjanaan semula atau peningkatan dalam oksigen (O^{2-}) telah dikesan tetapi tidak meningkatkan CPD. Na dikesan dalam beberapa sampel MB dan MO, disebabkan oleh tambahan garam dan nilai-nilai tinggi Na dalam sampel MO kerana gabungan Na^+ dalam struktur MO, kehadiran Na pada sampel yang dinyahaktifkan tidak mempengaruhi CPD. Terdapat peningkatan dalam Karbon (C) dalam semua sampel yang dinyahaktifkan, dengan lebih banyak spesies C dalam sampel MB berbanding MO. Kesimpulannya, sampel yang disinari dengan UV menghasilkan nilai CPD tertinggi dan pelbagai elemen baru terjerap dalam MB dan MO. Karbon $\text{C}=\text{O}$, $\text{C}-\text{O}$ dan $\text{C}-\text{C}$ adalah sebab utama penyahaktifan, dihasilkan dan terjerap pada permukaan TiO_2 . Adalah mungkin bahawa spesies-spesies ini dikesan pada penyambung O dan menjadi sumber paling mungkin generasi radikal $\cdot\text{OH}$. Aktiviti pemangkinfoto dengan pengurangan penyahaktifan boleh dikekalkan dengan sinaran UV yang mencukupi dengan penjanaan $\cdot\text{OH}$ secara berterusan. PH tidak mempunyai kesan ketara ke atas kadar penyahaktifan.

Keywords: TiO_2 , penyahaktifan, degradasi, sisa air tekstil, pemangkinfoto

ACKNOWLEDGEMENTS

I would like to express my appreciation to my supervisors Prof. Abdul Aziz Abdul Raman and Prof. Wan Mohd Ashri Wan Daud for their assistance, support, advice and guidance in the course of this research.

My gratitude goes to staff members and laboratory technicians in Chemical Engineering Department, for their assistance when needed.

I also appreciate the support provided by my colleagues.

My gratitude also goes to University of Malaya for granting me the opportunity to pursue my PhD program having unlimited access to laboratories, equipment, library resources and other supports and services during the period of my study.

I am also grateful to the Ministry of Higher Education Malaysia and University of Malaya Bright Spark Unit, which financially supported this work through a University of Malaya High Impact Research Grant (UM-MOHE UM.C/625/1/HIR/MOHE/38) and Institute of Research Management and Monitoring (IPPP) RPMS [PG094-2016A].

TABLE OF CONTENTS

Title Page	i
Original Literary Work Declaration.....	ii
Abstract.....	iii
Abstrak.....	v
Acknowledgements.....	viii
Table of Contents.....	ix
List of Figures.....	xiii
List of Tables	xvi
List of Symbols and Abbreviations	xviii
 CHAPTER 1: INTRODUCTION	1
1.1 Background	1
1.2 Problem statement	3
1.3 Aim.....	3
1.4 Objectives.....	3
1.5 Scope.....	4
1.6 Thesis organization	5
 CHAPTER 2: LITERATURE REVIEW	7
2.1 Introduction	8
2.2 Current challenges in Advanced Oxidation Process (AOP) with TiO ₂	8
2.2.1 Phase stability	9
2.2.2 Particle behavior in Bulk.....	10
2.2.3 Reaction conditions.....	10
2.2.4 Nature of contaminants	11
2.2.5 Light attenuation	11
2.2.6 Dye classification.....	12

2.2.7	Real textile wastewater kinetics	12
2.3	Essential photoreactor requirement	15
2.4	Water splitting reaction on rutile TiO ₂ (110) and anatase TiO ₂ (101) surface.....	17
2.5	Reaction rate and catalyst deactivation in photocatalysis	24
2.6	Three types of TiO ₂ activity inhibition in photocatalysis.....	25
2.6.1	<i>Active hole (*) deactivation</i>	26
2.6.2	<i>Inhibition by consuming •OH</i>	39
2.6.3	<i>Inhibition due to inability of O^{2•-} to prevent electron recombination</i>	42
2.7	Future of advanced oxidation process with TiO ₂	44
2.8	Summary of literature review.....	45
CHAPTER 3: METHODOLOGY		47
3.1	Introduction	47
3.2	Materials.....	47
3.3	Experimental design and method of analysis	47
3.3.1	Characterization of fresh TiO ₂ anatase photocatalyst	49
3.3.1.1	<i>Crystalline phase determination with X-ray diffraction (XRD)</i>	49
3.3.1.2	<i>Surface area and particle size were analyzed with Brunauer-Emmett-Teller (BET).....</i>	49
3.3.1.3	<i>Elemental composition determination with X-ray photoelectron spectroscopy (XPS)</i>	50
3.3.1.4	<i>Fourier-transform-infrared spectroscopy (FTIR) analysis to determine organic, polymeric and inorganic materials</i>	50
3.3.2	Kinetic studies of photodegradation of methylene blue and methyl orange solutions with Cl ⁻ or SO ₄ ²⁻ using TiO ₂ at different reaction conditions..	51

3.3.2.1	<i>The independent variables from response surface methodology (RSM)</i>	51
3.3.2.2	<i>Reproducibility/Error analysis</i>	53
3.3.2.3	<i>Stimulus-response method</i>	56
3.3.2.4	<i>Chemical actinometry technique</i>	57
3.3.2.5	<i>UV irradiation depth</i>	57
3.3.3	Kinetic studies in form of cumulative percent degradation of photodegradation of methylene blue and methyl orange solutions with Cl^- or SO_4^{2-} using TiO_2	59
3.3.3.1	<i>Data collection</i>	59
3.3.4	Relationship between adsorbed species and cumulative percent degradation.....	67
3.3.5	Propose a practice for photocatalyst deactivation analysis	67
3.4	Safety.....	67
CHAPTER 4: RESULTS AND DISCUSSIONS		68
4.1	Introduction	68
4.2	Characterization of fresh (T_F) TiO_2	68
4.2.1	X-ray diffraction of T_F	68
4.2.2	Brunauer-Emmett-Teller (BET).....	69
4.2.3	Fourier-transform infrared spectroscopy (FTIR)	69
4.2.4	X-ray photoelectron spectroscopy (XPS)	70
4.3	Kinetic studies of methylene blue and methyl orange photodegradation	71
4.3.1	Photodegradation products of Methylene blue with Cl^- or SO_4^{2-} at varying reaction conditions	73
4.3.2	Photodegradation products of Methyl orange with Cl^- or SO_4^{2-} at varying reaction conditions	76

4.4	Surface analysis of deactivated TiO ₂ samples from cumulative percent degradation study.....	79
4.4.1	<i>Fourier transform infrared spectroscopy (FTIR) comparison of T_F, T_{MB1}-T_{MB12} and T_{MO1}-T_{MO12} samples</i>	82
4.4.2	<i>X-ray photoelectron spectroscopy (XPS) of T_F, T_{MB1}-T_{MB12} and T_{MO1}-T_{MO12} samples</i>	84
4.4.2.1	<i>Percent atomic concentration changes in Titanium (Ti)</i>	86
4.4.2.2	<i>Percent atomic concentration changes in Oxygen (O)</i>	91
4.4.2.3	<i>Percent atomic concentration changes in Carbon (C)</i>	97
4.4.2.4	<i>Percent atomic concentration changes in Nitrogen (N)</i>	103
4.4.2.5	<i>Percent atomic concentration changes in Sulfur (S)</i>	106
4.4.2.6	<i>Percent atomic concentration changes in Sodium (Na)</i>	111
4.4.2.7	<i>Percent atomic concentration changes in Potassium (K)</i>	117
4.4.2.8	<i>Effect of Cl⁻ and SO₄²⁻ on scavenging active holes and competitive adsorption</i>	118
4.5	Recommended practice for deactivation analysis in photocatalysis	120
CHAPTER 5: CONCLUSION AND RECOMMENDATION		123
5.1	Conclusion.....	123
5.2	Recommendation for future work	125
References.....		126
LIST OF PUBLICATIONS AND PAPERS PRESENTED		135
Academic articles		135
Conference Proceeding		136

LIST OF FIGURES

Figure 2.1: Flow diagram of topics reviewed leading to research gap	7
Figure 2.2: Plot of the different surfaces studied. S^1 , S^2 , S^3 , S^4 and S^5 (Valdes et al., 2008)	21
Figure 2.3: The TiO_2 anatase (101) surface. a, Ball-and-stick model with an adsorbed water molecule. Water oxygen and hydrogen atoms are plotted in yellow and white, respectively, TiO_2 atoms are blue (Ti) and red (O) (He et al., 2009)	22
Figure 2.4: The TiO_2 anatase (101) surface showing empty-states STM image of the clean surface ($115 \times 72 \text{ \AA}^2$, $V_{\text{sample}} = +1.61 \text{ V}$, $I_{\text{Tunnel}} = 1.58 \text{ nA}$), taken at room temperature. Each oval-shaped bright spot extends across both under coordinated surface O_{2c} and Ti_{5c} atoms (He et al., 2009).....	23
Figure 2.5: Effect of increasing concentration of chloride on rates of oxidation (slopes) of salicylic acid, aniline and ethanol, each equivalent to 100 μg of carbon in 20 mL of solution (Abdullah et al., 1990)	27
Figure 2.6: Effects of increasing concentration of nitrate on rates of oxidation (slopes) of salicylic acid, aniline and ethanol, each equivalent to 100 μg of carbon in 20 mL of solution (Abdullah et al., 1990)	27
Figure 2.7: Effects of increasing concentration of sulfate on rates of oxidation (slopes) of salicylic acid, aniline and ethanol, each equivalent to 100 μg of carbon in 20 mL of solution (Abdullah et al., 1990)	28
Figure 2.8: Effects of increasing concentration of phosphate on rates of oxidation (slopes) of salicylic acid, aniline and ethanol, each equivalent to 100 μg of carbon in 20 mL of solution (Abdullah et al., 1990)	28
Figure 2.9: Photocatalytic inhibition in the presence of different anions Cl^- , SO_4^{2-} , CO_3^{2-} , NO_3^- and with no anion added (Y. Wang et al., 2013).....	29
Figure 2.10: The change of decomposition value (%) of Sirious Gelb GC sample with irradiation in Na_2SO_4 salt media at pH 3.5 in TiO_2/UV and $Ag-TiO_2/UV$ systems (Ozkan et al., 2004)	30
Figure 2.11: The change of decomposition value (%) of Sirius Gelb GC sample with irradiation time in $Na_2HPO_4 \cdot 2H_2O$ salt media at pH 3.5 in TiO_2/UV and $Ag-TiO_2/UV$ systems (Ozkan et al., 2004).....	31
Figure 2.12: The change of decomposition value (%) of Sirius Gelb GC sample with irradiation time in $NaCl$ salt media at pH 3.5 in TiO_2/UV and $Ag-TiO_2/UV$ systems (Ozkan et al., 2004).....	31

Figure 2.13: The change of decomposition value (%) of Sirius Gelb GC sample with irradiation time in Na_2CO_3 salt media at pH 3.5 in TiO_2/UV and $\text{Ag-TiO}_2/\text{UV}$ systems (Ozkan et al., 2004).....	32
Figure 2.14: The change of decomposition value (%) of Sirius Gelb GC sample with irradiation time in Na_2NO_3 salt media at pH 3.5 in TiO_2/UV and $\text{Ag-TiO}_2/\text{UV}$ systems (Ozkan et al., 2004).....	39
Figure 2.15: Effect of Cl^- concentration on the photocatalytic degradation of MO over HPW-Y- TiO_2 (Y. Wang et al., 2013)	40
Figure 2.16: Effect of halide ions on the amounts of $^1\text{O}_2$ formed in TiO_2 (P25) photocatalysis (Daimon et al., 2008)	43
Figure 2.17: Schematic diagram of the proposed practice.....	45
Figure 3.1: Flow diagram of major aspects of research activities	48
Figure 3.2: Flow diagram of procedure of kinetic studies of photodegradation of MB and MO in form of cumulative percent degradation (CPD)	61
Figure 3.3: Photoreactor set-up for kinetic studies and deactivation analysis.....	62
Figure 4.1: X-ray diffraction of T_F indicating TiO_2 in the anatase phase.....	69
Figure 4.2: FTIR of T_F indicating characteristic TiO_2 vibrations.....	70
Figure 4.3: XPS survey spectra of T_F	70
Figure 4.4: Photocatalytic degradation pathway of Methylene blue (Houas et al., 2001)	74
Figure 4.5: First order linear transforms of disappearance of MB under UV-irradiation	74
Figure 4.6: First order linear transforms of disappearance of MB without UV irradiation	75
Figure 4.7: Concentration (ppm) changing with time (mins) of MB samples $\text{T}_{\text{OMB1}}-\text{T}_{\text{OMB12}}$	75
Figure 4.8: Photocatalytic degradation pathway of Methyl orange (Baiocchi et al., 2002)	76
Figure 4.9: First order linear transforms of disappearance of MO under UV-irradiation	77
Figure 4.10: First order linear transforms of disappearance of MO without UV	77

Figure 4.11: Concentration (ppm) changing with time (mins) of MO samples T_{oMO1} - T_{oMO12}	78
Figure 4.12: 10-60h of MB samples T_{MB1} - T_{MB12} percent degradation and CPD per sample	80
Figure 4.13: 10-60h of MO samples T_{MO1} - T_{MO12} percent degradation and CPD per sample	80
Figure 4.14: Relationship between SS PAC and CPD per MB sample.....	81
Figure 4.15: Relationship between SS PAC and CPD per MO sample.....	81
Figure 4.16: FTIR of the samples T_F and T_{MB1} - T_{MB12} of MB.....	83
Figure 4.17: FTIR of the samples T_F and T_{MO1} - T_{MO12} of MO	83
Figure 4.18: XPS survey spectra of samples T_F and T_{MB1} - T_{MB12} of MB.....	84
Figure 4.19: XPS survey spectra of samples T_F and T_{MO1} - T_{MO12} of MO	85
Figure 4.20 Schematic diagram for the proposed practice of photocatalyst performance analysis	121

LIST OF TABLES

Table 2.1: Summary of references and remarks on effects of inorganic anions on active hole of titanium dioxide (TiO ₂) in aqueous media	33
Table 2.2: Summary of references and remarks on surface reaction of titanium dioxide (TiO ₂) in gaseous media	36
Table 2.3: Effect of anions on photodegradation of 4-FP (%) with TiO ₂ -P25 (Selvam et al., 2007)	42
Table 3.1: Independent variables, their levels and category	53
Table 3.2: Samples with matching reaction conditions as variables.....	54
Table 3.2: Rate of mineralization of methylene blue without salt without UV irradiation at pH4 for 10hours sample T _{MBR1}	64
Table 3.3: Rate of mineralization of methylene blue without salt without UV irradiation at pH 4 for 10hours sample T _{MBR2}	64
Table 3.4: Rate of mineralization of methylene blue without salt without UV irradiation at pH4 for 10hours sample T _{MBR3}	65
Table 3.5: Rate of mineralization of methylene blue without salt without UV irradiation at pH4 for 10hours sample T _{MBR4}	65
Table 3.6: Rate of mineralization of methylene blue without salt without UV irradiation at pH4 for 10hours sample T _{MBR4}	66
Table 3.7: Rate of mineralization of methylene blue without salt without UV irradiation at pH4 for 10hours sample T _{MB1}	66
Table 4.1: XPS Survey Spectra of elemental composition and Percent Atomic concentration of T _F , T _{MB1} -T _{MB12} of MB.....	85
Table 4.2: XPS Survey Spectra of elemental composition and Percent Atomic concentration of T _F , T _{MO1} -T _{MO12} of MO	86
Table 4.3: High Resolution Spectra of Ti2p species on T _F , T _{MB1} -T _{MB12} of MB.....	87
Table 4.4: High Resolution Spectra of Ti2p species on T _F , T _{MO1} -T _{MO12} of MO	88
Table 4.5: High Resolution Spectra of O1s species on T _F , T _{MB1} -T _{MB12} of MB.....	93
Table 4.6: High Resolution Spectra of O1s species on T _F , T _{MO1} -T _{MO12} of MO	94

Table 4.7: High Resolution Spectra of C1s species on T _F , T _{MB1} -T _{MB12} of MB	98
Table 4.8: High Resolution Spectra of C1s species on T _F , T _{MO1} -T _{MO12} of MO	99
Table 4.9: High Resolution Spectra of N1s species on T _F , T _{MB1} -T _{MB12} of MB	104
Table 4.10: High Resolution Spectra of N1s species on T _F , T _{MO1} -T _{MO12} of MO	104
Table 4.11: High Resolution Spectra of S2p species on T _F , T _{MB1} -T _{MB12} of MB	108
Table 4.12: High Resolution Spectra of S2p species on T _F , T _{MO1} -T _{MO12} of MO	109
Table 4.13: High Resolution Spectra of Na1s species on T _F , T _{MB1} -T _{MB12} of MB	113
Table 4.14: High Resolution Spectra of Na1s species on T _F , T _{MO1} -T _{MO12} of MO	114
Table 4.15: High Resolution Spectra of K2p species on T _F , T _{MO1} -T _{MO12} of MB	117
Table 4.16: High Resolution Spectra of K2p species on T _F , T _{MO1} -T _{MO12} of MO	117

LIST OF SYMBOLS AND ABBREVIATIONS

C_e	:	Dye concentration at equilibrium, $mg\ L^{-1}$
C_o	:	Initial dye concentration, $mg\ L^{-1}$
D_o	:	Photocatalyst dose, mg
$^1\Delta_g$:	Singlet molecular oxygen
e_{CB}^-	:	Conduction band electrons, <i>coulombs</i> , C
h_{VB}^+	:	Valence band holes, <i>coulombs</i> , C
I_o	:	Radiation intensity, <i>watt per steradian</i> (W/sr)
I_d	:	Irradiation depth, m
k_{app}	:	Apparent pseudo-first-order rate constant, s^{-1}
K	:	Adsorption coefficient, $mL\ g^{-1}$
M	:	Mass of catalyst, mg
n_{Fe}	:	Amount of Fe^{2+} ions after irradiation, mg
N_S	:	Number of occupied sites
N	:	Number of sites
N_A	:	Number of aggregates
Φ	:	Quantum yield
ρ_{app}	:	Apparent density of the TiO_2 colloid, kg/m^3
q_e	:	Equilibrium adsorption, mg/g
R_A	:	Mean average radius of the aggregate, m
R_{AO}	:	Value of R_A at intercept on x -axis, m
r	:	Reaction rate, $mol\ dm^3\ s^{-1}$
T_F	:	Fresh anatase titanium dioxide
θ	:	Surface coverage
V	:	Reactor volume, m^3

Abbreviations

AOP	:	Advanced oxidation process
BET	:	Brunauer-Emmett-Teller
CPD	:	Cumulative percent degradation
DFT	:	Density Functional Model
DNA	:	Deoxyribonucleic acid
EDCs	:	Endocrine-disrupting chemicals
FTIR	:	Fourier Transform Infrared Spectroscopy
GC-MS	:	Amount of Fe^{2+} ions after irradiation, <i>mg</i>
MB	:	Methylene blue
MO	:	Methyl orange
$\cdot OH$:	Hydroxyl radical
PAC	:	Percent atomic concentration
PZC	:	Point of Zero Charge
RIFs	:	Refractive index functions
TPD	:	Temperature Programmed Desorption
TOC	:	Total Organic Carbon
TiO ₂	:	Titanium dioxide
UV	:	Ultraviolet
VASP	:	Vienna <i>ab initio</i> simulation package
XPS	:	X-ray Photoelectron Spectroscopy
XRD	:	X-Ray Diffraction

CHAPTER 1: INTRODUCTION

1.1 Background

Growth of human civilization has witnessed increase in production from the textile industries with subsequent discharge of wastewater and toxic dyes. These effluents are detrimental to humans, aquatic life, the environment and other microorganisms (Borker & Salker, 2006). Additionally, dyes reduce light penetration (Prado et al., 2008), pollute and destroy aesthetic ecosystems. Public outcries are on the increase regarding the deleterious effects of textile dyes such as azo dyes on the earth ecosystems (Hong et al., 1998; Ohko et al., 2001), prompting for better wastewater treatment systems. AOP is one of the relatively new treatment systems that have been researched extensively and is likely to fit the wastewater treatment networks envisaged for effective water recycle and reuse when commercialization is achieved. AOP are technologies based on the generation of highly reactive species, the hydroxyl radicals. These oxidative species degradation the dissolved or dispersed organic compounds in the aquatic media, and are known to mineralize the target pollutants completely (Madhavan et al., 2000). Where photocatalysts are employed in AOPs, titanium dioxide (TiO_2) and its modified forms are prominent. In addition to possessing good attributes such as extreme stability even in electrolyte solution and the most efficient photoactivity to date, TiO_2 is cheap. However, the practical technology envisaged for TiO_2 -photocatalysis remains elusive because of factors such as deactivation, mass transfer and photon transfer limitations.

More work need to be done to make photoreactors available for commercial use, part of the needed research input was reviewed by (Gerven et al., 2007). The authors presented investigations into photoreactor intensification processes in the areas of mass and photon transfer limitations and provide recommendations on how to fabricate a working photoreactor. Further known standard reactor design considerations which need emphasis is maintaining photocatalyst activity over a certain period, which is the primary concern

of this research. This concern is more pertinent in textile wastewaters where effect of ions such as Cl^- , NO_3^- , SO_4^{2-} , CO_3^{2-} , and PO_4^{3-} , added as industrial dye-enhancers were reported to have detrimental effect on the activity of TiO_2 in three main areas namely scavenge and deactivate the photogenerated holes (h_{VB}^+), scavenging on $\cdot\text{OH}$, and in some instances, the action of these ions, reduces the amount of singlet molecular oxygen of $^1\Delta_g$ state ($^1\text{O}_2$) generated during the photocatalytic process leading to reduction in reaction rate (Farouk et al., 2016).

Therefore, in this work, studies of surface activity on TiO_2 surface leading to deactivation of h_{VB}^+ active sites will be of importance. TiO_2 activity inhibition and deactivation have been investigated in both aqueous media and in gas over TiO_2 shown in Table 2.1 and Table 2.2 respectively, where deposition on the photocatalyst surface by intermediates and other end products like carbon were reported to reduce the rate of photodegradation (Einaga, 2002). Often, the investigations carried out did not emphasize the distinction between gaseous and aqueous media photodegradation on the photocatalyst surface. The early studies of TiO_2 deactivation in aqueous media in the presence of inorganic ions CO_3^{2-} , Cl^- , NO_3^- , SO_4^{2-} blocking the active sites, was put forward by using Langmuir-Hinshelwood (L-H) mechanism. To explain the dynamics involved in the adsorption-desorption (due to the anions) on the semiconductor surface (TiO_2) leading to deactivation, the authors offered models. Their models reflect only analysis of contaminants not textile related, thus necessitating further investigation of this phenomenon with dyes and other complexities related to textile wastewater. Though Ghaly et al., (2007); Wang et al., (2013) investigated the phenomenon in dyes, no surface analysis of adsorbed species was presented. For possible commercialization of AOPs, the complexity in structure of different classes of contaminants in wastewaters must be put into consideration as alcohols, aldehydes, dyes interact differently with the TiO_2 surface in aqueous mixtures. Studying the adsorbed intermediates and end products on the surface

leading to deactivation will provide a platform for confirming sources of deactivation and provide information on the requirement of an effective photocatalyst surface for use in design of future photocatalyst, adding to the new knowledge used in density functional theory (DFT) analysis in optimizing the reaction conditions in photocatalysis leading to sustainable systems.

1.2 Problem statement

Deactivation of TiO_2 in photoreactors have been reported for dye containing wastewater. This wastewater may contain ions especially Cl^- and SO_4^{2-} that aggravate deactivation mainly by surface active site blockage, but no systematic study was carried out to show the effect of these ions on TiO_2 surface after deactivation in aqueous media. There is also a challenge on how to assess photocatalyst performance in relation to adsorbed species and how to articulate this knowledge to prolong the life of photocatalyst. In this research two types of dyes a cationic dye methylene blue and anionic dye methyl orange, that react differently in photocatalysis, will be added Cl^- or SO_4^{2-} and studied at different reaction conditions and adsorbed species determined.

1.3 Aim

The aim of this work is to identify main cause of surface deactivation of anatase TiO_2 photocatalyst for enhanced treatment of recalcitrant dye wastewaters.

1.4 Objectives

To achieve the aim of this study the following objectives are outlined:

1. Characterization of fresh TiO_2 anatase catalyst to determine structure, physico-chemical properties and adsorption capacity of the photocatalyst.

2. Kinetic evaluation of photodegradation of cationic dye (MB) and anionic dye (MO) solution with Cl^- or SO_4^{2-} , with or without UV irradiation, at pH4 or pH10 through activity determination of TiO_2 anatase.
3. Determine the effect of Cl^- and SO_4^{2-} addition on TiO_2 anatase deactivation in photodegradation of MB/MO dye solution in form of cumulative percent degradation with or without UV irradiation, at pH4 or pH10 through surface analysis.
4. Propose a procedure on conducting photocatalyst deactivation study systematically.

1.5 Scope

The scope will cover studies of degradation of cationic MB and anionic MO dyes in acidic and basic pH with Cl^- or SO_4^{2-} using TiO_2 as a photocatalyst. The reaction conditions and photocatalyst and other materials were methodically selected to reflect what is used in the industry and literature.

1. TiO_2 anatase was selected due to its commercial availability as an effective photocatalyst and available literature on water splitting reactions on its surface.
2. Methylene blue (cationic dye) and Methyl orange (anionic dye) were chosen as model dyes because they have opposite polarity, and this will affect the way each of them get adsorbed on the TiO_2 surface. Additionally, both have photodegradation pathway in literature.
3. NaCl and Na_2SO_4 were selected as they are among frequently used dye enhancers in textile industry.
4. UV source was chosen and modified from a commercially available UV light.
5. The pH4 and pH10 were chosen to reflect extreme basic and acidic pH conditions available from textile wastewater.

1.6 Thesis organization

This thesis contains five chapters with different facets reflecting the topic and objectives of the research.

Chapter 1: Introduction

This chapter briefly introduces background on AOP, the advantages of using TiO_2 as a photocatalyst in photoreactors, the deactivation of TiO_2 in textile wastewater due to added salts and how they affect photoreactor performance. Research problem statement, aim, objectives and scope of the study.

Chapter 2: Literature review

This chapter discusses the current challenges and future prospects in photoreactor bed design, in terms of photocatalyst deactivation in textile wastewaters. The three types of deactivation in photocatalysis in aqueous media was discussed. A comparison of surface reactions in gaseous media and conditions favoring the optimum reaction conditions in aqueous media that may extend photocatalyst life was also discussed. It also covers surface reactions including water splitting reactions on TiO_2 leading to generation of $\cdot\text{OH}$ radicals that oxidizes dyes and other recalcitrant wastewaters.

Chapter 3: Materials and Methods

This chapter presents the materials and equipment used, it also presents the methods followed to generate the required data to achieve the objectives of this study. It outlined the set of experiments to assess the performance of a photocatalyst as the surface adsorbed species accumulate.

Chapter 4: Results and Discussion

This chapter presents the result and discussion part of the rate of deactivation of TiO_2 photocatalyst, and surface analysis of fresh and deactivated photocatalyst in different reaction conditions. In this chapter, the results are presented in five parts to reflect the objectives as follows:

1. General (XRD, BET, XPS, FTIR) characterization of fresh TiO_2 to determine its initial composition and its suitability for the analysis was ascertained, presented and discussed. It provides information on objective (1).
2. Kinetics of degradation of cationic dye (methylene blue) and anionic dye (methyl orange) with Cl^- or SO_4^{2-} , with or without UV irradiation and varying pH using TiO_2 were determined and compared with the known degradation pathway for Methylene blue and Methyl orange, it provides information on objective (2).
3. This section provides information on objectives (3). XPS and FTIR analysis of deactivated TiO_2 anatase samples from both methylene blue and methyl orange, using the cumulative percent degradation analysis were presented, with detailed analysis of changes in elemental composition of titanium (Ti), Oxygen (O), Carbon (C), Nitrogen (N), Sulfur (S), Sodium (Na) on TiO_2 surface. The discussions were under four subcategories UV effect, pH effect, Cl^- effect and SO_4^{2-} effect each subcategory was discussed with respect to MB or MO dyes.
4. A schematic on the practice for photocatalyst deactivation analysis was proposed. This section provides information on objective (4).

Chapter 5: Conclusion and Recommendations

This chapter presented the concluding part of this research and provide recommendations for possible future research in this area.

CHAPTER 2: LITERATURE REVIEW

The topics discussed in the literature review and how they relate to the research gap are given in Fig. 2.1:

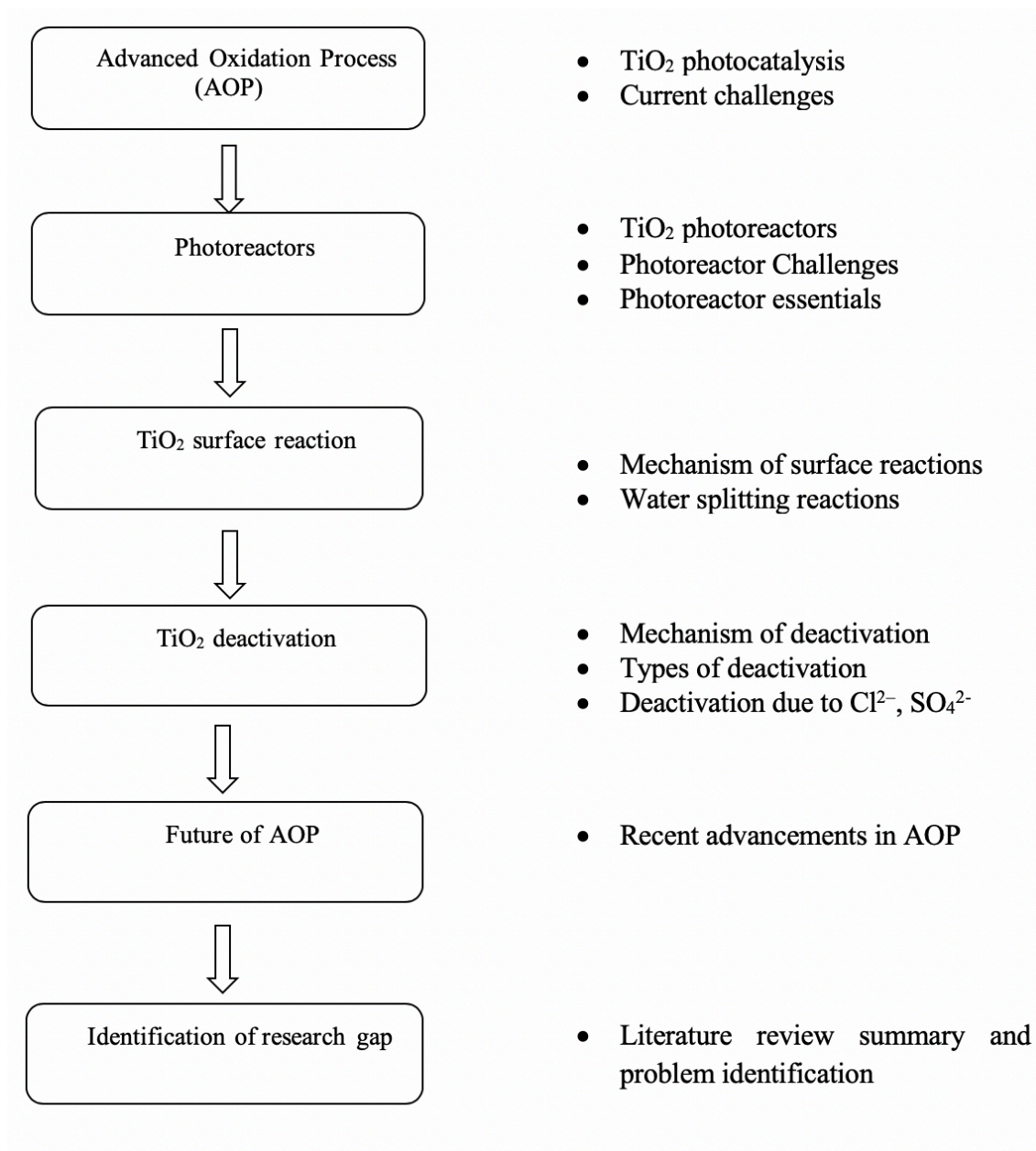


Figure 2.1: Flow diagram of topics reviewed leading to research gap

2.1 Introduction

Advanced oxidation process has been used to treat recalcitrant wastewaters, where efficiency is still being challenged due to variation of wastewaters, such that each wastewater might require a customized photoreactor. Among these recalcitrant wastewaters are the textile wastewaters (Borker & Salker, 2006). Numerous photodegradation processes of dyes and other chemicals have been studied in aqueous and gaseous media, resulting in better reactor design and raising prospects of commercialization (Gerven et al., 2007). In the areas of wastewater recycle and reuse, surface analysis of deactivated photocatalyst will enhance the knowledge base in the synthesis and design of better photocatalysts including sulfur resistant photocatalysts (P. Yu & Cardona, 2010) and specialty resins highlighted in (Farouk et al., 2016) for improved reactor performance. It will also enhance the understanding of H₂O splitting reaction and how it relates to photocatalytic degradation kinetics on solid surfaces in aqueous media. The H₂O splitting reaction is considered to be the initial step on TiO₂ surface leading to generation of oxidants where electrons reduce oxygen to superoxide radicals O₂^{•-} and holes can oxidize water to hydroxyl radicals •OH (Kafizas et al., 2016; Mills & Le Hunte, 1997). •OH is believed to be the principal oxidant that causes bond breakage of dyes such as MB and MO leading to intermediates and possibly final products (Houas et al., 20010). Such analysis will allow photocatalytic reactors to fit into wastewater treatment networks, to polish the treated water where conventional systems are unable to remove the carcinogenic components.

2.2 Current challenges in Advanced Oxidation Process (AOP) with TiO₂

Researches focusing on application of Advanced Oxidation Process (AOP) have shown potential in the way the photoreactors are designed. Despite such developments, the technology is yet to replace the existing treatment systems in the industry. Data collected from a survey by our research team of over 80 major global water treatment

companies, revealed that only about 43% used some form of AOP, mostly UV and Ozonation. Only about 4% used photocatalysis at pilot scale. This is a clear indication of lack of patronage of the technology. Among the most used photocatalysts, TiO_2 is the most important. It possesses good properties like high stability in electrolyte solution. It is also cheap and has the most efficient photocatalyst activity.

If TiO_2 is chosen for the application of such technology, the effect of ions in the solution matrix on the life span of TiO_2 reactor beds could be properly resolved by studying the electronic, structural and optical properties of the TiO_2 nanoparticles. This knowledge when combined with quantum chemistry as in (Cinar, 2017) will modify the pattern of research methods, result presentations and discussions in the areas of photocatalysis. Some of the factors that need be considered, highlighted and discussed in detail during photoreactions are as follows:

2.2.1 Phase stability

The pattern of research methods and discussion in reported cases of TiO_2 deactivation in aqueous suspensions does not reflect the differences of lattices or phase stability of TiO_2 , while these differences (in lattices) play a major role in computational and experimental analysis. Early thermodynamic analyzes on phase stability of nanocrystalline anatase and rutile were performed by (Zhang & Banfield 1998). Penn & Banfield (1999) had indicated that anatase clusters are dominated by 101 surfaces, while rutile clusters are usually dominated by 110 surfaces according to computational results of (Ramamoorthy et al., 1994). Zhang & Banfield (1998) concluded that when the particle size is reduced under ca. 14 nm, the anatase structure becomes more stable than rutile. The reason for the change in phase stability is the higher free energy of rutile, arising from the energetics of the dominating surface facet types in such small particles (Auvinen, 2013). These details are to be considered during future simulations and

experimentations.

2.2.2 Particle behavior in Bulk

The behavior at bulk also deserves consideration. In the case of the bulk quantities, rutile is the most stable crystal structure of TiO_2 . While for nanoparticles, however, the anatase structure becomes more favorable. This has been observed experimentally for example in the case of the TiO_2 thin layers (Kaariaainen et al., 2009). The driving force behind this phase transformation is the surface energetics of different TiO_2 surfaces. The nanoparticle is a closed object, limited by surface boundaries and the surface-to-bulk ratio is drastically increased when compared to larger particles, and the different surface energies start to play a more important role in the particle energetics. Moreover, existence of surface or bulk electron trap states occurring in colloidal TiO_2 is also another issue worth considering (Yates, 2009).

2.2.3 Reaction conditions

Furthermore, in the reports of TiO_2 deactivation in aqueous media, reaction conditions are often not well specified (apart from pH, and opacity), despite the fact that photoreactions are sensitive to reaction conditions. Phenomenon of photo induced hydrophilic effect (R. Wang et al., 1998; Yates, 2009) and its conditions are often disregarded and it is an acknowledged phenomenon in the studies of surface science describing a process where UV irradiation in air causes water droplets to wet the TiO_2 film surface, resulting in a lowering of the contact angle over time. While temperature is also a factor when molecules or atoms come in contact with a surface, numerous temperature dependence analysis especially in gas- TiO_2 photocatalysis have been reported in Temperature Programmed Desorption (TPD) (Fan et al., 2012; Larson & Falconer, 1994) because it provides information on how reaction temperature affects

binding energies of adsorbate and surface, but its effect is often ignored in the discussions of aqueous photodegradation.

2.2.4 Nature of contaminants

The complexity of different classes of contaminants in wastewaters has to be put into consideration as alcohols, aldehydes, dyes interact differently on the TiO_2 surface in aqueous mixtures. In some instances, the discussion of results did not provide details of the mechanisms involved and the models not well explained. Some authors, for example attempted to explain the deactivation mechanism between TiO_2 and anions. They initially concluded that Point of Zero Charge (PZC) is not sufficient in explaining the complex mechanism involved at the interface between the particles and the liquid. An alternative explanation for the observed salt effects was that the organic solutes and inorganic anions are engaged in competitive adsorption and reaction processes at the liquid- TiO_2 interface (Abdullah et al., 1990; Ghaly et al., 2007). Langmuir-Hinshelwood (L-H) mechanism was used in explaining the dynamics involved in the adsorption-desorption on the semiconductor surface and they offered a model. There is need for verification of such models theoretically with molecular orbital calculations and Density Functional Model (DFT) based calculations such as described in (Selli et al., 2017). It is apparent that all the modern applications of TiO_2 will demand better understanding of the optical and electronic properties of this semiconductor especially nano-sized form.

2.2.5 Light attenuation

Textile effluents from the dyeing and rinsing steps represent the most colored fraction of textile wastewaters, and are characterized by extreme fluctuations in many quality indicators such as pH, color, etc. (Carmen & Daniela, 2012). These might pose a challenge leading to slow degradation rate and possible activity inhibition of TiO_2 . Thus, light attenuation (due to strong coloration), the intermediates formed, and effect of pH

are parameters of concern.

Light attenuation in dye wastewaters is a major problem not only to the environment, but during photodegradation with visible-light using photocatalysts whose kinetics is dependent on the concentration of the dye (Rochkind et al., 2015). When UV-active photocatalysts are used to degrade molecules that do not absorb UV light, it seldom results in Langmuir-Hinshelwood type of kinetics (rate increases with increasing concentration of dye) until rate-saturation is achieved. A different outcome is observed in a visible-light absorbing contaminant (dye) and a visible light absorbing photocatalyst matrix. Increasing the concentration of the dye reduces the rate of degradation, due to increased absorption of light by free dye molecules in the solution (Rochkinnd et al 2015; Konstantinou & Albanis, 2004). Alahiane et al., (2014) investigated the effects of the initial concentration of RY 145 dye on the photocatalytic efficiency with concentrations from 5 to 40 mg/l and observed that increasing the dye concentration reduces the efficiency of degradation and same was reported in earlier studies (Liu et al., 2006; Senthilkumaar & Porkodi 2005).

2.2.6 Dye classification

Dyes can be classified on the basis of structure, function, or both, can also be categorized as acidic (anionic), basic (cationic), direct, disperse, reactive and other classes. These classifications point to differential behavior in TiO₂ colloid. Metal oxides such as TiO₂ have surfaces that can be assumed to be surfaces of hydroxyls and can participate in acid-base reactions as well as ion exchange, this information suggests that pH will have an effect on the photodegradation efficiency of dyes (Rajeshwar et al., 2008) and necessitates investigations into Point of Zero Charge (PZC), which is usually evaluated in connection with the pH of an electrolyte and surface of a mineral or metal oxide, and the PZC value is assigned to a given substrate or colloidal particle (Rajeshwar

et al., 2008). Any change in solution pH is going to affect the surface charge of TiO₂ particles and reposition the potentials of the photocatalytic reactions. Which will in turn, bring a change of the reaction rate. Epling & Lin, (2002) selected 15 dyes with different characteristics, they observed average bleaching rate of anionic dyes to be noticeably faster than both cationic and neutral dyes, the slowest among the two to be bleached was the neutral dye. While Baran et al., (2008) under different conditions concluded that TiO₂ adsorbed almost only cationic dyes, except for the anionic Quinizarine (adsorption efficiency of 21.8%) and the cationic color index (C.I.) Basic Orange 2 which displayed no adsorption.

Structure of dye molecules are typically made up of relatively large number of functional groups, often leading to several types of mechanisms with different intermediate products and final products during photodegradation processes. Two different photocatalysts rates of decolorization will not necessarily compare with their mineralization rates. Often, the absorption spectrum of their intermediates partially overlaps with that of the dye depending on the type of the intermediates or on the degradation mechanism (Rochkind et al., 2015). Complete mineralization of dyes have often been accomplished (Lachheb et al., 2002) and at times it also indicates the degraded intermediates, besides CO₂, H₂O and inorganic salts, are mainly low- or non-toxic colorless organic acids (Li et al., 2007). In azo dyes, attack on the azo bond (C-N=N-), is followed by opening of the aromatic rings leading to aromatic amines or phenolic compounds as intermediate products. Further opening of the aromatic (in other cases naphthalene rings) yields a variety of carboxylic acids that decarboxylate into CO₂ (Rochkind et al., 2015). Not only intermediates, end products like benzene and substituted benzenes could be formed from Point of Zero Charge •OH degradation of azo dyes containing a phenylazo substitutions (Spadaro et al., 1994). However, the lack of complete mineralization of dyes containing the triazine group, where a stable cyanuric

acid is formed can pose a challenge (Hu et al., 2003). Other observations revealed that inorganic anions that can have inhibitory impacts on the TiO_2 are generated during photodegradation. Liu et al., (2005) suggested that the breakage of azo bond is the first step of the photocatalytic dye degradation due to the relatively slow Total Organic Carbon (TOC) reduction likely caused by the transformation of parent compounds into smaller organic intermediates, such as acetic acids, phenols, aldehydes. The early breakdown products then underwent further oxidation leading to the production of CO_2 . They also noted the inorganic anion SO_4^{2-} formed progressively and the amount of SO_4^{2-} increased more than 30% per 4h. Dyes containing sulfur atoms are mineralized into sulfate ions (Hu et al., 2003). Chlorinated dye molecules release chloride ions (Konstantinou & Albanis, 2004). Dyes containing nitrogen may release NH_4^+ , NO_3^- and sometimes N_2 , depending on the initial oxidation state of the nitrogen atoms (Rochkind et al., 2015; Tanaka et al., 2000). The final degradation products (NH_4^+ , NO_3^- , NO_2^- , SO_4^{2-} and Cl^-) lead to variation of pH in the colloidal solution (Tanaka et al., 2000), which will have an impact on the reaction rate. The knowledge of the relevant intermediates and end products, pH and photon diffusion in photodegradation has become relevant to further understand possible causes of catalyst activity inhibition in photocatalysis of textile related wastewaters.

2.2.7 Real textile wastewater kinetics

For a real textile wastewater there will be challenges especially with the kinetics since it is to be considered as a multicomponent system. Depending on the type of textile industry, the wastewater could contain suspended solids, wax, contains grease, resin and dyes (Alinsafi et al., 2007; Buthiyappan et al 2016). For example, in batik industry wastewater in Malaysia, apart from the dark color from the dye related compounds, there could be high content of organic compounds such as benzenes, esters, hydrocarbons, and alkyl halide. Therefore, after filtration and other treatment methods, for photocatalytic

treatments, the solution will be considered as a multicomponent system. The kinetic study would be considered as an organic matter index for the COD value because of the complexity of the wastewater (Buthiyappan et al., 2016). In some studies such complex mixtures were tested to investigate the degradation efficiency (COD removal) with zero, first and second order reaction kinetics and the suitable reaction order will be considered (Buthiyappan et al., 2016; Nitoi et al., 2013).

2.3 Essential photoreactor requirement

For the purpose of process intensification of photocatalytic reactors, many photoreactors have been designed to address issues of mass transfer limitations like the slurry systems, spinning disc reactor, the monolith reactor, and the microreactor. In addition, optimization of the amount of illuminated surface (photon transfer) has explored optical fibers and Light Emitting Diodes (LEDs) (Gerven et al., 2007; Izadifard et al 2013; Jo & Tayade, 2014; Lazar et al., 2012; Ray, 1999; Vaiano et al., 2014) and is likely to be the way forward. Concern in photon generation investments prompt investigations into photocatalysts with improved photon efficiency. The enhancement of photocatalytic activity (has been achieved through the doping of ZnO and TiO₂ nanoparticles by engineered coupling of N-doped TiO₂ (Sacco et al., 2012) and N-doped ZnO with ZnS-based phosphors (Vaiano et al., 2015). N-doped TiO₂ coupled with CaAl₂O₄:(Eu, Nd), as a source of light, prolonged the photocatalytic activity for more than three hours after turning off the light (H. Li et al., 2010). Other composites were able to absorb Ultraviolet (UV), visible and Near Infrared (NIR) lights simultaneously to proceed photocatalytic reactions effectively (Wu et al., 2014). Elsewhere, up-conversion luminescence agents were coupled with nano TiO₂ to enhance its degradation ability, the agents prepared effectively turned visible lights to ultraviolet lights absorbed by nano TiO₂ particles to produce the electron-cavity pairs (J. Wang et al., 2006). Sacco et al., (2015) evaluated the photocatalytic activity of N-TiO₂/ZSP for the removal of atrazine under Ultraviolet A

(UVA) light irradiation and observed an enhanced performance compared to either pure N-TiO₂ nanoparticles or bare ZnS-based phosphors microparticles (ZSP). Codoped TiO₂ catalyst was found to degrade dyes faster than the undoped catalyst under solar light illumination indicating the effect of doping, C, N, B and F on TiO₂ to enhance performance in visible light (Lee et al., 2008). Maximizing surface area and photon efficiency was used to explore scale-up in photoreactor design (Vaiano et al., 2015). The simulation of the kinetic processes in photocatalytic oxidation of organic pollutants in optimizing the design of photoreactors will simplify future design procedure and increase predictability of reaction results (Brandi et al., 2002; Eckert et al., 2015). Other noticeable variable is the pH of the solution. Jawad et al., 2014 applied response surface methodology (RSM) to verify the influence of pH in addition to photon transfer. More TiO₂ thin film surface improvements were also achieved (Gurylev et al., 2015; Vaiano et al., 2015) as well as composites (Zhang et al., 2015). Other synthesized nanoparticles like gold and silver have indicated a potential in the effective mineralization of dyes (MeenaKumari & Philip, 2015).

The next important aspect that requires urgent panacea is how photocatalyst surface loses its activity due to inhibitors and poisons, which often block the active sites and reduce chances of maximum contact. This poses technical and economic challenges (Sie, 2001). These challenges are more manifest in textile wastewater, which usually contain a lot of added salts such as NaCl, Na₂SO₄ to improve colorfastness. These salts dissociate into ions for example Cl⁻, SO₄²⁻, CO₃²⁻ NO₃⁻, and PO₄³⁻ in the dyeing media, they tend to combine with other chemical species to form intermediates or simply attach themselves with the active holes (*) (Abdullah et al., 1990), scavenge on •OH (Wang et al., 2013) and in some instances halides (Br⁻ and I⁻) reduce the amount of singlet molecular oxygen of ¹Δ_g state (¹O₂) generated during the photocatalytic process thereby reducing the reaction rate (Daimon et al., 2008). Reviews on TiO₂ photocatalysis are either on

application-driven perspective where authors report how kinetics of photocatalytic reactions are affected by factors or reviews from the field of surface science perspective where authors present water splitting reactions at CUS (Henderson, 2011). In order to understand the activity inhibition of TiO_2 by anions in aqueous mixtures (textile wastewaters), there is need for an approach from both perspectives. The photoadsorption and photodesorption of substances on TiO_2 surface ranging from water (Henderson, 2002), H_2 , CO , CO_2 , NO , SO_2 , NH_3 and H_2S (Diebold, 2003), organic molecules (Diebold, 2003) have been studied and reviewed in an effort to understand the mechanism behind their interaction with the surface. Point defects (predominantly oxygen vacancies) are created in the bulk or at surfaces, they cause important changes in the electronic structure that affect the performance of the semiconductor in various applications (Ganduglia-Pirovano et al., 2007). In colloidal TiO_2 the oxygen and crystalline lattice vacancy is where chemisorption occurs, while Photodesorption is caused by photogenerated holes. Much of the interest in studying originated from the photocatalytic splitting of water on TiO_2 electrodes (Linsebigler et al., 1995). Efforts have been focused on what forms of water (molecular or dissociated) exist on the surface lattice (anatase or rutile) and what are the important parameters in controlling the adsorption behavior. For a working photoreactor, it has to be optimized in three aspects; mass transfer, photon transfer and desirable surface properties to minimize surface inactivity.

2.4 Water splitting reaction on rutile $\text{TiO}_2(110)$ and anatase $\text{TiO}_2(101)$ surface

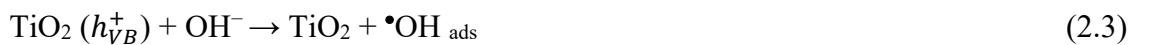
There are a number of studies of gases-over TiO_2 photocatalytic oxidation (PCO) systems, where deactivation have been reported (Alberici et al., 2001; Mendez-Roman et al., 1998; Shang et al., 2002). Some authors claim that TiO_2 photocatalytic detoxification of compounds is generally more efficient in the gas-over TiO_2 than in the liquid-over TiO_2 (Shang et al., 2002), but it is certain that the mechanisms of deactivation also differ between the two processes. The variation in mechanism was observed in relation to the

amount of deposits on the catalyst surface in gas-solid degradation when water was introduced. Einaga et al., (2002) investigated gas-solid heterogeneous photocatalytic decomposition of benzene, toluene, cyclohexane and cyclohexene over TiO_2 at room temperature and their reactivity compared. Reaction rates of toluene, cyclohexene and benzene increased with increasing humidity, while opposite is the case for cyclohexane. They suggested that increasing amount of carbon deposits was responsible for the lowered activity of TiO_2 for the photooxidation of benzene, toluene and cyclohexene in dry air. They postulated that the water vapor could reduce the formation of carbon deposits consistently on the TiO_2 surface and accelerated their decomposition.

Mendez-Roman & Cardona-Martinez (1998) observed while passing a mixture of gas-phase toluene and water vapor over any of the oxides $\text{SiO}_2\text{--TiO}_2$, or TiO_2 , the presence of water reduces the formation of surface species and concluded that its either the water competes for the sites where the species are formed, or it partially regenerates the active sites. It was reported by d'Hennezel et al., (1998) that photodegradation of benzene follows two routes, $\bullet\text{OH}$ radical oxidation or direct hole oxidation, and later observed by Li et al., (2007) that for the former, $\bullet\text{OH}$ takes part in the photoreactive process and continued dehydroxylation without water vapor causes surface deactivation. While for the latter, the direct hole-oxidation route produces radical cations of benzene, which might react with the next benzene molecule resulting in the polymerization of benzene which deactivates the catalyst surface. Sun et al., (2003) highlighted that the reaction atmosphere (i.e. gas-phase or aqueous solution) is very important for the decomposition of silicon-containing organic compounds on TiO_2 photocatalysts. These observation by various authors on TiO_2 surface shows and affirm that different reaction conditions results in different surface behavior as recently confirmed with near-ambient-pressure XPS analysis of TiO_2 surface (Krishnan et al., 2017). Unfortunately, in the few observed deactivation phenomena in aqueous media containing inorganic anions and TiO_2 ,

mechanisms and details of surface reactions were sketchy. In instances where TiO₂ deactivation is in aqueous solution, it will be of interest to engage water-TiO₂ interface analysis. TiO₂ in an aqueous mixture possess surface oxygen vacancy defects and defects in the crystalline lattice that provide new localized energy states not available in the perfect crystal, chemisorption occurs at the oxygen and crystalline lattice vacancies, while at the photogenerated holes photodesorption is said to occur. All the activities at these defects are important but most importantly are the activities at the photogenerated holes that will be of interest in this research. In order to make the necessary points concerning the decrease in photoreaction claimed by many authors it is important to identify those important reactions that control (rate limiting) the degradation process. The series of reactions on a semiconductor surface range from simplistic, well understood, to very complex and yet to be properly understood.

In summary and simplistic form, the relevant reactions at the semiconductor surface (TiO₂) causing the degradation of dyes can be expressed as follows (Konstantinou & Albanis, 2004):





The relevant reactions to focus in order to address the issues of activity inhibition in terms of hole scavenging are Eqs. (2.2) and (2.3). In Eq. (2.2) where the water molecule gets adsorbed at the photogenerated hole to form $\bullet\text{OH}_{\text{ads}}$ and Eq. (2.3) where OH^- was oxidized to $\bullet\text{OH}_{\text{ads}}$. If the anions like Cl^- from the textile or dye solution matrix could scavenge the photogenerated hole (Ghaly et al., 2007; Y. Wang et al., 2013) there will be a reasonable decrease in reaction rate (assuming the same for Eq. (2.7)). Likewise, if the photogenerated $\bullet\text{OH}$ in Eqs. (2.2) and (2.3) were to be scavenged by anion like Cl^- there will be reasonable decrease in reaction rate (Selvam et al., 2007; Stapleton et al., 2010) (assuming the same for Eq. (2.6)). When the conduction band electrons (e_{CB}^-) in Eq. (2.4) oxidized halide, Cl^\bullet , (Cl^- can be oxidized to Cl^\bullet with the valence band holes h_{VB}^+) reacts easily with the conduction band electrons (e_{CB}^-) it will hinder the conversion of $\text{O}_{2(\text{ads})}$ to $\text{O}_2^{\bullet-}$ and a net decrease in degradation rate will be observed (Daimon et al., 2008; Hirakawa & Nosaka 2002) (assuming the same for Eq. (2.8)).

These type of activities on the semiconductor surface makes studies of water adsorption on TiO_2 very significant and it has been investigated with a variety of experimental (Wendt et al., 2006; Zhang et al., 2006) and theoretical techniques (Valdes et al., 2008) comprehensive review have also been presented by Henderson (2002).

The studies use more recent techniques and mathematic models to predict with a level of accuracy the rate limiting steps in water splitting reactions at nanoscale for both rutile and anatase. To elucidate the rate limiting step in water splitting reactions, (Valdes et al., 2008) considered two different surface terminations S^1 and S^2 in Fig. 2.2 of the rutile $\text{TiO}_2(110)$ face, that are relevant in water oxidation processes and density functional theory (DFT) calculations.

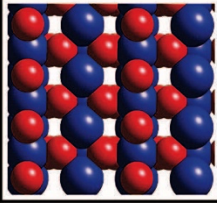
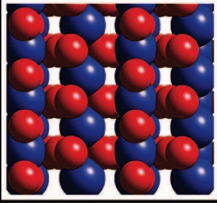
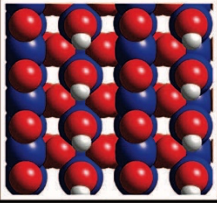
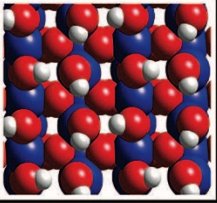
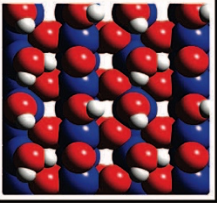
S ¹	S ²	S ³	S ⁴	S ⁵
$\Delta G=0$ eV	$\Delta G=7.40$ eV $-4eU$ -4 kT ln10 pH	$\Delta G=4.58$ eV $-2eU$ -2 kT ln10 pH	$\Delta G=0.87$ eV	$\Delta G=0.53$ eV
				

Figure 2.2: Plot of the different surfaces studied. S¹, S², S³, S⁴ and S⁵ (Valdes et al., 2008)

Valdes et al., (2008) concluded that oxidation of water on the rutile TiO₂(110) surface requires a moderate overpotential (0.78 V for pH = 0), and that the rate-limiting step for the oxidation process at the coordinatively unsaturated sites (CUS) is as given in Eq. (2.9).



They further observed that the relevant surface termination for the photo-oxidation of water is the completely oxygen covered surface (S²). Finally, that the illumination of the TiO₂(110) surface with light provides enough over-potential for the photo-oxidation to proceed spontaneously. It is the wide band gap of rutile TiO₂ that explains the low photoenergy conversion factor of this material.

Both rutile and anatase have these CUS where water-splitting reactions are initiated. Once the important reaction steps are identified, it will be easier to predict the behavior of the ions at the CUS. It is worth mentioning that majority of the earliest works on TiO₂ were on rutile(110) whereas it is the metastable anatase form that is generally considered photocatalytically more efficient, and should be investigated more due its application in photocatalysis industry (He et al., 2009). Anatase (101) surface happened to be favored as the surface with the lowest energy (Gong et al., 2006). Vittadini et al., (1998) applied density functional calculations of water adsorbed on the (101) and (001) surfaces of TiO₂ anatase at various coverage (θ), from low θ to $\theta = 1$. Their results support the idea that

on the anatase surface, two distinct states of the adsorbed water are present, one related to undissociated water on the (101) (adsorption at fivefold coordinated Ti sites) and (100)/(010) majority surfaces, and the other to dissociated water on the anatase (001) minority surface.

He et al., (2009) investigated anatase (101) with the intention of providing insight into reactions of H_2O with the anatase (101) surface. Their investigations confirm earlier predictions by Herman et al., (2003) about the structure of anatase (101), as having a morphology with five-fold coordinated Ti (Ti_{5c}) and two-fold coordinated surface O (O_{2c}) atoms arranged in rows along the [010] direction and that the water molecule is bound to a Ti_{5c} atom and forms weak hydrogen bonds with the two neighboring O_{2c} atoms as shown in Fig. 2.3. The centered rectangular surface unit cell, marked in Fig. 2.4, contains two equivalent $\text{Ti}_{5c}/\text{O}_{2c}$ surface atoms. The arrow marks a water monomer, probably adsorbed at a subsurface defect site.

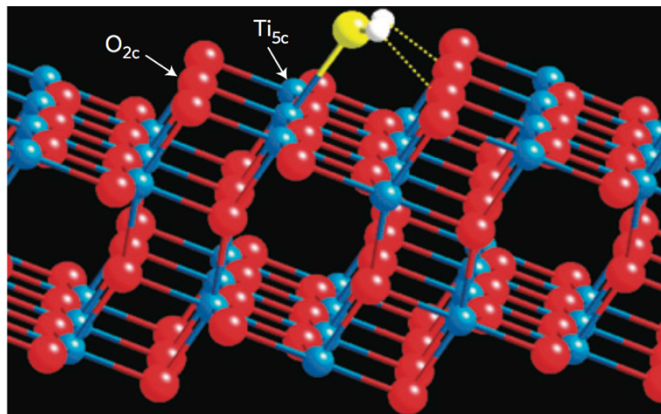


Figure 2.3: The TiO_2 anatase (101) surface. a, Ball-and-stick model with an adsorbed water molecule. Water oxygen and hydrogen atoms are plotted in yellow and white, respectively, TiO_2 atoms are blue (Ti) and red (O) (He et al., 2009)

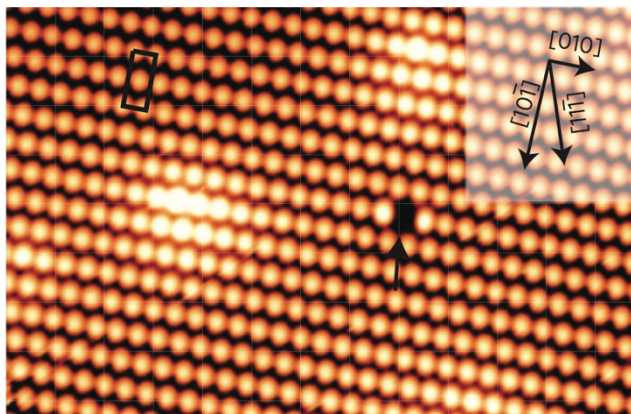


Figure 2.4: The TiO₂ anatase (101) surface showing empty-states STM image of the clean surface ($115 \times 72 \text{ \AA}^2$, $V_{\text{sample}} = +1.61 \text{ V}$, $I_{\text{Tunnel}} = 1.58 \text{ nA}$), taken at room temperature. Each oval-shaped bright spot extends across both under coordinated surface O_{2c} and Ti_{5c} atoms (He et al., 2009)

Furthermore, Zhao & Liu, (2014) used charged-slab first principles calculations integrated with a periodic continuum solvation model to analyze the initiating steps of water splitting on the TiO₂ surfaces, rutile (110) and anatase (101), at the solid–water interface. It was found that the first proton removal of water ($\text{H}_2\text{O} + h\nu_{VB}^+ \rightarrow \text{OH} + \text{H}^+$) during dissociation is sensitive to the crystalline phase and surface not the surface hole. The rutile (110) surface is more active for water splitting, with the calculated barrier of O-H bond breaking being 0.2 eV lower compared to that on anatase (101).

The higher activity of rutile is not due to the redox level of the hole (the position of the valence band maximum) but caused by the more favorable local bonding geometry of the surface. The authors observed that the capture of the hole occurs after the dissociation of H₂O. It is the final state of the H₂O dissociation, i.e. the OH anion and the solvated proton, state 2, that captures a hole to form the state 2⁺. In the state 2⁺, the hole may be transferred to the OH anion to form an OH radical or be trapped on the lattice O nearby the OH anion.

The proposed deactivation phenomenon on TiO₂ by Abdullah et al., (1990) mirrors the findings of Zhao & Liu (2014) with regards to the activities at the TiO₂ surface leading to the generation of radicals in an aqueous solution. Abdullah et al., (1990) went further

to propose the interaction of inorganic ions, organic solutes and other entities present in aqueous media that are engaged in a competitive adsorption at the photogenerated hole.

2.5 Reaction rate and catalyst deactivation in photocatalysis

Abdullah et al., (1990) predicted the deactivation mechanism at the TiO₂ surface in aqueous solution based on Langmuir-Hinshelwood Kinetics Model. Model 2, case 3 was proposed, the model assumed that all oxidizing sites at the surface are available for adsorption by organic solutes and inorganic anions. The inorganic anion for example Cl⁻ reacts competitively with organic solute for the positive holes to give a radical anion species, which subsequently reacts with adsorbed organic solute to give CO₂ eventually. Their model is similar to H₂O splitting reactions only that unlike in H₂O being dissociating into OH⁻ then reacting with the hole to form •OH, it is the Cl⁻ that transform into the radical anion specie Cl• thereby degrading the organic solute.



For example, for sulfate and phosphate ions, Eq. (2.10) will be:



and the fractional coverage θ_A

$$\theta_A = \frac{K_A[A^{-}]}{1 + K_S[S] + K_A[A^{-}]} \quad (2.14)$$

therefore, it is assumed that the average rate of CO₂ formation at 50% decomposition is given as:

$$\left\{ \frac{k_{CO_2} * 0.5K_S[S]^0 + k_A K_A[A^-] * \text{no. of atoms in } S}{(1 + K_S[S]^0 + K_A[A^-])} \right\} \quad (2.15)$$

where A and S are inorganic (SO_4^{2-} or $H_2PO_4^-$) and organic solutes respectively, k_A is the mean specific reaction rate constant for CO_2 formation from i intermediates multiplied by $K_{O_2}P_{O_2}/(1 + K_{O_2}P_{O_2})$, K_S is the adsorption coefficient of S , K_A is the adsorption coefficient of A , k_{CO_2} is the mean specific reaction rate constant for CO_2 , \bullet_{ox} is the oxidizing surface active sites.

From Eq. (2.15) the limiting value for r_{CO_2} would depend on two factors; the equilibrium adsorption constants for the various anions and the reaction rate constant for the reaction between the inorganic anion radical and the organic solute. The model was seen to consider the differences in observed limiting values in the cause of analysis. Therefore, the inhibitory effect of anionic species often encountered in photocatalytic oxidation can be reasonably explained by the mechanism (Model 2, case 3).

The marked effect of sulfate and phosphate was caused by the stronger surface adsorption and larger values of K_A than the other anions. The explanation given for the higher detrimental effect of phosphate more than the effect of sulfate might be due to the faster rate of reaction between $SO_4^{\bullet-}$ and the organic solutes to give CO_2 than the corresponding reaction with $H_2PO_4^{\bullet}$ which is slower. If the mechanism is accepted then the first step of water splitting reactions (He et al., 2009; Valdes et al., 2008) to produce $\bullet OH$ is assumed to have been displaced by the competitive adsorption reaction between either $SO_4^{\bullet-}$ or $H_2PO_4^{\bullet}$ on to the sites as the case may be, thus hindering $\bullet OH$ production.

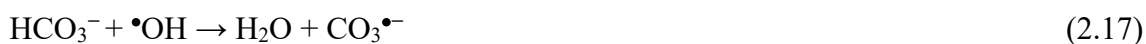
2.6 Three types of TiO_2 activity inhibition in photocatalysis

There are three types of TiO_2 activity inhibition identified in photocatalysis: active hole (*) deactivation, inhibition by consuming the $\bullet OH$ and inhibition due to inability of

O₂ to prevent electron recombination.

2.6.1 *Active hole (*) deactivation*

Inorganic ions in textile wastewaters have been known to inhibit surface reactions of TiO₂ by blocking the active hole. These ions are from sodium salts like NaCl, Na₂SO₄, Na₂CO₃ widely used in dyeing process. Na₂CO₃ is usually added in dyeing bath to adjust the pH for color fastness, while sodium chloride is used for transferring the dyestuff to the fabric. The dye industry wastewater is expected to contain a certain amount of CO₃²⁻ and Cl⁻ both species can scavenge •OH and (*) as shown in Eqs. (2.16) - (2.19).



Abdullah et al., (1990) demonstrated the effects of NO₃⁻, ClO₄⁻, Cl⁻, SO₄²⁻ or PO₄³⁻ on photocatalytic oxidation of salicylic acid, aniline and ethanol. They choose the pH of 4.1 ± 0.1 and each of the organic solutes added in 20 mL of solution was equivalent to 100 µg of organic carbon, these specifications were maintained throughout the investigations. A 7m-long 65-turn glass spiral reactor made of boron silicate glass of 6mm-o.d. and 1mm-wall thickness (spiral volume of 90cm³) with inner surface coated with TiO₂ Degussa P25 was used. UV illumination was used in the experiment and the temperature of the experimental set-up was 50°C (25°C higher than the ambient temperature).

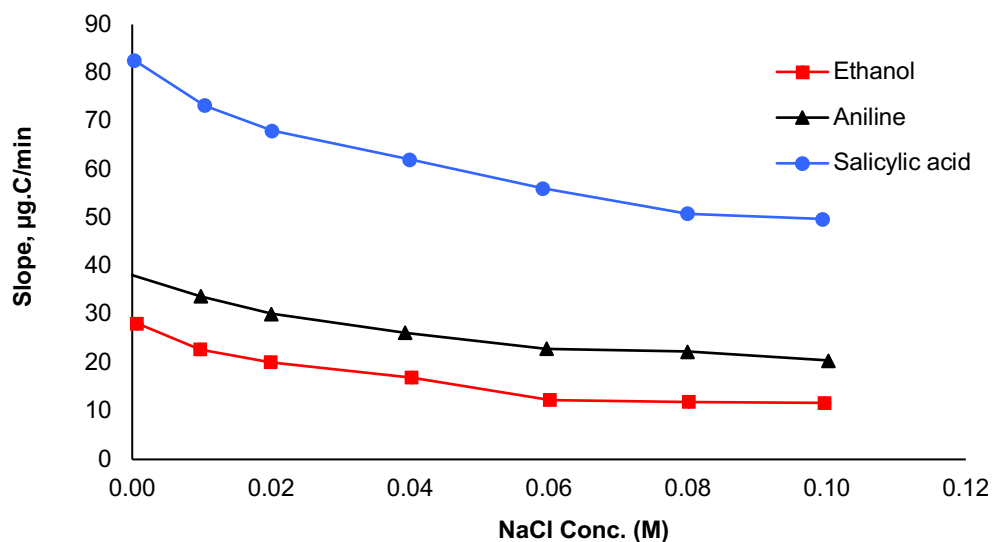


Figure 2.5: Effect of increasing concentration of chloride on rates of oxidation (slopes) of salicylic acid, aniline and ethanol, each equivalent to 100 µg of carbon in 20 mL of solution (Abdullah et al., 1990)

The authors demonstrated the effect of increasing the concentration of NaCl on salicylic acid, aniline, and ethanol in Fig. 2.5. For all the three samples, the slope continued to decrease with higher concentration of added chloride. They attribute the effect to both blockage of active sites and scavenging on the radical species.

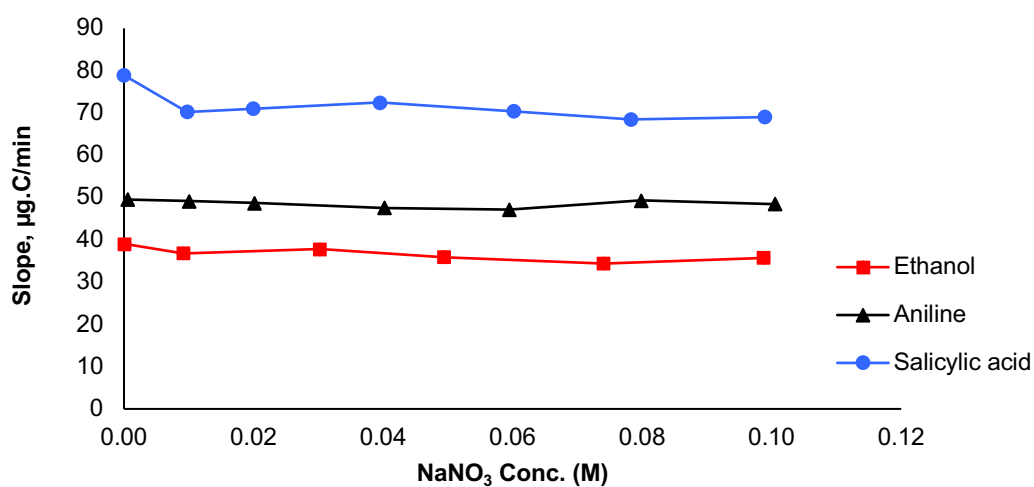


Figure 2.6: Effects of increasing concentration of nitrate on rates of oxidation (slopes) of salicylic acid, aniline and ethanol, each equivalent to 100 µg of carbon in 20 mL of solution (Abdullah et al., 1990)

Effect of Nitrate ions NO_3^- Fig. 2.6 on the rates of oxidation salicylic acid, aniline and ethanol were not appreciable and believed to be due to partial blockage of the active sites.

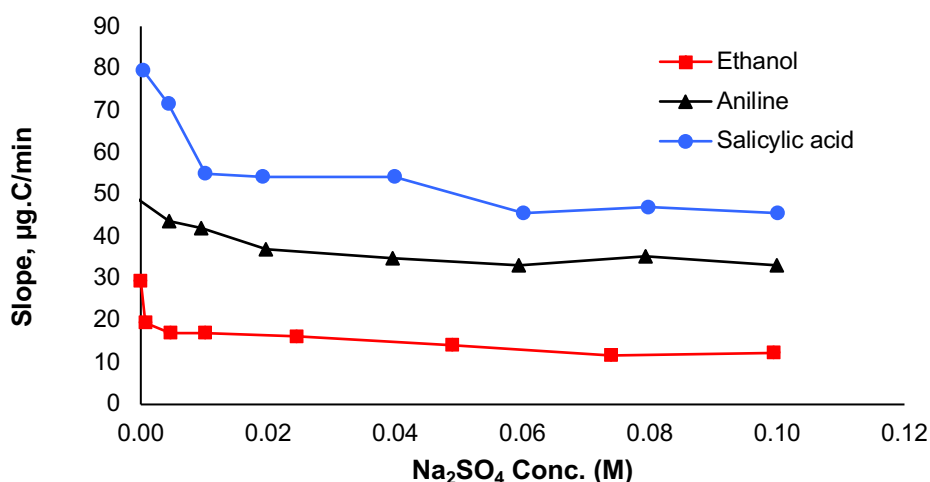


Figure 2.7: Effects of increasing concentration of sulfate on rates of oxidation (slopes) of salicylic acid, aniline and ethanol, each equivalent to 100 μg of carbon in 20 mL of solution (Abdullah et al., 1990)

Figure 2.7 presents the effect of sulfate ions, which decreases the reaction of all the organic compounds. The effect of phosphate ions H_2PO_4^- Fig. 2.8 were thought to have adsorbed on the surface of the catalyst.

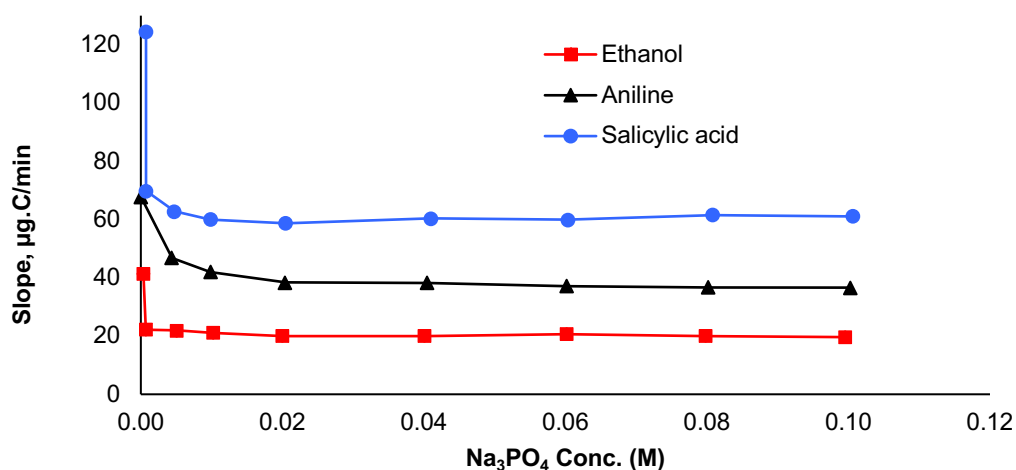


Figure 2.8: Effects of increasing concentration of phosphate on rates of oxidation (slopes) of salicylic acid, aniline and ethanol, each equivalent to 100 μg of carbon in 20 mL of solution (Abdullah et al., 1990)

They noticed that the behavior of phosphates is similar to that of sulfates in that the photocatalytic activity was markedly inhibited as soon as the ions were introduced. Therefore, sulfates or phosphates, even at millimolar concentration, could be rapidly adsorbed onto the catalyst surface and reduce the oxidation rates by 20-70%.

Ghaly et al., (2007) also reported the detrimental effect of CO_3^{2-} and Cl^- due to hole scavenging activities in a Maxoline Navy 2 RM 200% basic dye aqueous solution with TiO_2 -A (pure anatase) as photocatalyst in slurry form. Even with pure anatase, instead of Degussa P-25 as in Abdullah et al., (1990) and by using a dye not salicylic acid, aniline or ethanol, the pattern of degradation was as predicted. Additionally, Wang et al., (2013) demonstrated the inhibitory effect in mineralization of methyl orange by inorganic anions Cl^- , SO_4^{2-} , CO_3^{2-} and NO_3^- at the same concentration (10mmol/L) using a doped photocatalyst of TiO_2 a nanocomposite with the formula $\text{H}_3\text{PW}_{12}\text{O}_{40}\text{-Y-TiO}_2$ (HPW-Y- TiO_2) in Fig. 2.9.

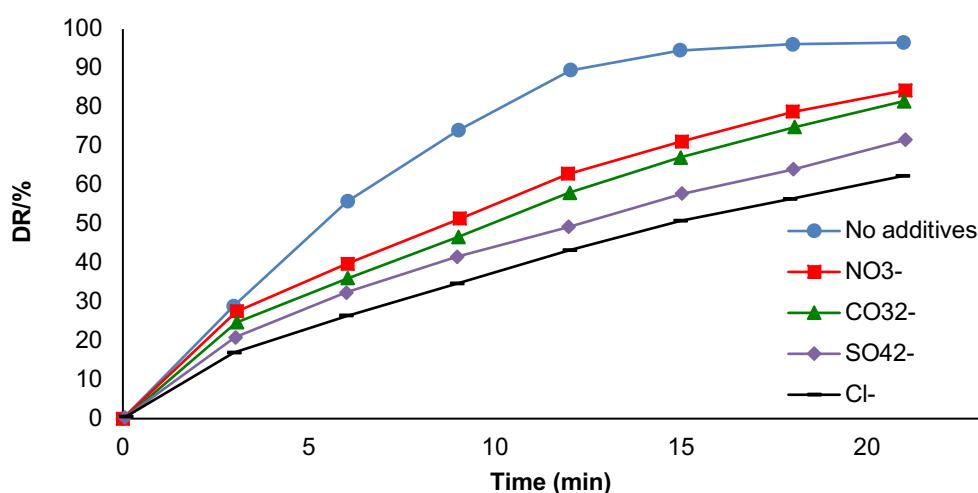


Figure 2.9: Photocatalytic inhibition in the presence of different anions Cl^- , SO_4^{2-} , CO_3^{2-} , NO_3^- and with no anion added (Y. Wang et al., 2013)

The figure shows normal degradation with no additive having a higher gradient than the curves obtained with subsequent addition of the salts. They suggested the inhibition to be as a result of radical scavenging and competitive adsorption. Generally, the level of

inhibition on MO degradation caused by inorganic additives can be presented in the order of $\text{Cl}^- > \text{SO}_4^{2-} > \text{CO}_3^{2-} > \text{NO}_3^-$ (Guillard et al., 2003).

Ozkan et al., (2004) investigated photocatalytic degradation of Sirius Gelb GC used in the textile industry, at an optimized pH = 3.5. A modified TiO_2 with silver and a non-modified TiO_2 were used. They observed that the Silver-loading (Ag-loading) enhances catalyst performance by shortening the degradation period of the titania than unloaded titania. Even when inorganic anions were added to the aqueous mixture, the activity retardation was less noticeable in the system with $\text{Ag-TiO}_2/\text{UV}$ than in the TiO_2/UV system. They noticed that Ag-TiO_2 catalyst surface is influenced much less than TiO_2 catalyst (by the anions) because the TiO_2 surface have fewer number of holes to be filled with anions than in the Ag-TiO_2 catalyst surface which have higher number of holes per area than the same amount of pure TiO_2 used in the investigations.

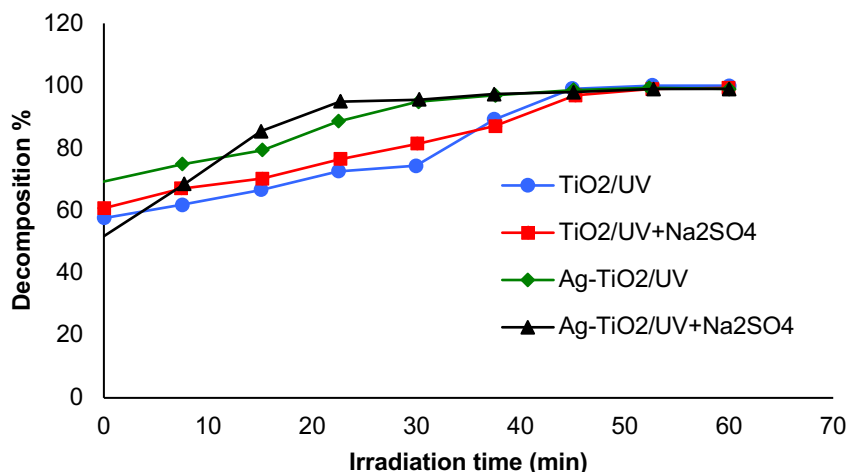


Figure 2.10: The change of decomposition value (%) of Sirious Gelb GC sample with irradiation in Na_2SO_4 salt media at pH 3.5 in TiO_2/UV and $\text{Ag-TiO}_2/\text{UV}$ systems (Ozkan et al., 2004)

In Figure 2.10, the effectiveness of TiO_2/UV and $\text{Ag-TiO}_2/\text{UV}$ system were increased in the presence SO_4^{2-} at a time between 2.5-8 mins and at a time of 0-10 mins respectively. This is contrary to what was reported by Abdullah et al., (1990); Habibi et al., (2005); Selvam et al., (2007); Wang et al., (2013), in their observations, there was no instance

where SO_4^{2-} enhances the degradation rate. In all the cases, it was observed to have reduced the degradation instead of enhancing it. Even though in Selvam et al., (2007), SO_4^{2-} was seen to cause the least reduction in degradation.

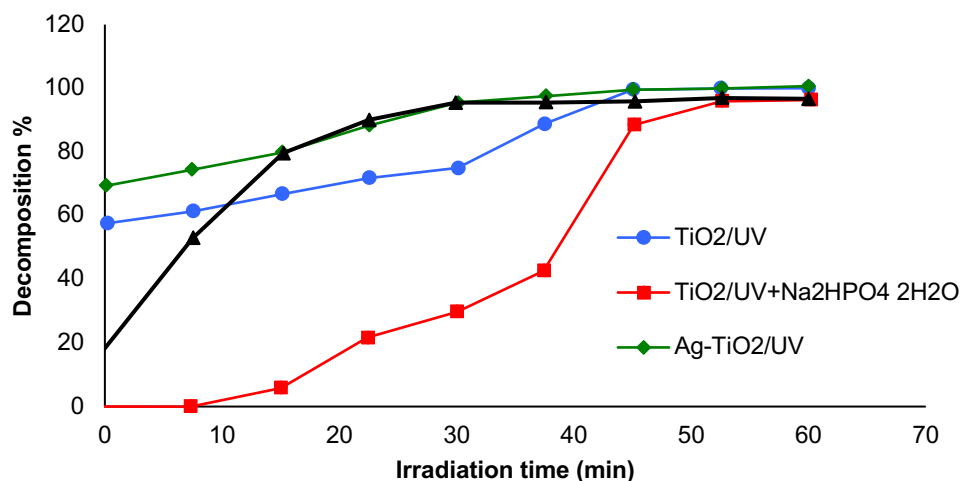


Figure 2.11: The change of decomposition value (%) of Sirius Gelb GC sample with irradiation time in $\text{Na}_2\text{HPO}_4 \cdot 2\text{H}_2\text{O}$ salt media at pH 3.5 in TiO_2/UV and $\text{Ag-TiO}_2/\text{UV}$ systems (Ozkan et al., 2004)

Figure 2.11 shows the effect of phosphate group ion HPO_4^{2-} on the degradation with more detrimental effect especially in pure TiO_2 where a remarkable decrease in degradation was noticed at the 0-20 mins and a decrease in degradation for $\text{Ag-TiO}_2/\text{UV}$ was not remarkable within the same time interval of 0-20 mins.

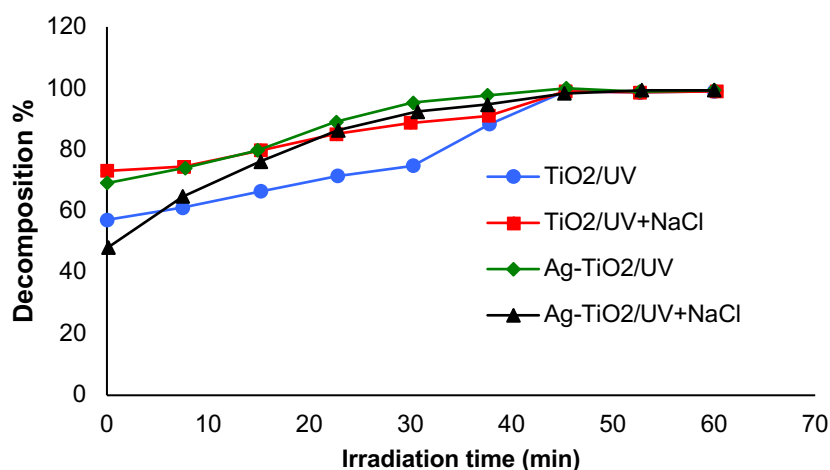


Figure 2.12: The change of decomposition value (%) of Sirius Gelb GC sample with irradiation time in NaCl salt media at pH 3.5 in TiO_2/UV and $\text{Ag-TiO}_2/\text{UV}$ systems (Ozkan et al., 2004)

The effect of HPO_4^{2-} as reported by is in agreement with the observation in (Abdullah et al., 1990).

In Figure 2.12 Ozkan et al., (2004) observed Cl^- to significantly increase the degradation rate in pure TiO_2 from 0-20 mins, and only a slight decrease was observed in Ag- TiO_2/UV . This observation contradicts (Abdullah et al., 1990; Ghaly et al., 2007; Selvam et al., 2007; Y. Wang et al., 2013), while on the other hand the decrease in degradation using Ag- TiO_2/UV agrees with literature.

Figure 2.13 shows the effect of CO_3^{2-} as reported by Ozkan et al., (2004) on the degradation rate for both TiO_2/UV and Ag- TiO_2/UV it agreed with the observations reported by (Ghaly et al., 2007; Selvam et al., 2007; Y. Wang et al., 2013).

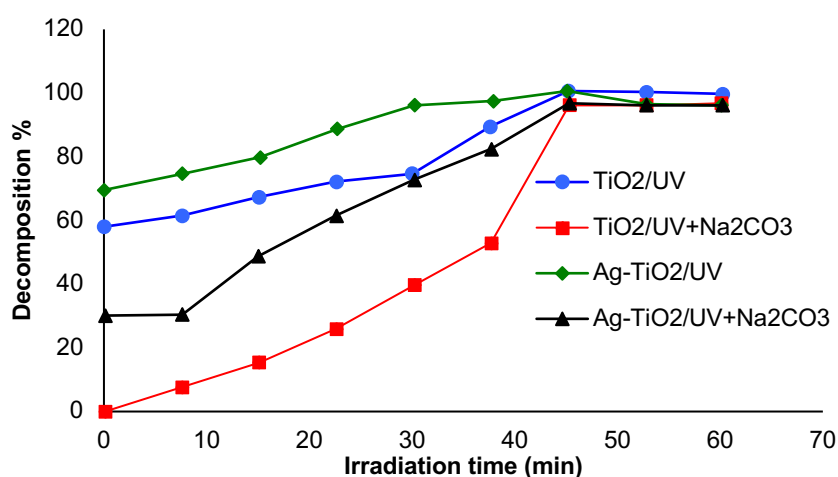


Figure 2.13: The change of decomposition value (%) of Sirius Gelb GC sample with irradiation time in Na_2CO_3 salt media at pH 3.5 in TiO_2/UV and Ag- TiO_2/UV systems (Ozkan et al., 2004)

Table 2.1: Summary of references and remarks on effects of inorganic anions on active hole of titanium dioxide (TiO₂) in aqueous media

S/No.	Reference	TiO ₂ type	Wastewater	Reactor type	Temperature °C	pH	Inhibitor	Remarks
1	Abdullah et al., (1990).	TiO ₂ Dagussa P25.	1. Salicylic acid, 2. Aniline 3. Ethanol.	Continues flow reactor (spiral boron silicate glass) inner surface coated with TiO ₂ Dagussa P25 with a UV 20-W light.	50	4.0±0.2	NaCl Percholates and Nitrates. Sulfates or phosphates.	Active hole blockage was observed in all three. There was reduction in degradation at pH 4.0±0.2 but not noticeable degradation at other pH values. No significant reduction in the oxidation rates was observed. Reduces the oxidation rates significantly by 20-70%.
2	Ghaly et al., (2007).	TiO ₂ -A pure anatase, supplied by Merck).	Maxilon Navy 2 RM 200% basic dye.	Continues flow, Parabola cylindrical concentrator solar photoreactor TiO ₂ slurry form, UV.	Room temperature.	7.1-7.4 and TOC=5 g/L.	Na ₂ CO ₃ and NaCl.	Hole scavenging activities by Cl ⁻ was observed. At optimum operating conditions of: 1 g/L TiO ₂ , 1.5 ml/L H ₂ O ₂ , pH=3-5, the inhibition effect is twice as much as at 5g/L dye concentration.
4	Selvam et al., (2007).	TiO ₂ -P25 Degussa (Germany). particle size of 30nm and BET specific area 56m ² /g.	4-fluorophenol (4-FP).	Batch, UV 330nm Heber multilamp photoreactor model HML-MP 88).	Room temperature.	4, 7 and 9 and TOC = 50 to 200 mg/l.	CO ₃ ²⁻ , HCO ₃ ⁻ , Cl ⁻ >NO ₃ ⁻ , SO ₄ ²⁻ and Fe ³⁺ , Fe ²⁺ , Mg ²⁺ , Cu ²⁺ ions.	In pH 4, the inhibition was in the order of CO ₃ ²⁻ >HCO ₃ ⁻ >Cl ⁻ >NO ₃ ⁻ >SO ₄ ²⁻ . The effect of CO ₃ ²⁻ , HCO ₃ ⁻ and Cl ⁻ being most significant. The order of efficiency was found to be pH 7>pH 9>pH 4, this result was attributed to point of zero charge PZC phenomenon.

‘Table 2.1, continued’

S/N	Reference	TiO ₂ type	Wastewater	Reactor type	Temperature °C	pH	Inhibitor	Remarks
5	Stapleton et al., (2010).	TiO ₂ P-25 Degussa.	2-Chloropyridine, (2-CPY) 2-fluoropyridine (2-FPY), 2-Hydroxypyridine (2-HPY).	Batch.	50	Each salt is 2.7±0.4mM.	HCl and NaCl.	Large amounts of HCl or NaCl, reduced the degradation rate of 2-HPY, due to hole scavenging. While addition of NaCl in stoichiometric amounts had little effect. Addition of either HF or H ₂ SO ₄ doubled degradation rate. Increase in 2-HPY degradation attributed to sulfation of TiO ₂ surface by SO ₄ ²⁻ .
6	(Guillard et al., 2003)	TiO ₂ Degussa P-25.	Methylene Blue (MB).	Batch.	20.	Basic and Neutral pH.	NO ₃ ⁻ , SO ₄ ²⁻ , HCO ₃ ⁻ , CO ₃ ²⁻ , SO ₄ ²⁻ , HSO ₄ ⁻ , H ₂ PO ₄ ⁻ .	Hole deactivation at basic and neutral pH in decreasing order is: CO ₃ ²⁻ > H ₂ PO ₄ ⁻ > SO ₄ ²⁻ > SO ₄ ²⁻ > NO ₃ ⁻ . The degradation rate of MB with added Na ₂ CO ₃ was higher at basic pH than at neutral pH.
7	Ozkan et al., (2004).	TiO ₂ and modified Ag-TiO ₂ with silver (Ag-TiO ₂).	Sirius Gelb GC.	Batch.	Room temperature.	3.5, 7.0 and 11.0.	C ₆ H ₅ O ₇ ³⁻ , CH ₃ COO ⁻ , C ₂ O ₄ ²⁻ , CO ₃ ²⁻ , SO ₃ ²⁻ , HPO ₄ ²⁻ , NO ₃ ⁻ , Cl ⁻ , SO ₂ ⁻	TiO ₂ /UV system degradation increases with addition of NO ₃ ⁻ , Cl ⁻ , SO ₂ ⁻ in the first 25mins and reached 95-99%. After 25min no noticeable effect of salt addition. Both TiO ₂ and Ag-TiO ₂ were negatively affected by CH ₃ COO ⁻ , C ₂ O ₄ ²⁻ , CO ₃ ²⁻ , SO ₃ ²⁻ , HPO ₄ ²⁻ , C ₆ H ₅ O ₇ ³⁻ . Ag-TiO ₂ enhances catalyst performance better than TiO ₂ .

‘Table 2.1, continued’

S/No.	Referen	TiO ₂ type	Wastewater	Reactor type	Temperature °C	pH	Inhibitor	Remarks
8	Habibi, et al., (2005).	TiO ₂ anatase.	1-C.I. Direct 80, 3BL, 2-C.I. Direct Blue 160, RL 3-C.I. Reactive Yellow 2, X6G.	Photodegradation cell of 200 ml in volume. High pressure mercury lamp 400 W.			Cl ⁻ , NO ₃ ⁻ , SO ₄ ²⁻ .	All three Dye degradation rate gradually decreased with increasing Cl ⁻ , NO ₃ ⁻ , SO ₄ ²⁻ concentrations. The decrease was attributed to adsorption of the anions on TiO ₂ surface in acidic medium.
9	Kavitha & Palanisamy (2010).	TiO ₂ -P25 (Degussa).	Vat Yellow 4.	Batch reactor solar and UV lamp were used.	Room temperature.		Cl ⁻ , HCO ₃ ⁻ .	At pH less 6.6 when TiO ₂ surface was positively charged, Cl ⁻ were attracted and scavenge on active hole.

Table 2.2: Summary of references and remarks on surface reaction of titanium dioxide (TiO₂) in gaseous media

S/No.	Referenc	TiO ₂ type	Waste-air	Reactor type	Temperature °C	pH	Inhibitor	Remarks
1	Peral & Ollis, (1997).	P25 TiO ₂ (Degussa).	Decamethyltetrasiloxane (DMTS), indole, pyrrole and dimethyl sulfide (CDS).	A flow reactor (cylindrical vessel), UV.	Room temperature.	200mgm ⁻³ gas mixtures of different chemicals and 1000 mgm ⁻³ of water and air flowrate 50 cm ³ min ⁻¹ used in all the experiments.	Carbon and heteroatom (N S or Si)	Si, N and S shows irreversible catalyst deactivation in DMTS, pyrrole and indole, with no deactivation on DS.
2	Shang et al., (2002)	TiO ₂ nanoparticles, anatase, crystal size 12nm, spec. surf. area 40.5m ² g ⁻¹ .	C ₇ H ₁₆ -O ₂ , SO ₂ -O ₂ and C ₇ H ₁₆ -SO ₂ -O ₂ .	Batch reactor, UV light.	Room Temperature.	0.4% v/v heptane or 0.4% SO ₂ , or 0.4% heptane and 0.4% SO ₂ , and each with 20% O (v/v) and ultrapurity N as balanced gas to reach 1 Atm pressure.	C and S	C ₇ H ₁₆ -O ₂ -TiO ₂ system, no catalyst deactivation over 200h. SO ₂ -O ₂ -TiO ₂ and C ₇ H ₁₆ -SO ₂ -O ₂ -TiO ₂ systems there was deactivation. Reaction products SO ₂ or sulfuric acid causes poisoning and conclusively substrates containing C and S causes poisoning.
3	Fan et al., (2012).	Titanium dioxide on gold (Au/TiO ₂).	CO	Flow reactor (dielectric barrier discharge).	Room temperature.	Gas mixture (simulated air, 80% N ₂ /20% O ₂) containing 960–970 ppm of CO fed into reactor at 600 mL/min and 50% 'relative humidity.	3 types of deactivations 1: Agglomeration of gold particles 2: accumulation of carbonate-like species. 3: [NO _y] _s during N ₂ /O ₂ plasma regeneration.	As gas hourly space velocity (GHSV) increases the rate of deactivation increases due to carbonate species. Surface poisoning by [NO _y] _s species was observed during regeneration.

‘Table 2.2, continued’

S/No.	Reference	TiO ₂ type	Waste-air	Reactor type	Temperature °C	pH	Inhibitor	Remarks
4	Ameen & Raupp,(1999)	TiO ₂ -P25 Degussa.	o-xylene and o-xylene-air.	Powder-bed microreactor flow reactor, UV irradiation.	Room temperature.	o-xylene 25 ppmv and known % humidity.	o-xylene and o-toluic acid.	Deactivation rate increases as the concentration of the water vapor in the inlet stream decreases.
5	Kozlov et al., (2003).	100% anatase with specific surface BET = 347 m ² /g.	Diethyl sulfide (DES).	434ml Batch reactor, UV irradiation.	Room temperature.	0.5µl of DES and 2µl of water.	Diethylsulfone and carboxylates.	The observed deactivation was always highest close to the last run.
6	Alberici et al., (2001).	TiO ₂ Degussa P-25.	Pyridine, propylamine and diethylamine in presence and absence of oxygen.	Annular plug flow photoreactor, UV irradiation.	Room temperature.	Pyridine (63ppmv), diethylamine (235 ppmv) and propylamine (99 ppmv).	NH ₄ ⁺ and NO ₃ ⁻ ions.	Deactivation was observed in all cases.
7	Xie & Lin, (2007).	Pure TiO ₂ , TiO ₂ film on Al ₂ O ₃ , SiO ₂ , or CaO.	Formaldehyde in air.	1.2 m ³ Batch reactor, UV irradiation.	Room temperature	Formaldehyde (~38%) in water vapor.	Si, Al, and Ca migrating into TiO ₂ film.	Bronsted acid sites at the TiO ₂ /SiO ₂ interface inhibit •OH production because Al ³⁺ substitute Ti ⁴⁺ in the TiO ₂ lattice creating oxygen recombination center of e _{CB} ⁻ •OH production.
8	Cao et al., (2000).	Nanoscale TiO ₂ (pore size 35–44 nm), Degussa P25 and platinum loaded on TiO ₂ .	Toluene, Toluene-water.	Flow reactor, UV irradiation.	Room temperature.	Percent concentrations were used.	Intermediates, e.g. benzaldehyde and benzoic acid.	Partially oxidized intermediates, e.g. benzaldehyde and benzoic acid, on active sites causes deactivation. High humidity/water in the feed stream significantly inhibited the oxidation rate.

‘Table 2.2 continued’

S/No.	Reference	TiO ₂ type	Waste-air	Reactor type	Temperature °C	pH	Inhibitor	Remarks
9	Sun et al., (2003).	TiO ₂ thin films prepared on one side of silica-coated soda lime glass.	Octamethyltrisiloxane (OMTS).	Batch reactor, UV irradiation.	Room temperature.	OMTS and synthetic air.	Hydroxylated SiO _x (x=3~4).	No other decomposition products (or intermediates) were detectable. OMTS was the only deposit of ~7 monolayers in the 5 th cycle.

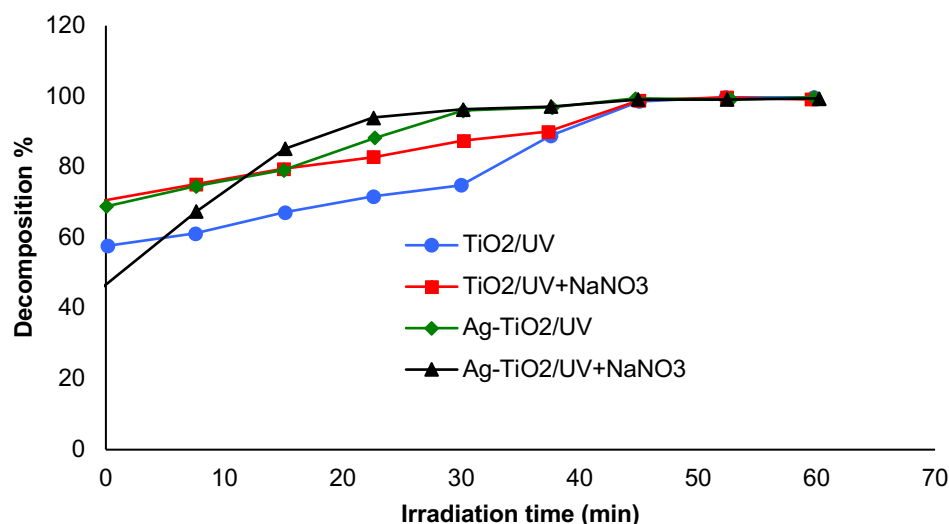


Figure 2.14: The change of decomposition value (%) of Sirius Gelb GC sample with irradiation time in NaNO₃ salt media at pH 3.5 in TiO₂/UV and Ag-TiO₂/UV systems (Ozkan et al., 2004)

Additionally, Ozkan et al., (2004) investigated the effect of NO₃⁻ and observed minimal improvement in the degradation of TiO₂/UV and Ag-TiO₂/UV at 0-10 min and 3-8 min respectively Fig. 2.14.

The observations were relatively close to what was observed by Abdullah et al., (1990) that NO₃⁻ does not have an appreciable effect and Wang et al., (2013) observations that NO₃⁻ have the least effect among the anions tested (Cl⁻ > SO₄²⁻ > CO₃²⁻ > NO₃⁻). Selvam et al., (2007) also reported NO₃⁻ as having one of the least effects (CO₃²⁻ > HCO₃⁻ > Cl⁻ > NO₃⁻ > SO₄²⁻). The results presented by Ozkan et al., (2004) does not resolve the issue of whether the Ag-TiO₂/UV performed better than TiO₂. The literature of deactivation in both aqueous and gaseous media are given in Table 2.1 and Table 2.2 respectively.

2.6.2 Inhibition by consuming •OH

Wang et al., (2013) demonstrated the inhibitory effect in mineralization of methyl orange by inorganic anions Cl⁻, SO₄²⁻, CO₃²⁻ and NO₃⁻ by consumption of •OH. They observed that the introduction of Cl⁻ and other ions facilitated the consumption of •OH

(Eq. 2.20) in the dye degradation of methyl orange. Similarly, CO_3^{2-} eliminates $\bullet\text{OH}$ as shown in Eqs. (2.21) and (2.22):

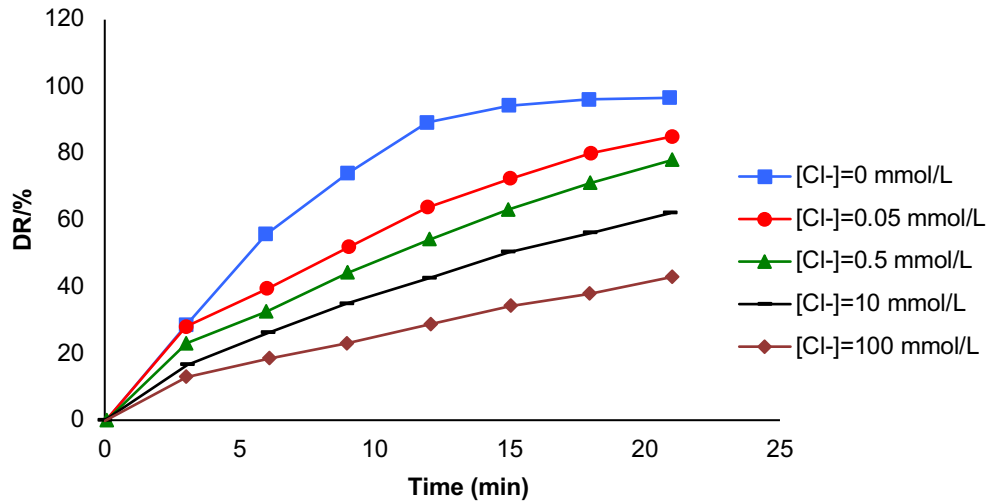


Figure 2.15: Effect of Cl^- concentration on the photocatalytic degradation of MO over HPW-Y-TiO₂ (Y. Wang et al., 2013)



They observed that concentration has significant effect on the reaction rate. Higher Cl^- concentration culminates into higher reduction as shown in Fig. 2.15.

Stapleton et al., (2010) investigated the kinetics and mechanisms of photolytic/TiO₂-photocatalytic degradation of substituted pyridines in aqueous solutions, the effect of ions was demonstrated. 2-Chloropyridine ($\text{C}_5\text{H}_4\text{NCl}$), referred to as 2-CPY; and 2-fluoropyridine ($\text{C}_5\text{H}_4\text{NF}$), referred to as 2-FPY, with purity greater than 98% was supplied by Fluka. 2-Hydroxypyridine ($\text{C}_5\text{H}_4\text{NOH}$), referred to as 2-HPY, with purity of 97% was supplied by Aldrich. Deionized water was used to prepare the aqueous solutions. titanium

dioxide (TiO₂ P-25) having purity greater than 97% was supplied by Degussa (average particle size of 21 nm, a ratio of anatase:rutile mixture of 70:30, HCl content of less than 0.3 wt.%). Tert-Butanol (C₄H₁₀O) with purity of 99% was supplied by Riedel-de Haen. All reagents were used without further treatment or purification. It was clear that with a mixture of 70:30 anatase:rutile the pattern of degradation is predictable and agrees with literature.

The authors observed that destruction rate of 2-HPY was affected by addition of HCl which had the most notable detrimental effect. Addition of HCl or NaCl (chloride ions) in large amounts reduced the degradation rate, while addition of NaCl in stoichiometric amounts had little effect. HCl addition had the most notable detrimental effect on 2-HPY degradation rate due to synergistic effects of pH reduction and Cl⁻ addition. The effect of each acid on 2-HPY was unique. This explained that lower degradation rates in the presence of HCl or NaCl could not be attributed to pH, but rather the presence of chloride anions. The Cl⁻ act as •OH radical scavengers.

Selvam et al., (2007) demonstrated the effect of inorganic anions at two different pH of 4 (acidic) and 9 (basic) on the degradation of 4-fluorophenol (4-FP) by addition of Na₂CO₃, NaHCO₃, NaCl, NaNO₃, NaSO₄ as presented in Table 2.3. The reaction condition was [4-FP] = 100ppm; catalyst suspension = 100mg; anions = 0.1 M; irradiation time = 30 min; airflow rate = 8.1 ml s⁻¹; $I = 1.381 \times 10^{-3}$ einstein l⁻¹ s⁻¹.

In the illuminated TiO₂ system, after 30 min irradiation, at pH4, 37.55%, 40.12%, 48.22%, 64.80% and 72.17% of degradations were observed with Na₂CO₃, NaHCO₃, NaCl, NaNO₃, Na₂SO₄, respectively. The order of inhibition of these anions are CO₃²⁻ > HCO₃⁻ > Cl⁻ > NO₃⁻ > SO₄²⁻. The main inhibition effect is due to adsorption on TiO₂ surface. The decrease in percentage degradation is more severe with CO₃²⁻ > HCO₃⁻, Cl⁻ these observations are in agreement with earlier observations by (Abdullah et al., 1990).

Table 2.3: Effect of anions on photodegradation of 4-FP (%) with TiO₂-P25 (Selvam et al., 2007)

Anion	pH 4	pH 9
Na ₂ CO ₃	37.55	35.87
NaHCO ₃	40.12	38.57
NaCl	48.22	46.22
NaNO ₃	64.80	62.87
NaSO ₄	72.17	70.17

2.6.3 *Inhibition due to inability of O₂^{•−} to prevent electron recombination*

If the amount of dissolved O₂ is altered by an appreciable amount thereby preventing scavenging activity of O₂ on the photo-generated electrons from recombining with the holes, a significant change in reaction rate will be noticed as reported in literature (Hirakawa & Nosaka, 2002; Ishibashi et al., 2000). O₂^{•−} is formed during the UV irradiation on TiO₂ photocatalysts, while simultaneously it decays by the reaction of h_{VB}^+ and/or h_{TR}^+ (Eqs. 2.26 and/or 2.27). The existence of additional ions that can scavenge the holes would influence the amount of O₂^{•−} produced. By changing the redox potentials of the additives, therefore, the energy level of effective holes might be affected. Daimon et al., (2008) demonstrated how formation and decay of singlet molecular oxygen of (¹Δ_g) state (¹O₂) in TiO₂ (Dagussa P25, Nippon Aerosil) was affected by different experimental conditions. Comparison between the effects on ¹O₂ and O₂^{•−} suggested that ¹O₂ was formed by the electron transfer mechanism where molecular oxygen was reduced to O₂^{•−} by photogenerated electrons, followed by subsequent oxidation of O₂^{•−} to ¹O₂ by photogenerated holes. Their work featured 18 commercially available TiO₂, suspended in a 1cm x 1cm x 4.5cm quartz cell containing 3.5mL of 0.01M NaOH aqueous solution which were used at different conditions to allow for better generalized conclusion. The production of singlet molecular oxygen ¹O₂ in a photocatalytic process favors the degradation process of organic compounds by counteracting recombination of valence electron with active hole.

Daimon et al., (2008) investigations revealed how anions like I^- , SCN^- , Br^- , affected the degradation process. Fig. 2.16 shows an initial higher amount of $^1\text{O}_2$ and gradual decline up to a concentration of about 0.23mM followed by a steady state for each of the three ions in each of the three suspensions. The halides reduced the amount of singlet molecular oxygen of $^1\Delta_g$ state ($^1\text{O}_2$) generated during the photocatalytic process. The formation of $^1\text{O}_2$ decreased at $\text{pH} < 5$ and $\text{pH} > 11$, indicating that the intermediate $\text{O}_2^{\bullet-}$ is stabilized at the terminal OH site of the TiO_2 surface in the pH range of $5 < \text{pH} < 11$.

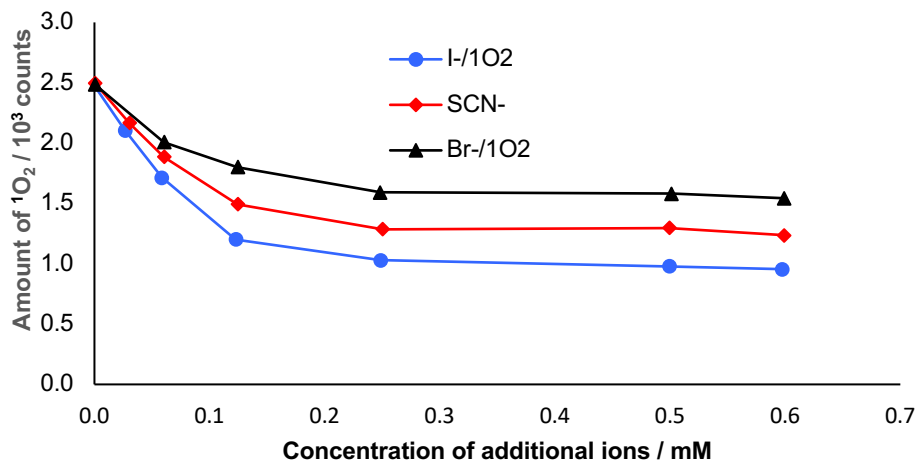
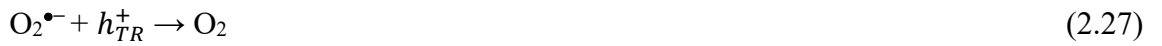
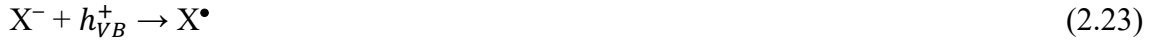


Figure 2.16: Effect of halide ions on the amounts of $^1\text{O}_2$ formed in TiO_2 (P25) photocatalysis (Daimon et al., 2008)

The effect of these halide ions on $\text{O}_2^{\bullet-}$ production was explained by (Hirakawa & Nosaka, 2002). If we assume X as a halide, X^- can be oxidized to X^\bullet with the valence band holes h_{VB}^+ (Eq. (2.23)) but not reduced by the conduction band electrons (e_{CB}^-). Then the reduction of O_2 in Eq. (2.24) cannot be directly influenced by the addition of X^- . But if on the other hand, the oxidized halide, X^\bullet , reacts easily with the conduction band electrons (e_{CB}^-) in Eq. (2.25) after out-competing the reduction of O_2 (Eq. (2.24)), thereby decreasing the formation of $\text{O}_2^{\bullet-}$. In other words, X^- plays a role in the effective recombination through the oxidation and succeeding reduction, resulting in an increase in the $(e_{CB}^-)-(h_{VB}^+)$ recombination process. Thus, the addition of X^- having a lower

oxidation potential resulted in less $O_2^{\bullet-}$ formation as represented in Fig. 2.16 (Daimon et al., 2008).



2.7 Future of advanced oxidation process with TiO₂

The studies on surface science have demonstrated the uniqueness of surface performance of either rutile or anatase in the reaction outcome in photocatalysis hence different consideration for each lattice is required.

Theoretical and experimental methods are to be used to approach the study of surfaces of photocatalysts. Optical and electronic behavior of small TiO₂ particles at the atomic level can be studied computationally and model the absorption characteristics and refractive index functions (RIFs) of TiO₂ particles, in order to predict how the quantum-size effect and particle size affect these properties (Selli, Fazio, & Di Valentin, 2017). The effects of structure on the light absorption characteristics, defects and how they affect surface reactions in an aqueous environment can be determined using DFT based packages for example GPAW software package, Vienna *ab initio* simulation package VASP, Gaussian 09 (or their improved versions) should be used to analyze the interaction and then validated findings with experiments. For the experimental aspect, where Temperature Programmed Desorption (TDP) cannot be used, X-ray Photoelectron

Spectroscopy (XPS), Fourier Transform Infrared Spectroscopy (FTIR), Gas Chromatography-Mass Spectrometry (GC-MS) and X-Ray Diffraction (XRD) can be used to monitor both the deposition on TiO_2 surface and the components of complex mixtures in view.

The future of using AOP reactors base on optimized reaction conditions through optimized catalyst surface will enhance water recycle and reuse by following a simple practice (Fig. 2.17). This practice entails the identification of ions with severe effect on photocatalyst performance and where structural modification will not be applicable, remedy their detrimental effect by introducing pre or post treatment (ion exchange resins) where necessary.

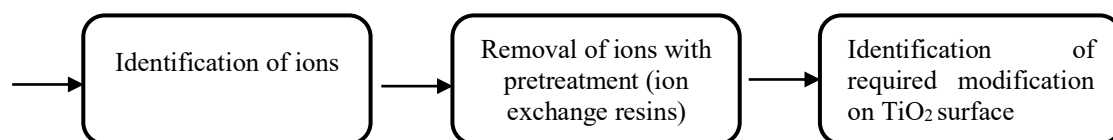


Figure 2.17: Schematic diagram of the proposed practice

2.8 Summary of literature review

The literature revealed advanced oxidation process (AOP) as an option for treatment of recalcitrant wastewaters and textile wastewater is among such wastewaters. Though there are Fenton processes among the AOPs, it is known to have drawbacks, such as powdered catalyst recovery, formation of ferric hydroxide and pH limitations. While ozonation could be the most widely used treatment for textile wastewaters among the AOP systems, the other AOP option is the use of pure titanium dioxide or its doped form as a photocatalyst. In this area, much work has been done to solve the powdered catalyst recovery problem such that TiO_2 can be immobilized on a substrate surface to solve the mass transfer problem. Additionally, from various investigations, pH is not known to have a significant effect on its performance. Furthermore, findings in literature revealed

that the photon transfer problem have been resolved, a gap that need to be closed is sufficient investigation into deactivation of photocatalyst.

The photocatalyst deactivation mechanism in aqueous media unlike in gaseous media is less understood. It is also an area that can prevent the commercialization of the system. It became clear that there is a need to apply the existing knowledge in adsorption to understand the causes of deactivation of TiO_2 in aqueous media, because all the works in this area revealed success in complete mineralization of the recalcitrant compounds like dyes. Further investigations revealed few literature of textile wastewaters with dissolved salts, the salts were known to reduce the efficiency of the TiO_2 and argued extensively that the active sites are actually blocked on the TiO_2 surface, but none of such works provided any surface analysis. In addition, there were a few reports that such dissolved salts enhance the performance of the TiO_2 instead of reducing it. The issues of conflicting literature, lack of surface analysis and proper procedure to analyze TiO_2 deactivation in aqueous media form the basis of this investigation and provided the research gap.

CHAPTER 3: METHODOLOGY

3.1 Introduction

This section provides information on the materials and procedure used to carry out the characterization and photodegradation experiments. It also provides details about equipment and equipment-modifications to achieve the aim and objective of this research.

3.2 Materials

The chemicals were of analytical grade and used as received without further treatment. Anatase TiO_2 , sodium hydroxide (NaOH) and Perchloric acid (HClO_4) to adjust the pH, sodium chloride (NaCl) and sodium sulfate (Na_2SO_4) salts were supplied by Aldrich chemicals. Methylene blue (MB) (maximum absorbance 663-667nm) and Methyl orange (MO) (maximum absorbance 464nm) were obtained from R & M chemicals.

3.3 Experimental design and method of analysis

This research is made of two major components, characterization part and kinetic studies part. The characterization part involves the characterization of fresh TiO_2 to achieve objective (1) and characterization of deactivated TiO_2 after kinetic studies as part of objective (3). While the kinetics studies part was used in two sections, both sections have identical reaction conditions. The first section was the determination of degradation kinetics of methylene blue and methyl orange, which was also the determination of activity of TiO_2 to achieve objective (2). The second part of the kinetics was the determination of adsorbed species through kinetics based on cumulative percent degradation to achieve objective (3) and it requires slight modification of the experimental design.

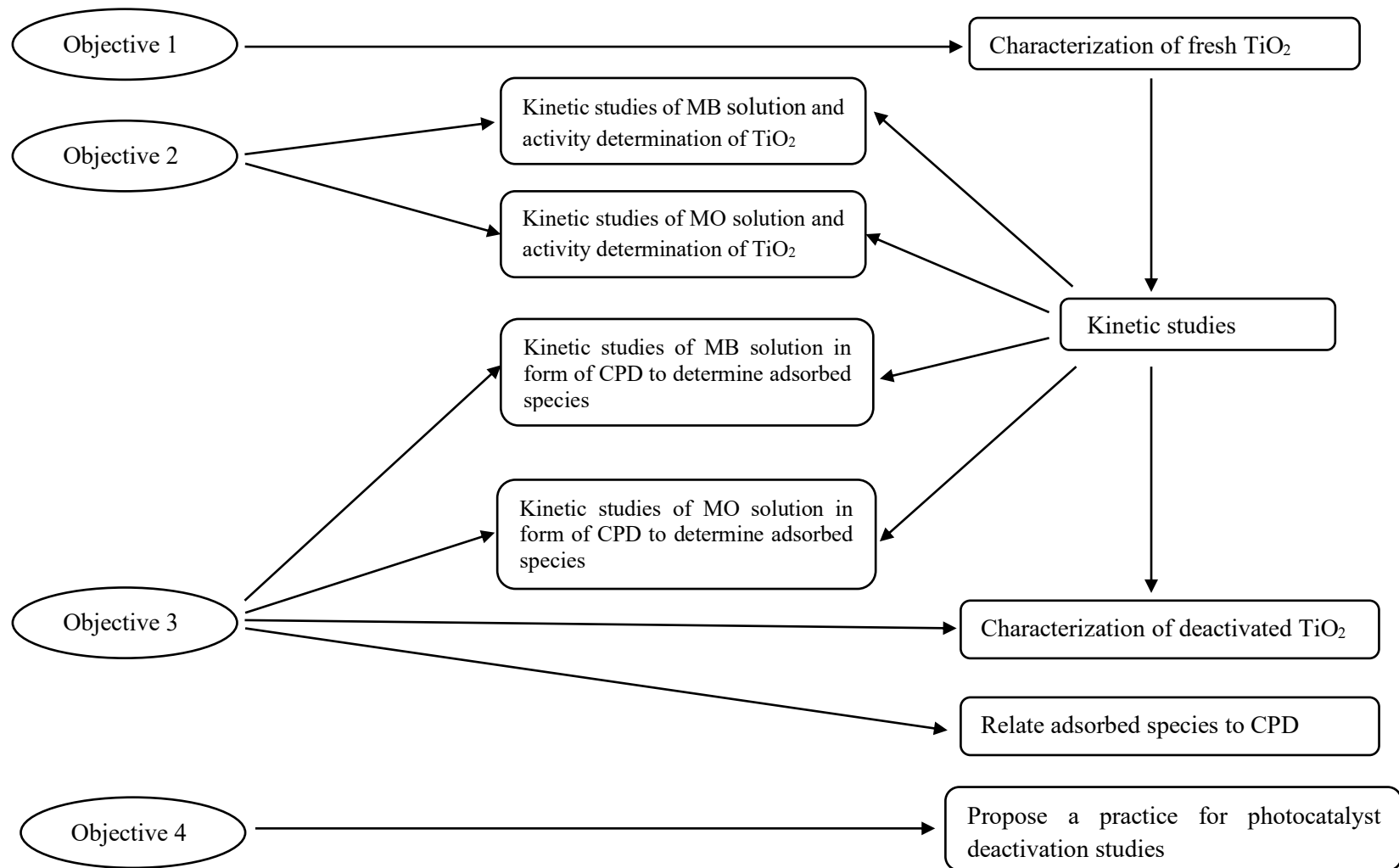


Figure 3.1: Flow diagram of major aspects of research activities

Both components are the means to achieve the objectives of this research, as shown in Fig. 3.1. Objective (4) was possible when all the objectives (1-3) have been useful in achieving the deactivation analysis. The following numbered sub-chapters provide more explanation on the objectives.

3.3.1 Characterization of fresh TiO₂ anatase photocatalyst

The characterization and analysis of fresh TiO₂ anatase will address objective (1) of this research. The physico-chemical characterization of the fresh anatase TiO₂ were to confirm its crystalline phase, morphology, size, surface area, elemental composition. This will allow for comparison with the deactivated samples for changes in organic, polymeric and inorganic materials on TiO₂ surface.

3.3.1.1 Crystalline phase determination with X-ray diffraction (XRD)

The XRD analysis provides information about the crystal structure, chemical composition, and physical properties of materials and thin films. The XRD machine with PANalytical Empyrean system diffractometer with copper (Cu), K α radiation was used to confirm the fresh TiO₂ sample as having anatase crystalline phase.

3.3.1.2 Surface area and particle size were analyzed with Brunauer-Emmett-Teller (BET)

The BET method is widely used in surface science for the calculation of surface areas of solids by physical adsorption of gas molecules. The surface area determination is to predict the activity of the TiO₂ photocatalyst and determine whether it compares with the industry standard, this test was also only on fresh TiO₂ conducted with Surface area analyzer Brunauer-Emmett-Teller (BET) Micromeritics ASAP2020, TRISTAR II 3020 Kr.

3.3.1.3 Elemental composition determination with X-ray photoelectron spectroscopy (XPS)

XPS can measure the elemental composition, empirical formula, chemical state and electronic state of the elements within a material. For high performance materials, the importance of knowledge of surface properties through surface chemistry, will influence catalytic activity among many factors. The elemental composition (titanium, oxygen, carbon, nitrogen, sulfur and sodium) of fresh and deactivated TiO₂ samples surface was carried out with XPS ULVAC-PHI quarter II analyzing machine for information on whether a change has occurred on fresh TiO₂ after deactivation. The XPS results will be discussed base on XPS survey spectra (SS) which was a generalized change in percent atomic concentration of the elements (Ti, O, C, N, S and Na) before (fresh TiO₂) and after deactivated TiO₂ photocatalyst. The other discussion is on XPS high resolution spectra (HRS) which is the detailed information on the type of species in each of the elements, for example O has three distinct class of adsorbed species with each having a unique affinity for a site on TiO₂, the three O species can only be assessed when deconvoluted and expressed in HRS.

3.3.1.4 Fourier-transform-infrared spectroscopy (FTIR) analysis to determine organic, polymeric and inorganic materials

The FTIR analysis uses infrared light to scan test samples and observe chemical properties, chemical bonds present and information about the specific bonding in the specimen. Among its uses is in contamination (Residue) analysis, it is used to identify organic, polymeric, and in some cases, inorganic materials. Group frequency peaks are typically strong in intensity and convey the presence of numerous organic functional groups. These include, but are not limited to, alcohols (-O-H), amines (-N-H), carbonyls (-C=O). The FTIR analyzer used was the Perkin Elmer FTIR-Spectrum 400.

3.3.2 Kinetic studies of photodegradation of methylene blue and methyl orange solutions with Cl^- or SO_4^{2-} using TiO_2 at different reaction conditions

This procedure is to provide steps to achieve objective (2). It states how the kinetics of photodegradation of MB and MO solutions were determined separately, using TiO_2 anatase as a photocatalyst at different reaction conditions in order to confirm the suitability of TiO_2 anatase for this analysis. This information affirms the photocatalytic ability of our chosen TiO_2 anatase photocatalyst and the expected order of reaction. In literature, the pattern of surface coverage in aqueous media, have been reported to obey the Langmuir-Hinshelwood mechanism as a first order kinetic equation. Langmuir-Hinshelwood kinetic model expressing relationship between reaction rate and surface coverage was used to investigate the kinetics of MB and MO adsorption in this work. The kinetics of degradation was measured with Spectroquant Pharo 300 (SR # 13041074) spectrophotometer and random check with TOC change was followed with Shimadzu TOC analyzer model TOC-L CSN (SR # H54405100077).

3.3.2.1 *The independent variables from response surface methodology (RSM)*

The need to optimize the experimental parameters requires application of response surface methodology (RSM), a tool suitable for analyzing the interaction between the parameters to get the best possible outcome. RSM employ lower order polynomial (Ye et al., 2014), in the realm of quadratic surface which will minimize the number of required experiments (Arami-Niya et al., 2012). The RSM has been used successfully in numerous chemical process applications (Baroutian et al., 2011; Ölmez 2009). In this research, a software package, Design expert (version 8.0.7.1) allow the use of RSM using central composite design (CCD) for the design of experiment. Additionally, the numerous publications especially review papers in photocatalysis, discussing the composition of textile wastewaters, optimal photocatalyst amounts, dye solution concentration, degradation time and other variables, narrowed the challenge of optimization of reaction

variables. Combining these sources of information is important as this work seeks the most desirable reaction conditions of dye degradation in photocatalysis to investigate the deactivation challenge.

The levels and ranges of the independent variables involved in this analysis were given in Table 3.1. The reaction conditions are to reflect a range of textile industry wastewater to be charged into a photoreactor. The investigations showed pH of textile wastewaters often fall within the range of 4 and 10 and the added salts fall within an average of 10g/L. The dye concentration from the industry can be high, but in the model wastewater in this research, a low concentration of dye was chosen so that the problem of light attenuation could be avoided. Thus, range of values were used to set the independent variables; dye concentration was fixed at 20ppm, amount of TiO_2 (photocatalyst concentration) was fixed at 0.4g in 200mL (2g/L) after numerous values were tried from the review by (Konstantinou & Albanis, 2004), amount of added salts (salt concentration) was fixed at 0.2g in 200mL (10g/L) from values recommend in (Abdullah et al., 1990; Ghaly et al., 2007; Ozkan et al., 2004; L. K. Wang et al., 2004; Y. Wang et al., 2013). While pH values were numeric between 4 and 10, they were considered binary categorical variables. UV-irradiation (with or without UV), type of salt (Na_2SO_4 or NaCl) were also considered binary categorical variables in form of yes or no (yes/no) as shown in Table 3.1. The responses (dependent variable) were the change in color and organic carbon content. The dyes were chosen to vary as cationic or anionic, these categorization (cationic or anionic) could also be viewed as a binary categorial variation.

Table 3.1: Independent variables, their levels and category

Independent variables	Amount/Level	Variable category
pH	4	vary
	10	
Mass of TiO ₂ (g/L)	2g/L	fixed
Total Reaction time (h)	60	fixed
Salt type	NaCl	yes/no
	Na ₂ SO ₄	
Salt concentration (g/L)	10	fixed
UV Irradiation	With UV	yes/no
	Without UV	
Dye type	MB	cationic
	MO	anionic
Dye solution concentration (ppm)	20	fixed

For each of the dyes; methylene blue the cationic dye and methyl orange the anionic dye, there were twelve (12) types of setup as shown in Table 3.2, representing different experimental conditions, to yield samples T_{MB1}-T_{MB12} for methylene blue and T_{MO1}-T_{MO12} for methyl orange.

3.3.2.2 Reproducibility/Error analysis

Reproducibility is the variation due to different operators using the same measuring instrument at different environmental conditions, as the need to redo the experiment arises. A reproducibility limit is the value below which, the difference between two test results obtained under reproducibility conditions may be expected to occur with a probability of approximately 0.95 (95%). Therefore, reproducibility can be reported as a standard deviation. In the raw data collection tables drawn in the design of experiment, showing dye solution color change, which were the change in initial and final values in the spectrophotometer measurements, provided easy calculation of standard deviation. This ensures that experimental errors were minimized.

Table 3.2: Samples with matching reaction conditions as variables

S/No.	Reaction condition	Reaction condition sample Abbreviation for filtrate	Reaction condition sample Abbreviation for photocatalyst	Fixed			Variable							
				Dye solution concentration (20ppm)	Mass of TiO ₂ (2g/L)	Total Reaction time (60h)	Salt type		pH		UV Irradiation		Dye type	
							NaCl	Na ₂ SO ₄	4	10	With UV	without UV	MB	MO
1	Methylene blue without salt at pH4 without UV	T _o MB1	T _{MB} 1	Yes	yes	yes	no	no	yes	no	no	yes	yes	no
2	Methylene blue with NaCl at pH4 without UV	T _o MB2	T _{MB} 2	Yes	yes	yes	yes	no	yes	no	no	yes	yes	no
3	Methylene blue with Na ₂ SO ₄ at pH4 without UV	T _o MB3	T _{MB} 3	Yes	yes	yes	no	yes	yes	no	no	yes	yes	no
4	Methylene blue without salt at pH4 with UV	T _o MB4	T _{MB} 4	Yes	yes	yes	no	no	yes	no	yes	no	yes	no
5	Methylene blue with NaCl at pH4 with UV	T _o MB5	T _{MB} 5	Yes	yes	yes	yes	no	yes	no	yes	no	yes	no
6	Methylene blue with Na ₂ SO ₄ at pH4 with UV	T _o MB6	T _{MB} 6	Yes	yes	yes	no	yes	yes	no	yes	no	yes	no
7	Methylene blue without salt at pH10 without UV	T _o MB7	T _{MB} 7	Yes	yes	yes	no	no	no	yes	no	yes	yes	no
8	Methylene blue with NaCl at pH10 without UV	T _o MB8	T _{MB} 8	Yes	yes	yes	yes	no	no	yes	no	yes	yes	no
9	Methylene blue with Na ₂ SO ₄ at pH10 without UV	T _o MB9	T _{MB} 9	Yes	yes	yes	no	yes	no	yes	no	yes	yes	no
10	Methylene blue without salt at pH10 with UV	T _o MB10	T _{MB} 10	Yes	yes	yes	no	no	no	yes	yes	no	yes	no
11	Methylene blue with NaCl at pH10 with UV	T _o MB11	T _{MB} 11	Yes	yes	yes	yes	no	no	yes	yes	no	yes	no
12	Methylene blue with Na ₂ SO ₄ at pH10 with UV	T _o MB12	T _{MB} 12	Yes	yes	yes	no	yes	no	yes	yes	no	yes	no
1	Methyl orange without salt at pH4 without UV	T _o MO1	T _{MO} 1	Yes	yes	yes	no	no	yes	no	no	yes	no	yes
2	Methyl orange with NaCl at pH4 without UV	T _o MO2	T _{MO} 2	Yes	yes	yes	yes	no	yes	no	no	yes	no	yes
3	Methyl orange with Na ₂ SO ₄ at pH4 without UV	T _o MO3	T _{MO} 3	Yes	yes	yes	no	yes	yes	no	no	yes	no	yes
4	Methyl orange without salt at pH4 with UV	T _o MO4	T _{MO} 4	Yes	yes	yes	no	no	yes	no	yes	no	no	yes
5	Methyl orange with NaCl at pH4 with UV	T _o MO5	T _{MO} 5	Yes	yes	yes	yes	no	yes	no	yes	no	no	yes
6	Methyl orange with Na ₂ SO ₄ at pH4 with UV	T _o MO6	T _{MO} 6	Yes	yes	yes	no	yes	yes	no	yes	no	no	yes
7	Methyl orange without salt at pH10 without UV	T _o MO7	T _{MO} 7	Yes	yes	yes	no	no	no	yes	no	yes	no	yes
8	Methyl orange with NaCl at pH10 without UV	T _o MO8	T _{MO} 8	Yes	yes	yes	yes	no	no	yes	no	yes	no	yes
9	Methyl orange with Na ₂ SO ₄ at pH10 without UV	T _o MO9	T _{MO} 9	Yes	yes	yes	no	yes	no	yes	no	yes	no	yes
10	Methyl orange without salt at pH10 with UV	T _o MO10	T _{MO} 10	Yes	yes	yes	no	no	no	ye	yes	no	no	yes
11	Methyl orange with NaCl at pH10 with UV	T _o MO11	T _{MO} 11	Yes	yes	yes	yes	no	no	yes	yes	no	no	yes
12	Methylene blue with Na ₂ SO ₄ at pH10 with UV	T _o MO12	T _{MO} 12	Yes	yes	yes	no	yes	no	no	yes	no	no	yes

Error analysis is the study of uncertainties in physical measurements, often the measurement error was monitored with a simple measurement model written as:

$$x_m = x + \varepsilon \quad (3.10)$$

Where x_m is the measured value, x is the ‘true’ or master value, and ε is the measurement error.

To ensure accuracy in the analysis, there was need to measure experimental error and to learn basic principles of error analysis through:

- Understanding the types and sources of experimental errors,
- Clearly and correctly report measurements and the uncertainties in those measurements, and
- Design experimental methods and techniques to improve measurement skills to reduce experimental errors.

Some of the sources of error noted in the course of experiment were:

(a) ***Weighing balances***

Same weighing balance was used to measure the amounts of TiO₂ and dye powder while cleaning the plate regularly after use.

(b) ***Color changes (spectrophotometer)***

During kinetic studies the deviation in the values in change of spectrophotometer readings were kept at minimum as unwanted deviations were discarded.

(c) ***Meters (pH meter)***

The same pH meter was used throughout the experiment and the calibration was checked regularly with the manufacturers known sample acidic/neutral/basic pH solutions.

(d) *Purity of materials*

The analysis of fresh TiO_2 revealed a minor impurity which was put into consideration during analysis. Same dye source, same TiO_2 source and same source water were used. The water source was especially important because of the sensitivity of XPS machine on detecting minute contaminations. There was an issue of adventitious carbon accumulating on materials kept in the atmosphere, which was addressed by keeping all materials in tight lid containers.

(e) *Timing*

Keeping the reaction time of 10h was also a challenge that require vigilance. Also, the time of filtration has be moderately the same to avoid irregular over exposure to the atmosphere.

(f) *External factors*

The temperature was maintained so as not to affect the vaporization of reactants. External light source could access the setup, also there was need to keep the UV source confined within the reactor for safety, these were considered by using foil paper to keep the reacting environment confined to only the desirable reaction conditions. The drying of the filtered deactivated TiO_2 was in a dark environment with minimum contamination from the atmosphere.

Prior to that, there were activities to optimize the photoreactor and light source as follows:

3.3.2.3 *Stimulus-response method*

The stimulus-response test was carried out in the laboratory reactor where complete mixing was achieved with Wids Laboratory instruments magnetic stirrer maintained at 350rpm.

3.3.2.4 Chemical actinometry technique

The chemical actinometry technique was used to determine the UV photon flux. The technique made use of potassium ferrioxalate as the reference substance, which underwent a light induced chemical reaction which the incident UV radiation provides the energy to convert ferric into ferrous ions given in Eq. 3.1 below:



The amount of Fe^{2+} ions (n_{Fe}) after irradiation can be measured spectrophotometrically. The quantum yield Φ for the conversion reaction was accurately measured at different wavelengths, for any irradiation wavelength there was a value for Φ .

The radiation intensity of the lamp I_0 , at time t , is given by Eq. 3.2:

$$I_0 = \frac{n_{\text{Fe}}}{\Phi \cdot t} \quad (3.2)$$

Where n_{Fe} was the number of moles of Fe (II), t is the time of irradiation. From Eq. 3.2 a plot of n_{Fe}/Φ against t will yield a straight line with I_0 radiation intensity as gradient.

3.3.2.5 UV irradiation depth

A batch cylindrical reactor 500ml beaker, internal diameter 9cm and 12.5cm height. The height corresponding to 200ml fluid in the batch reactor was set so that flux from Khind photocatalyst lamps 15W UV Malaysia emanates from a chosen distance (irradiation depth I_d) of 16.5cm having a wavelength of 360-400nm (UVA). Initially, the manufacturers have optimized the range of best distance 15-22.5 cm from the source of UV irradiation to the TiO_2 coated conical surface for effective $h\nu_{VB}^+$ and e_{CB}^- generation.

The irradiation depth I_d can be estimated from the Eq. 3.3:

$$I_d = \frac{V}{N_A S_P} \quad (3.3)$$

on rearranging;

$$\frac{1}{I_d} = \frac{N_A}{V} S_P \quad (3.4)$$

N_A/V the number of aggregates per unit of reactor volume is given as in Eq. 3.5:

$$N_A = \frac{D_O V}{\rho_{app} \left(\frac{4}{3}\right) \pi (R_{AO} + B D_O)^3} \quad (3.5)$$

where ρ_{app} is apparent density of the TiO_2 colloid, while the effective cross section of an aggregate for the interaction with the radiation S_P , and can be evaluated from the geometric optics approximation equation Eq. 3.6:

$$S_P = \pi R_A^2 \quad (3.6)$$

where R_A is the mean average radius of the aggregate and B is slope when R_A was plotted against photocatalyst dose D_O as R_A is defined in Eq. 3.7, R_{AO} is the value of R_A at intercept on x -axis.

$$R_A = B D_O + R_{AO} \quad (3.7)$$

Additionally, the UV irradiation was confined within the reactor by wrapping with aluminum foil. The environmental temperature was maintained such that the temperature of the colloid was maintained at 25°C in all the experimental setup.

3.3.3 Kinetic studies in form of cumulative percent degradation of photodegradation of methylene blue and methyl orange solutions with Cl^- or SO_4^{2-} using TiO_2

After confirming the rate of degradation of MB and MO solution approximately obeys the Langmuir-Hinshelwood mechanism, it was then followed with deactivation analysis. This procedure was used to achieve objective (3).

This is the step where there was need to modify the design of experiment to provide answer to the problem of photocatalyst deactivation, a major question stated in the objective. Though, there are numerous photodegradation experiments in literature, such that the amount of materials needed to optimize an experimental procedure is common place, the unique procedure and the detailed surface analysis in this research set it apart from other studies of photocatalyst deactivation in aqueous media. In this procedure, photocatalyst was used repeatedly in a reaction condition until it reached equilibrium adsorption or deactivated. At this stage the effect of species on photocatalyst surface would be analyzed. The experiment was designed in such a way that same experimental conditions set in achieving objectives (2) were used, but the procedure was modified.

3.3.3.1 Data collection

(a) *Kinetic studies of photodegradation of MB and MO solutions and activity of TiO_2*

The experimental conditions used in this kinetic study were identical to those used in the kinetic studies in form of CPD, only that the procedure is different. In the analysis of kinetics of photodegradation of dyes, change in concentration with reaction time are to be captured. Twelve data points starting from 10 to 120 minutes have been accepted in each experimental condition. The first experimental condition was having 200ml, 20ppm MB dye solution in batch reactor (500ml beaker), with no UV, no salt in pH4. The needed amount of photocatalyst was a fixed amount of 0.4g of pure, fresh titanium dioxide (TiO_2)

anatase (T_F) and allowed to run for a period of 10 minutes to obtain the first data point of T_{oMB1} , succeeding data points were at 10 minutes interval, adding 10 minutes to each subsequent point up to the 120th minute, using a centrifuge to obtain the filtrate at each interval for spectrophotometer and TOC analysis. Table 3.2 shows the twelve different experimental conditions for MB (T_{oMB1} - T_{oMB12}) and similar conditions for MO (T_{oMO1} - T_{oMO12}).

(b) ***Kinetic studies of photodegradation of MB and MO in form of cumulative percent degradation (CPD)***

To obtain each sample say T_{MB1} , a photocatalyst will be used (many times) up to six rounds to allow the collection of raw data to fit into Table 3.3-Table 3.8 and Fig. 3.2 outline the flow diagram of the experiment. Each round run for 10h making a total of 60h. It was the total of 60h that generate the cumulative percent degradation. In the first round, tagged as sample T_{MBR1} as shown in Table 3.3, the experimental condition was having 200ml, 20ppm MB dye solution in batch reactor (500ml beaker), assemblage shown in Fig. 3.3 with no UV, no salt in pH4. The needed amount of photocatalyst was a fixed amount of 0.4g of pure, fresh titanium dioxide (TiO_2) anatase (T_F) and allowed to run for a period of 10h. When it reached equilibrium adsorption (becomes deactivated), a Sastec Laboratory Equipment Model ST-CT500 (SR # 8913) Centrifuge of 50mL Conical Sterile Polypropylene Tubes and HERMILE Labortechnik GmbH, Model Z 206 A (SN # 60130537) were used to separate the T_{MBR1} photocatalyst from the suspension to obtain the filtrate for spectrophotometer and TOC analysis. The kinetics of disappearance was measured with Spectroquant Pharo 300 (SR # 13041074) spectrophotometer and TOC change was followed with Shimadzu TOC analyzer model TOC-L CSN (SR # H54405100077).

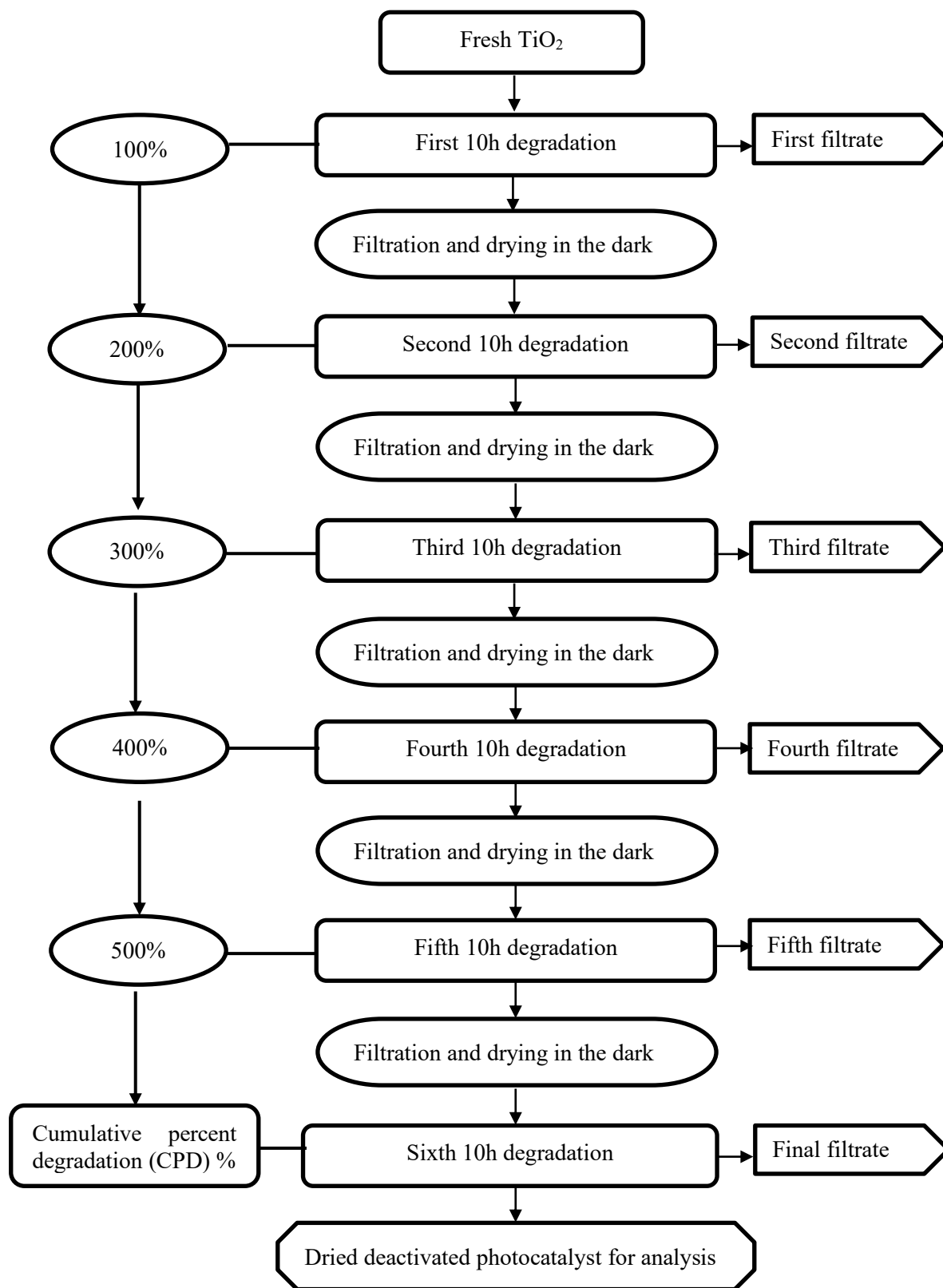


Figure 3.2: Flow diagram of procedure of kinetic studies of photodegradation of MB and MO in form of cumulative percent degradation (CPD)

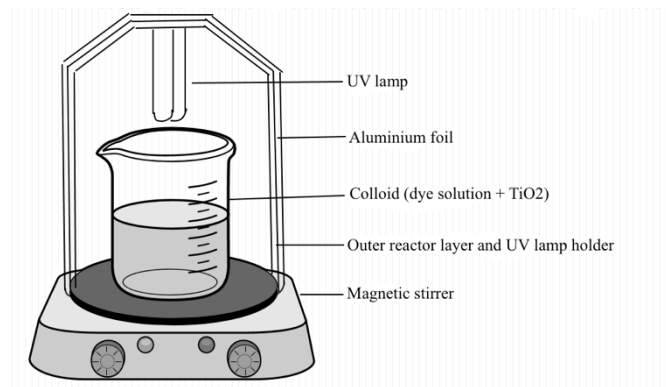
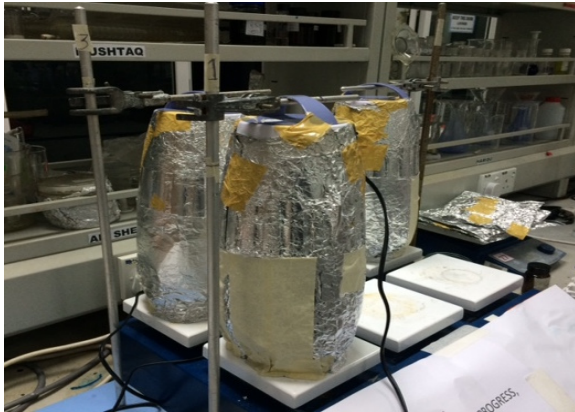


Figure 3.3: Photoreactor set-up for kinetic studies and deactivation analysis

Once the filtrate was taken, the sediment was further carefully transferred into a Rocker VF3 filtration set (with the pump attached) to finally obtain the filter cake of the used catalyst in a minimum dust environment on the GE Whatman, Nylon membrane filter and dried in the dark. When enough amount of T_{MBR1} was gathered, it was followed by second round to fit Table 3.4 with ten runs and same procedure to gather the dried sample as T_{MBR2} , then seven runs in third round Table 3.5 to gather the dried samples as T_{MBR3} , followed by fourth round with five runs shown in Table 3.6 to gather the dried samples as T_{MBR4} , then fifth round with three runs Table 3.7 to gather the dried samples as T_{MBR5} and finally sixth round Table 3.8 with one run to gather the final required dried samples as T_{MB1} . It is worth mentioning that, each round was designed to maintain consistency, also to obtain enough amount of used TiO_2 for the subsequent round (inevitable due to small reactor size). At the sixth final round, the dried T_{MB1} was taken for surface analysis using FTIR and XPS. Further analysis continued where eleven (11) different experimental conditions were selected for MB as shown in Table 3.2. The same procedure was repeated for Methyl orange to obtain sample T_{MO1} - T_{MO12} as shown in Table 3.2.

Primary Data

1 round

Table 3.2: Rate of mineralization of methylene blue without salt without UV irradiation at pH4 for 10hours sample T_{MBR1}

No. Degradation Experiment	Initial (TOC)	Final (TOC)	Change (TOC)	Initial (UV-VIS)	Final (UV-VIS)	Change (UV-VIS)	Time	Tripod
1			X _{TOC1}			X _{UV-VIS1}		
↓			↓			↓		
16			X _{TOC16}			X _{UV-VIS16}		
			$\frac{1}{16} \sum_{i=1}^{16} x_{\text{TOC}}$			$\frac{1}{16} \sum_{i=1}^{16} x_{\text{UV-VIS}}$		
Total Mass (TiO ₂ Residue) =								

2 round

Table 3.3: Rate of mineralization of methylene blue without salt without UV irradiation at pH 4 for 10hours sample T_{MBR2}

No. Degradation Experiment	Initial (TOC)	Final (TOC)	Change (TOC)	Initial (UV-VIS)	Final (UV-VIS)	Change (UV-VIS)	Time	Tripod
1			X _{TOC1}			X _{UV-VIS1}		
↓			↓			↓		
10			X _{TOC10}			X _{UV-VIS10}		
			$\frac{1}{10} \sum_{i=1}^{10} x_{\text{TOC}}$			$\frac{1}{10} \sum_{i=1}^{10} x_{\text{UV-VIS10}}$		
Total Mass (TiO ₂ Residue) =								

3 round

Table 3.4: Rate of mineralization of methylene blue without salt without UV irradiation at pH4 for 10hours sample T_{MBR3}

No. Degradation Experiment	Initial (TOC)	Final (TOC)	Change (TOC)	Initial (UV-VIS)	Final (UV-VIS)	Change (UV-VIS)	Time	Tripod
1 ↓ 7			X _{TOC1} ↓ X _{TOC7} $\frac{1}{7} \sum_{i=1}^7 x_{TOC}$			X _{UV-VIS1} ↓ X _{UV-VIS7} $\frac{1}{7} \sum_{i=1}^7 x_{UV-VIS7}$		
Total Mass (TiO ₂ Residue) =								

4 round

Table 3.5: Rate of mineralization of methylene blue without salt without UV irradiation at pH4 for 10hours sample T_{MBR4}

No. Degradation Experiment	Initial (TOC)	Final (TOC)	Change (TOC)	Initial (UV-VIS)	Final (UV-VIS)	Change (UV-VIS)	Time	Tripod
1 ↓ 5			X _{TOC1} ↓ X _{TOC5} $\frac{1}{5} \sum_{i=1}^5 x_{TOC}$			X _{UV-VIS1} ↓ X _{UV-VIS5} $\frac{1}{5} \sum_{i=1}^5 x_{UV-VIS5}$		
Total Mass (TiO ₂ Residue) =								

5 round

Table 3.6: Rate of mineralization of methylene blue without salt without UV irradiation at pH4 for 10hours sample T_{MBR4}

No. Degradation Experiment	Initial (TOC)	Final (TOC)	Change (TOC)	Initial (UV-VIS)	Final (UV-VIS)	Change (UV-VIS)	Time	Tripod
1 ⋮ 3			X _{TOC1} ⋮ X _{TOC3} $\frac{1}{3} \sum_{i=1}^3 x_{TOC}$			X _{UV-VIS1} ⋮ X _{UV-VIS3} $\frac{1}{3} \sum_{i=1}^3 x_{UV-VIS3}$		
Total Mass (TiO ₂ Residue) =								

6 round

Table 3.7: Rate of mineralization of methylene blue without salt without UV irradiation at pH4 for 10hours sample T_{MB1}

No. Degradation Experiment	Initial (TOC)	Final (TOC)	Change (TOC)	Initial (UV-VIS)	Final (UV-VIS)	Change (UV-VIS)	Time	Tripod
Fresh TiO ₂								
Deactivated TiO ₂								
Total Mass (TiO ₂ Residue) =ΣT _{MB1}								

3.3.4 Relationship between adsorbed species and cumulative percent degradation

This section is to achieve objective (3). The results of the characterized deactivated samples were analyzed in terms of elemental composition and compared with the characterized fresh TiO_2 , while both are related to the cumulative percent degradation.

3.3.5 Propose a practice for photocatalyst deactivation analysis

The data obtained from the analysis was seen to be sufficient to recommend a practice for photocatalyst performance analysis to achieve objective (4).

3.4 Safety

This research was carried out following the Laboratory Safety and Health Practices, Faculty of Engineering, University of Malaya, which complies with the Material Safety Data Sheet (MSDS) Malaysia, available from the Department of Occupational safety and Health, Ministry of Human Resources, Malaysia. To ensure compliance all incidences of substandard practices and conditions were eliminated. This was achieved by the use of required personal protective equipment and use of standard operating procedures. Care was taken to prevent fire, chemical reactivity and contact with chemicals. Proper disposal method was also applied. Special attention was also given to how the UV radiation was used in this research by covering the reactor with a reflective aluminium foil paper. All was done to prevent, minimize or eliminate risks.

CHAPTER 4: RESULTS AND DISCUSSIONS

4.1 Introduction

This chapter provides detailed results and discussions on the achieved objectives of this research. It provides the results of surface analysis of fresh TiO_2 anatase, whose composition is to compare with that of the deactivated TiO_2 samples, after photodegradation analysis. The subsequent discussion is on the kinetics of methylene blue, a cationic dye with added NaCl or Na_2SO_4 at varying pH and compared with literature. Followed by discussions on degradation rate of methyl orange an anionic dye with added NaCl or Na_2SO_4 at varying pH also compared with the literature. The succeeding section provides surface analysis of deactivated TiO_2 samples from methylene blue and methyl orange (with added NaCl or Na_2SO_4 and varying pH) solutions and how each relates with cumulative percent degradation type kinetics. This is where the new adsorbed species on deactivated samples identified using XPS and FTIR were compared with the earlier characterized fresh TiO_2 . Next section provides the significance of the relationship between the adsorbed species and reaction rate in form of CPD. Lastly, discussions and schematic of the propose practice for photocatalyst deactivation analysis was presented.

4.2 Characterization of fresh (T_F) TiO_2

4.2.1 X-ray diffraction of T_F

The X-ray diffraction (XRD) analysis of T_F in Fig. 4.1 exhibited two strong diffraction peaks in the (101) plane at 25.354° and in (200) plane at 48.077° , all subsequent peaks and unit cell parameters $a = 3.7830 \text{ \AA}$ and $c = 9.5100 \text{ \AA}$ are in good agreement with ICSD reference code 00-004-0477 indicating TiO_2 in the anatase phase.

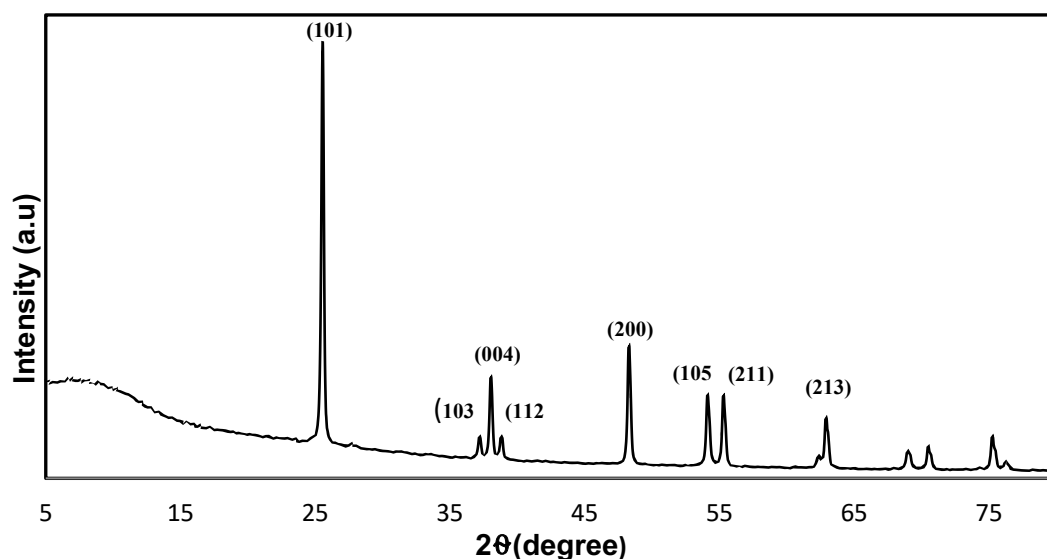


Figure 4.1: X-ray diffraction of T_F indicating TiO₂ in the anatase phase

4.2.2 Brunauer-Emmett-Teller (BET)

Analysis of quantities of specific surface area determined through BET theory gives information on how much adsorption capacity is available on the surface. The BET analysis of fresh TiO₂ indicate a surface area of 10.14m²/g, pore size 12.38nm and pore volume 0.0314cm³/g suitable for this analysis.

4.2.3 Fourier-transform infrared spectroscopy (FTIR)

FTIR analysis of T_F in Fig. 4.2 suggests the characteristic vibrations of the Ti–O–Ti stretch observed in the range 450–1000 cm⁻¹. The existence of C–O in the range of 1600 cm⁻¹ to 1500 cm⁻¹ was observed. These values have given information on the initial characteristics of chemical properties, chemical bonds present and information about the specific bonding in the fresh specimen. This information will be used to compare with the deactivated samples to determine the level of contamination (residue) and identify their nature, whether organic, polymeric, and in some cases, inorganic materials. There was presence of C–H in the range of 2950 to 2850 cm⁻¹.

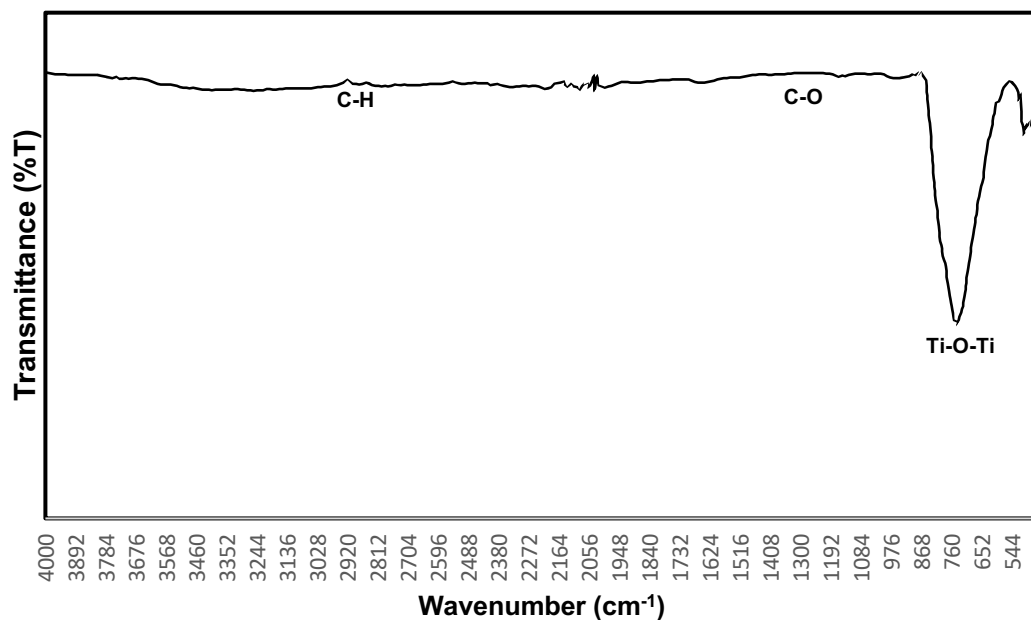


Figure 4.2: FTIR of T_F indicating characteristic TiO₂ vibrations

4.2.4 X-ray photoelectron spectroscopy (XPS)

XPS results measure the elemental composition, empirical formula, chemical state and

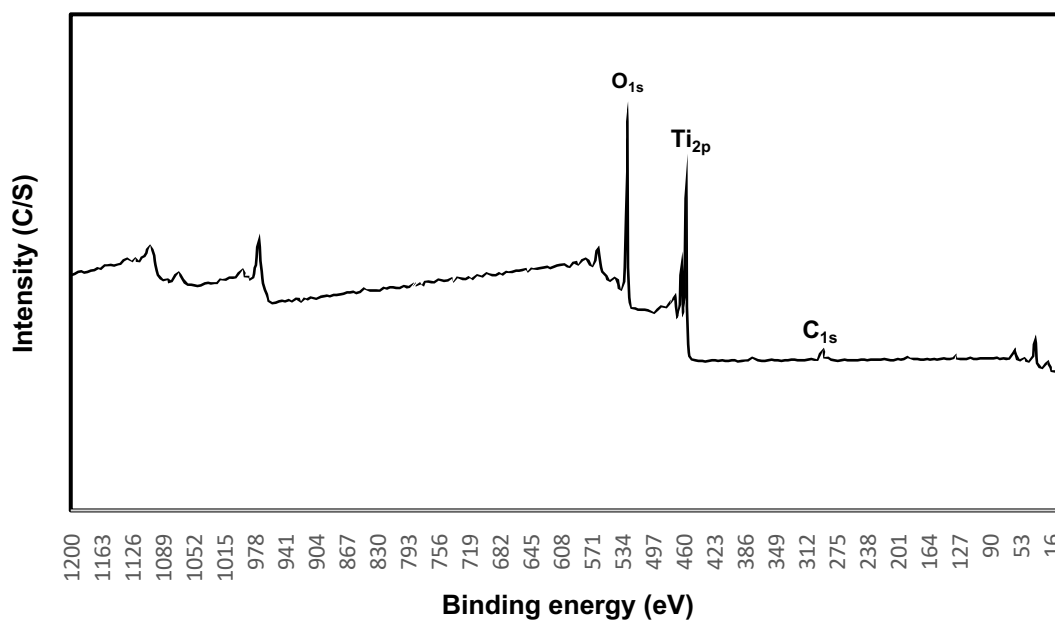


Figure 4.3: XPS survey spectra of T_F

electronic state of the elements within a material. For the fresh sample the XPS SS of T_F in Fig. 4.3 indicate a characteristic presence of Ti, O, C with a Ti⁴⁺ at level Ti 2p_{1/2} and Ti

2p_{3/2}. These results will allow for discussions based on XPS survey spectra (SS) and high resolution spectra (HRS), providing a comparison of changes in percent atomic concentration of existing elements in fresh TiO₂ and new elements in deactivated TiO₂ (after the kinetic studies in form of cumulative percent degradation).

4.3 Kinetic studies of methylene blue and methyl orange photodegradation

To avoid repeating major steps in photodegradation of azo dyes MB and MO used in this analysis, a general outlook can be provided before discussing their photodegradation kinetics pathway individually. In photodegradation of azo dyes (Lachheb et al., 2002; J.-y. Li et al., 2007) like MB and MO, attack on the azo bond (C-N=N-), is followed by opening of the aromatic rings leading to aromatic amines or phenolic compounds as intermediate products. Further opening of the aromatic (in other cases naphthalene rings) bears a variety of carboxylic acids that decarboxylate into CO₂ (Y. Liu et al., 2005; Rochkind et al., 2015). Not only intermediates, end products like benzene and substituted benzenes could be formed from •OH degradation of azo dyes containing a phenylazo substitutions (Spadaro et al., 1994). The early breakdown products then underwent further oxidation leading to the production of CO₂. They also noted the inorganic anion SO₄²⁻ formed progressively and the amount increased more than 30% per 4h (Y. Liu et al., 2005). Dyes containing sulfur atoms are mineralized into sulfate ions (Hu et al., 2003). Chlorinated dye molecules release chloride ions (Konstantinou & Albanis, 2004). Dyes containing nitrogen may release NH₄⁺, NO₃⁻ and sometimes N₂, depending on the initial oxidation state of the nitrogen atoms (Rochkind et al., 2015; Tanaka et al., 2000).

From the nature of the intermediate compounds in both elemental analysis from this work and the LC/MS data obtained from (Houas et al., 2001), it infers dissociative adsorption in photodegradation pathway of MB. Similar analogies were made in MO (Sheikh et al., 2016). The raw photodegradation kinetic data for MB and MO were shown

in Fig. 4.7 and 4.11 respectively. As the surface gets covered by the intermediates and final products, the surface coverage (θ) is defined in Eq. 4.1. At equilibrium adsorption Eq. 4.2, will lead to deactivation of the samples T_{oMB1}-T_{oMB12} in MB and T_{oMO1}-T_{oMO12} in MO:

$$\theta = \frac{N_s}{N} \quad (4.1)$$

where θ is dependent on number of occupied sites N_s and the total number of sites N for gas on solid surface, based on Langmuir-Hinshelwood (L-H) mechanism, which can be applied in this situation. It is believed that the deactivation corresponds to the equilibrium adsorption q_e Eq. 4.2:

$$q_e = \frac{V(C_o - C_e)}{M} \quad (4.2)$$

where C_o initial concentration of the dye solution, C_e the dye concentration at equilibrium and M the mass of catalyst and V is the volume of the dye solution.

Unlike in gaseous media where it is expected that the molecules of absorbent will get dissociated as they adsorb on catalyst surface directly, the essential initial reactions in aqueous media (apart from adsorption) is the generation of $\bullet\text{OH}$ and other oxidants (Kafizas et al., 2016). The $\bullet\text{OH}$ generation breaks the bonds in the mother compound and subsequently the intermediates gradually begin to bond on the TiO_2 surface, while other reaction path will lead to generation of CO_2 . In anatase TiO_2 , depending on the reaction conditions, the bridging oxygen will attract intermediates and final products (e.g. dissolved CO_2) leading to the gradual reduction in the generation of $\bullet\text{OH}$ due to decline in generation of photogenerated holes leading to subsequent loss of activity of the photocatalyst. This pattern of surface coverage in aqueous media, have been reported to

obey the Langmuir-Hinshelwood mechanism as a first order kinetic equation Eq. 4.3 (Houas et al., 2001; Sacco et al., 2012; Q. Zhang et al., 2012), where the rate r was (Sacco et al., 2012) found to be proportional to the surface coverage θ and proportional to concentrations (at low values) and C is the concentration of dye in solution at time t , k the rate constants, K the equilibrium adsorption constant and k_{app} the apparent pseudo-first-order rate constant.:

$$r = -\frac{dC}{dt} = \frac{kKC}{1+KC} = k_{app}C \quad (4.3)$$

As the Eq. 4.3 is integrated it becomes:

$$\ln \frac{C_0}{C} = k_{app}t \quad (4.4)$$

where C_0 is the initial dye concentration in solution, t is the reaction time. k_{app} as the effect of varying constraints (initial concentration, mass of catalyst, wavelength, temperature and radiant flux) was assigned as constant because none of its varying factors was investigated.

4.3.1 Photodegradation products of Methylene blue with Cl^- or SO_4^{2-} at varying reaction conditions

The initial photodegradation pathway of MB was linked to the severance of the C–S+=C functional group bonds, resulting in sulfate ions, feasibly through the formation of a sulfone, a sulfoxide and a sulfonic group as shown in Fig. 4.4 (Houas et al., 2001). Due to the traces of S and N in some of the deactivated samples (T_{MB1} – T_{MB12}) in this research, any of the path ways suggested by (Houas et al., 2001) in Fig. 4.4, might have been possible.

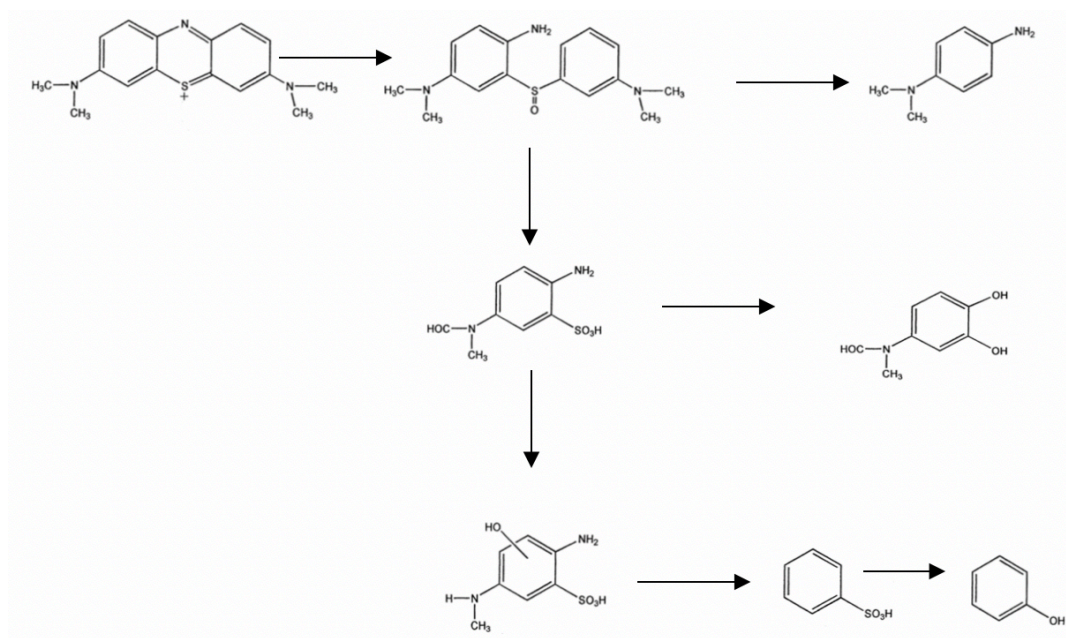


Figure 4.4: Photocatalytic degradation pathway of Methylene blue (Houas et al 2001)

From Eq. 4.4, the straight line when $\ln \frac{C_0}{C}$ was plotted against t , was seen in reactions with UV irradiation in MB in Fig. 4.5, could also be seen in reactions without UV in MB in Fig. 4.6. While in the plot of the raw data, there was a drop in the initial C_0 concentration of MB in Fig. 4.7 with time in all MB samples ($T_{0MB1}-T_{0MB12}$).

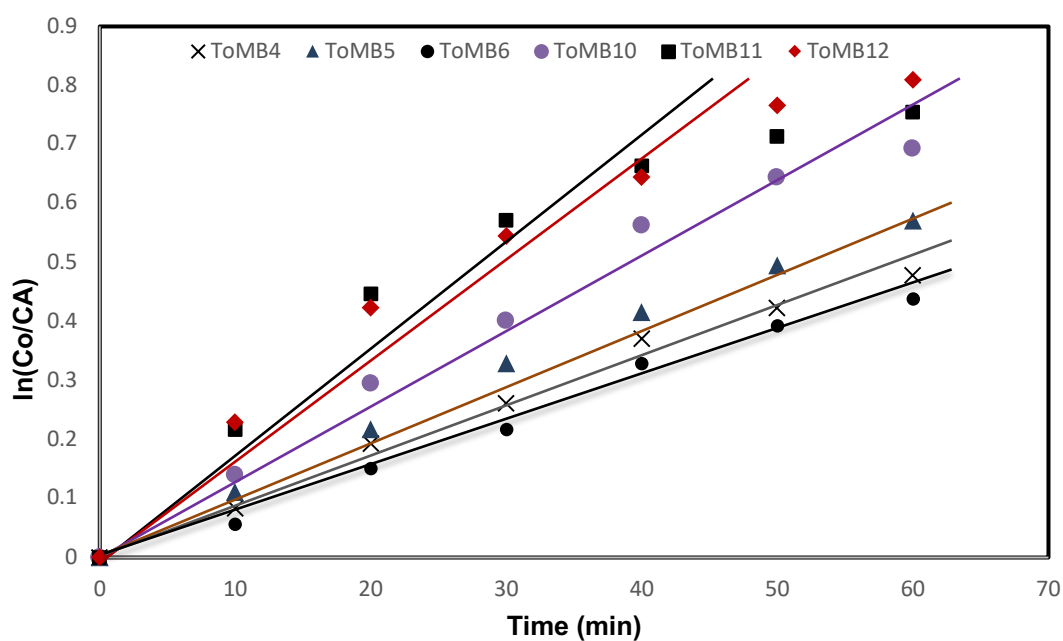


Figure 4.5: First order linear transforms of disappearance of MB under UV-irradiation

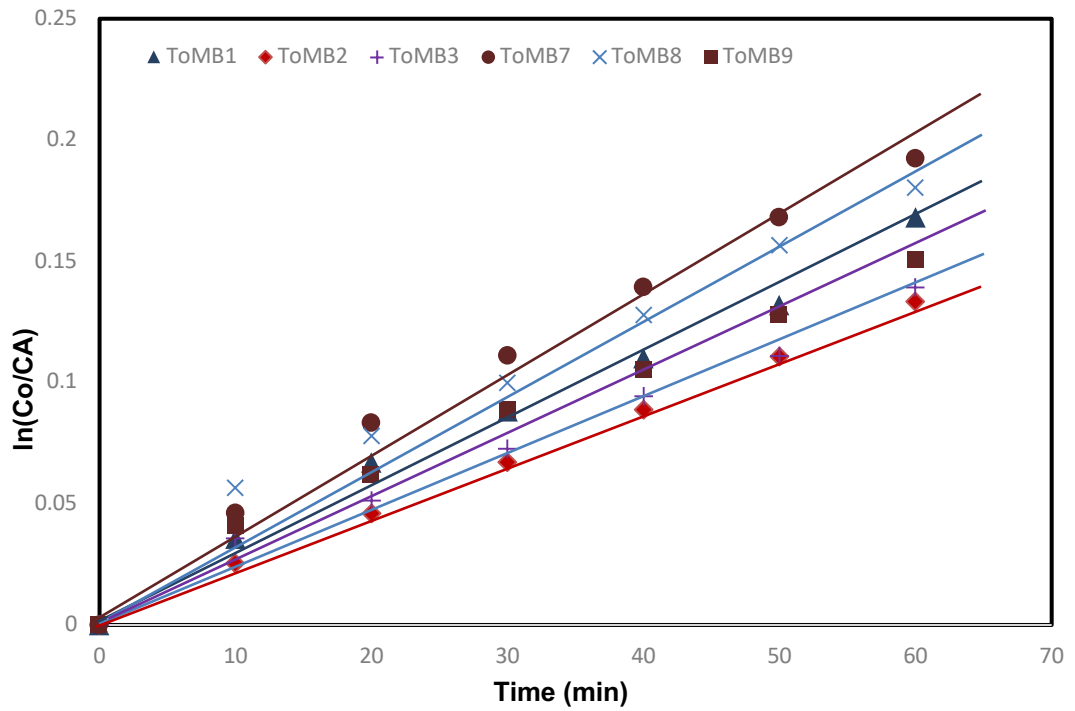


Figure 4.6: First order linear transforms of disappearance of MB without UV irradiation

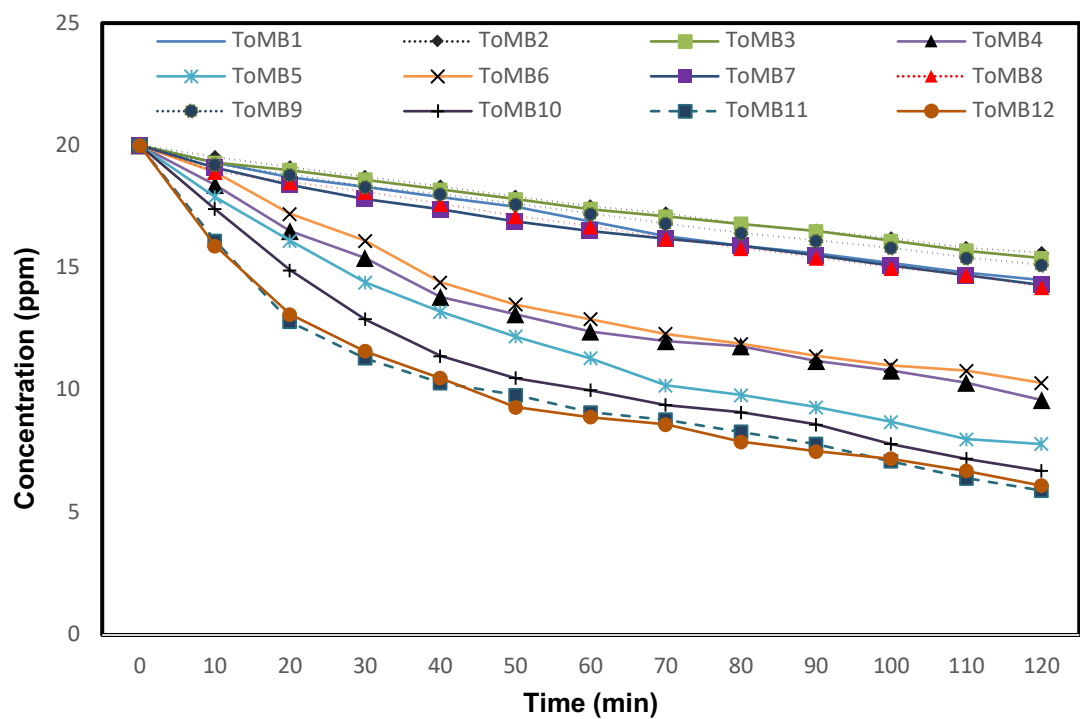


Figure 4.7: Concentration (ppm) changing with time (min) of MB samples T_{oMB1} - T_{oMB12}

4.3.2 Photodegradation products of Methyl orange with Cl^- or SO_4^{2-} at varying reaction conditions

From the LC-MS results, (Sheikh et al., 2016) assert that the different intermediate compounds, during the degradation pathway of MO, starts with the demethylation of MO or addition of a hydroxyl group to MO, mainly in ortho positions to azo and $\text{N}(\text{CH}_3)_2$ groups. Followed by introduction of the second hydroxyl group in the ring containing the SO_3^- group, as detected by HPLC/UV-VIS diode array and HPLC/MS techniques (Baiocchi et al., 2002) leading to the formation of intermediates as shown in Fig. 4.8. Further demethylation and removal of SO_2 generates fragments. Finally all intermediates were mineralized into CO_2 , SO_4^{2-} and NO_3^- (Sheikh et al., 2016; J. Yu et al., 2000).

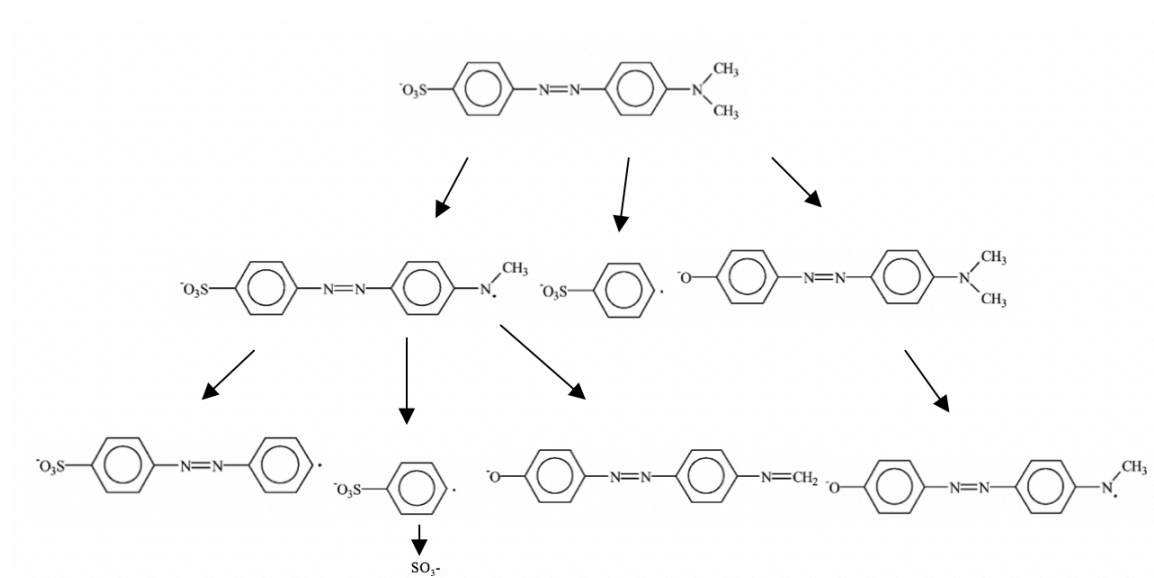


Figure 4.8: Photocatalytic degradation pathway of Methyl orange (Baiocchi et al., 2002)

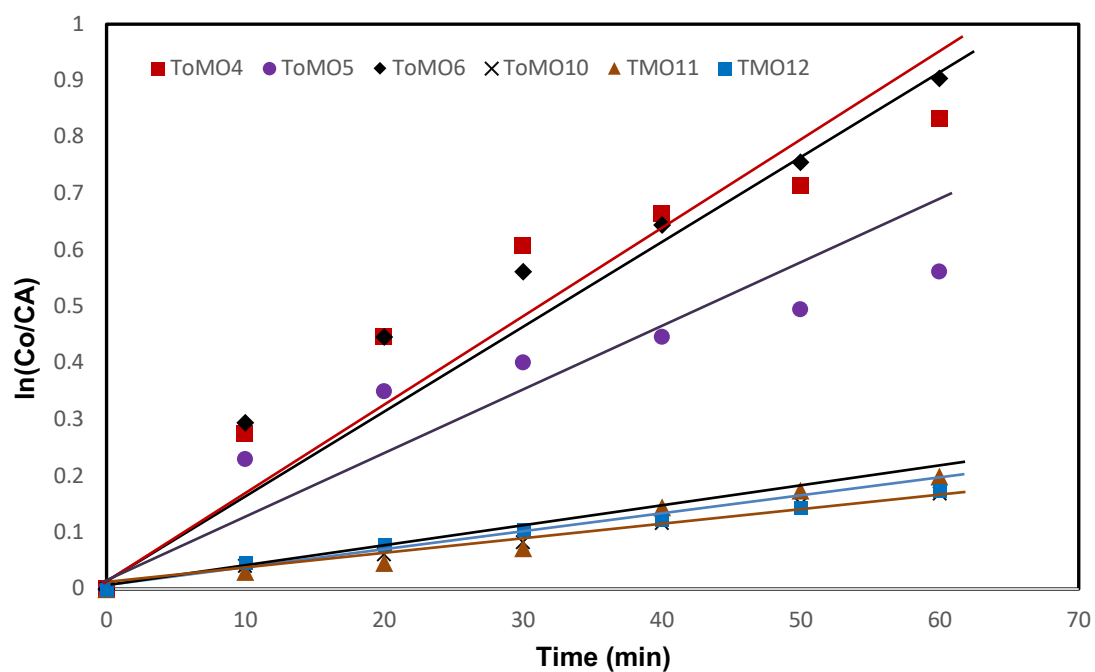


Figure 4.9: First order linear transforms of disappearance of MO under UV-irradiation

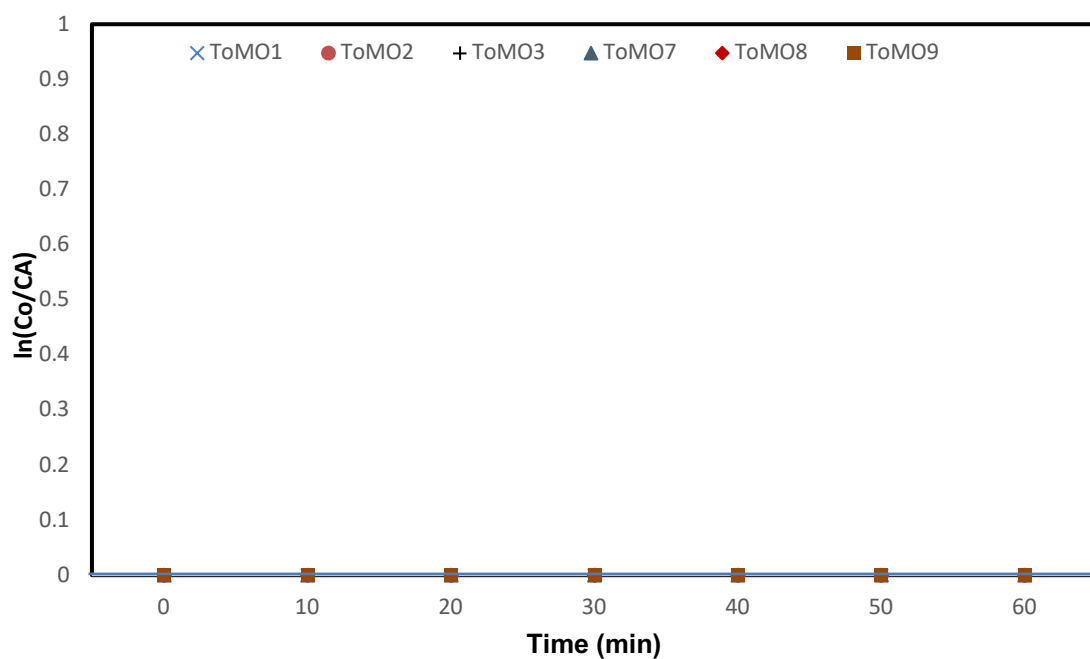


Figure 4.10: First order linear transforms of disappearance of MO without UV-irradiation

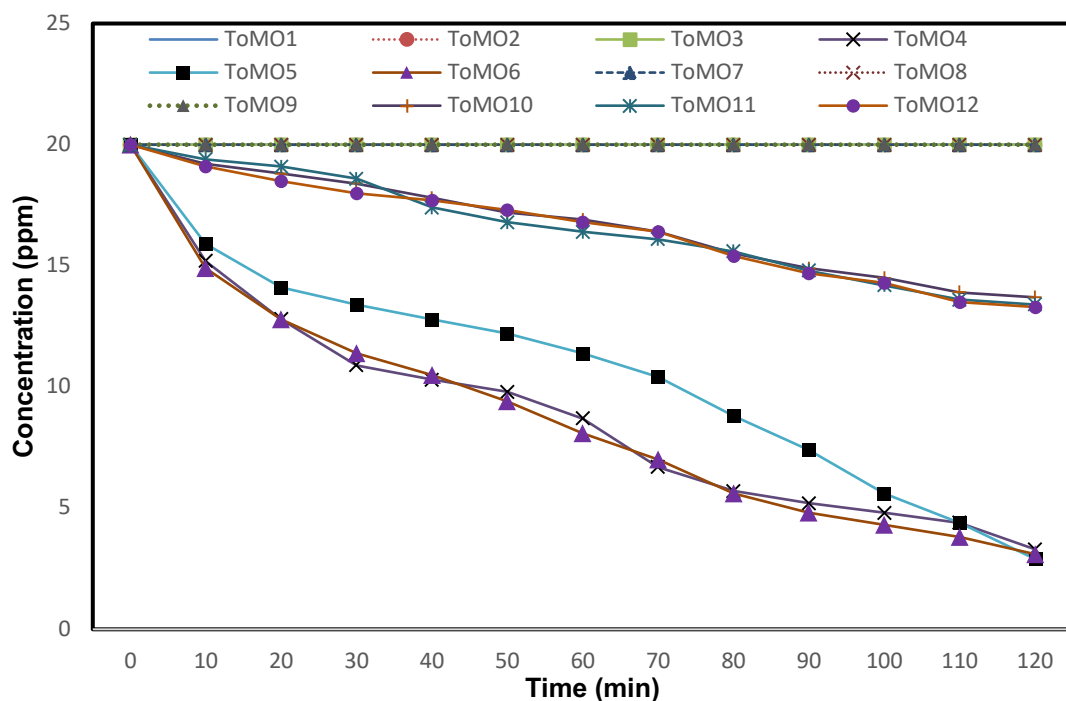


Figure 4.11: Concentration (ppm) changing with time (mins) of MO samples T_{0MO1} - T_{0MO12}

From Eq. 4.4, the straight line when $\ln \frac{C_0}{C}$ was plotted against t , was seen in reactions with UV irradiation in MO in Fig. 4.9, likewise seen in reactions without UV irradiation in Fig. 4.10. Even though the reactions without UV irradiation did not reveal a sufficient gradient to be seen to obey Langmuir-Hinshelwood mechanism (there was no detectable change in concentration of dye from the laboratory measurements), the surface had adsorbed some carbon species leading to surface coverage. Considering the raw data of MO, there was a drop in the initial C_0 concentration in Fig. 4.11 with time in all the MO samples (T_{0MO1} - T_{0MO12}). In both MB and MO there was gradual surface coverage as the reaction progresses that obeyed a pseudo first order kinetics. The surface coverage in MB was faster than in MO due to the nature of the molecule and intermediate species available in the individual colloid mixture.

In both MB and MO, the organic carbon mineralization in both dark and UV irradiation, was monitored with TOC evaluation, very low values and less initial sharp decrease were obtained for the samples in the dark, the samples with UV irradiations produces high TOC disappearance confirming the values obtained with the photospectrometer.

4.4 Surface analysis of deactivated TiO₂ samples from cumulative percent degradation study

In this work the CPD was introduced to express the cumulative performance of a photocatalyst based on its usage over fixed time interval. The analysis presented in Fig. 4.12 for MB and Fig. 4.13 for MO, shows that CPD values were used to express the 10hourly performance which also shows the gradual decline in performance with time. The CPD generated can be a reliable parameter for measuring the efficacy of a photocatalyst, where experimental conditions can be compared easily as one measures the life span of the photocatalyst involved. Other useful information is relating the CPD with PAC of each element involved in individual experimental conditions, this is shown in Fig. 4.14 and Fig. 4.15. This analysis provides an opportunity to ascertain the contribution of each element or its derivatives in the deactivation of the photocatalyst. In some circumstances, there might be a requirement in photoreactor design to compare the rate of degradation of different dyes as shown in Fig. 4.12 and Fig. 4.13 for MB and MO respectively.

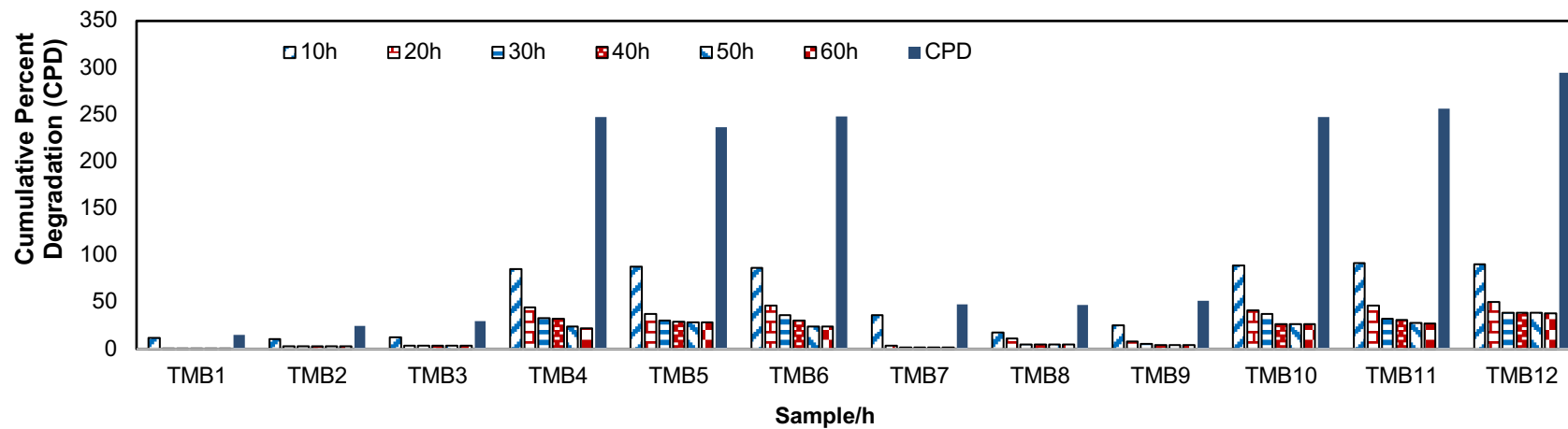


Figure 4.12: 10-60h of MB samples T_{MB1}-T_{MB12} percent degradation and CPD per sample

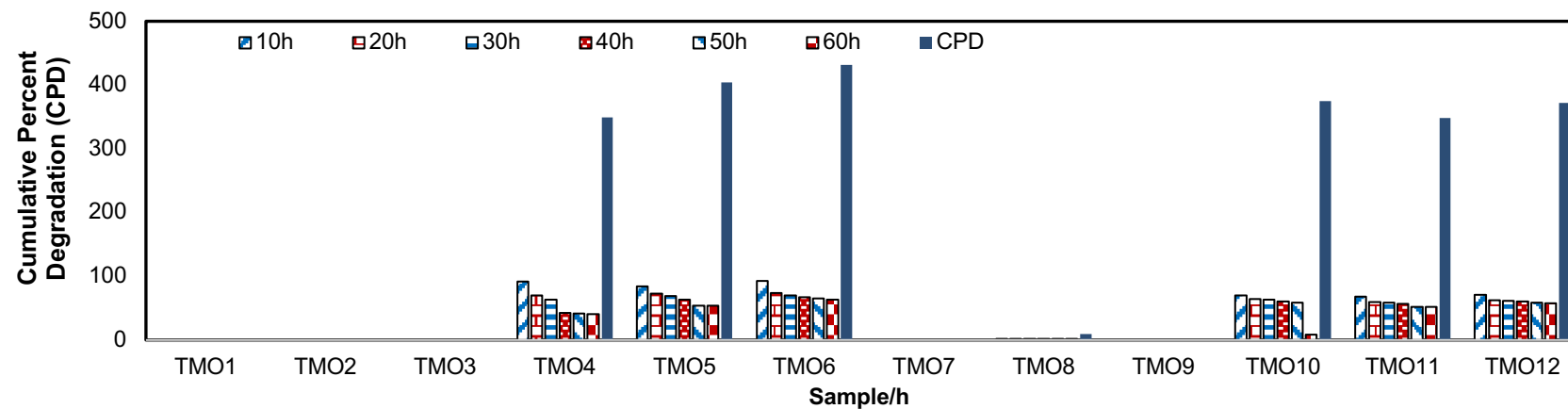


Figure 4.13: 10-60h of MO samples T_{MO1}-T_{MO12} percent degradation and CPD per sample

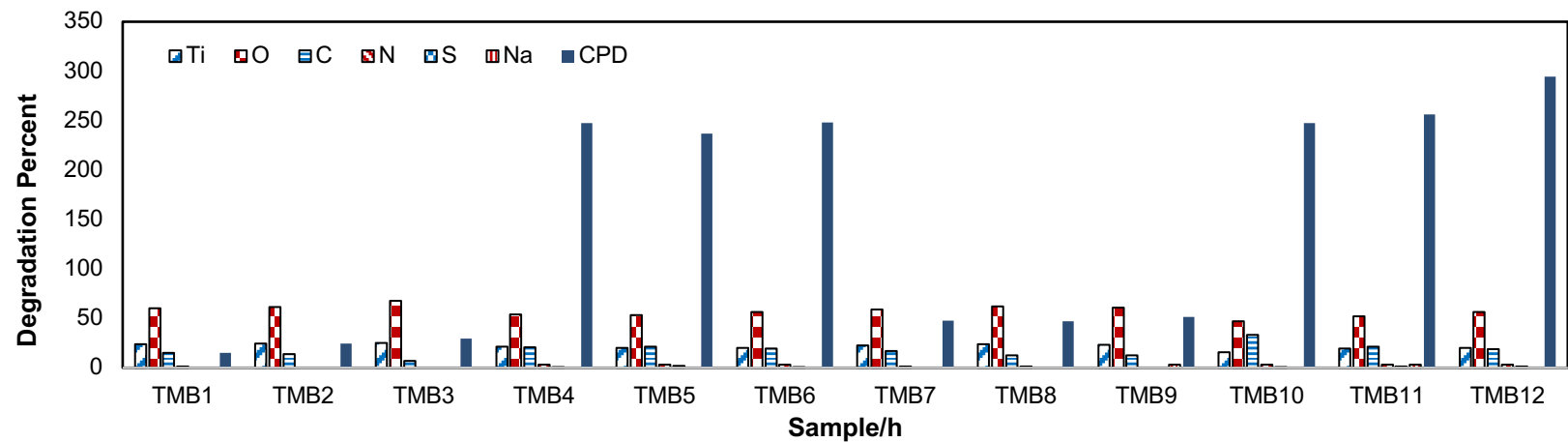


Figure 4.14: Relationship between SS PAC and CPD per MB sample

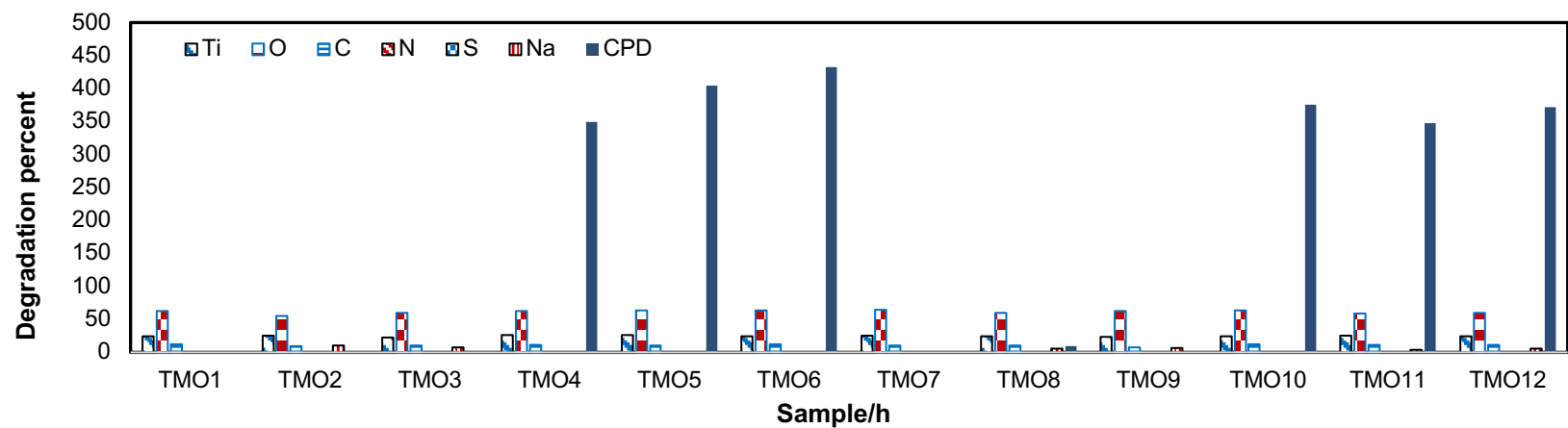


Figure 4.15: Relationship between SS PAC and CPD per MO sample

These figures easily compare the 10 hourly up to 60 hour performance of the photocatalyst in MB and MO solutions. In the first 10h, samples with UV irradiation performed better in reactions involving MO and could be used for longer time than in MB. In the 20h analysis most samples have shown a decline in performance, same as 30h analysis, as the analysis enters the 4th round, performance appears to be declining only slightly especially for MO.

The surface analysis in this section is to compare T_F and deactivated samples of MB (T_{MB1} - T_{MB12}) and MO (T_{MO1} - T_{MO12}) obtained from the cumulative percent degradation analysis, such that all the variables including the variations in pH, salts (NaCl and Na_2SO_4), UV and dyes are discussed concurrently. This comparison presents the FTIR and XPS results of T_F and deactivated samples of MB and MO samples, such that any change in T_F in composition due the new adsorbed species can be observed.

4.4.1 *Fourier transform infrared spectroscopy (FTIR) comparison of T_F , T_{MB1} - T_{MB12} and T_{MO1} - T_{MO12} samples*

The differences between species in T_F and the new adsorbed species in deactivated samples, were observed when comparing the FTIR results of T_F and all the deactivated samples of MB in Fig. 4.16 and in MO Fig. 4.17. The peaks between 3000 cm^{-1} and $2,850\text{ cm}^{-1}$ were assigned to C-H stretching vibrations of alkane groups seen to have increased in all the samples (both MB and MO) except T_F . The new peaks at the positions 970 - 1280 cm^{-1} in all the samples shows C-O stretching (both MB and MO). C-N at 1335 - 1250 cm^{-1} stretch (alcohols, carboxylic acids, esters and ethers) were not seen in T_F , but seen in all MB samples except T_{MB2} , T_{MB3} , T_{MB9} , these peaks of C-N were not seen in any of the MO samples (T_{MO1} - T_{MO12}).

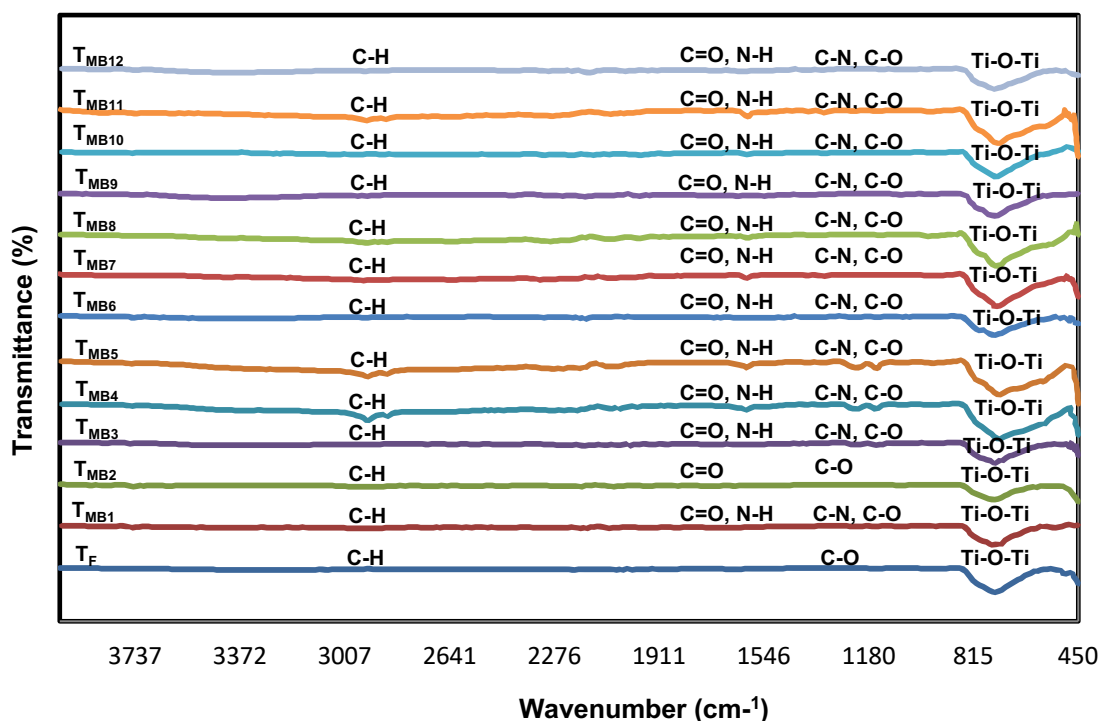


Figure 4.16: FTIR of the samples T_F and T_{MB1} - T_{MB12} of MB

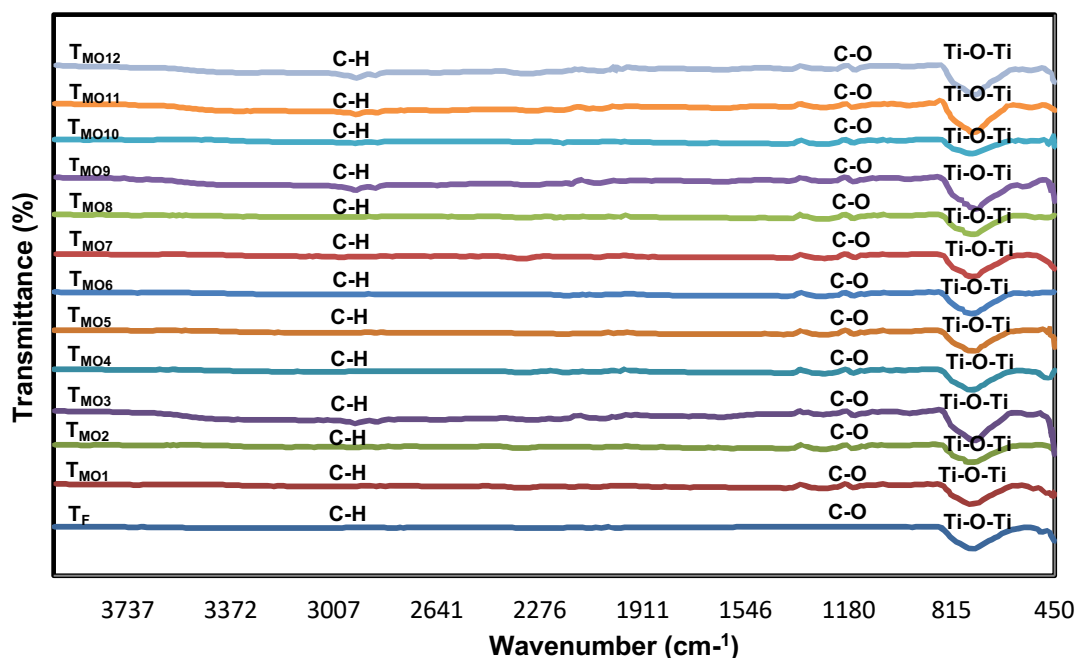


Figure 4.17: FTIR of the samples T_F and T_{MO1} - T_{MO12} of MO

Existence of N-H bending (1° -amines) in the range 1650 cm^{-1} to 1580 cm^{-1} was seen in all samples except T_F , T_{MB2} , T_{MB3} , T_{MB9} , but not seen in any of the MO samples (T_{MO1} - T_{MO12}). In all MB samples except T_{MB2} , it is probable that there was an amide due to the N-H and C=O overlap at 1650 cm^{-1} to 1550 cm^{-1} and overlap C-O and C-N in the range

1080 cm^{-1} and 1360 cm^{-1} suggesting an amine. None of these specie overlaps were seen in MO samples.

4.4.2 X-ray photoelectron spectroscopy (XPS) of T_F , T_{MB1} - T_{MB12} and T_{MO1} - T_{MO12} samples

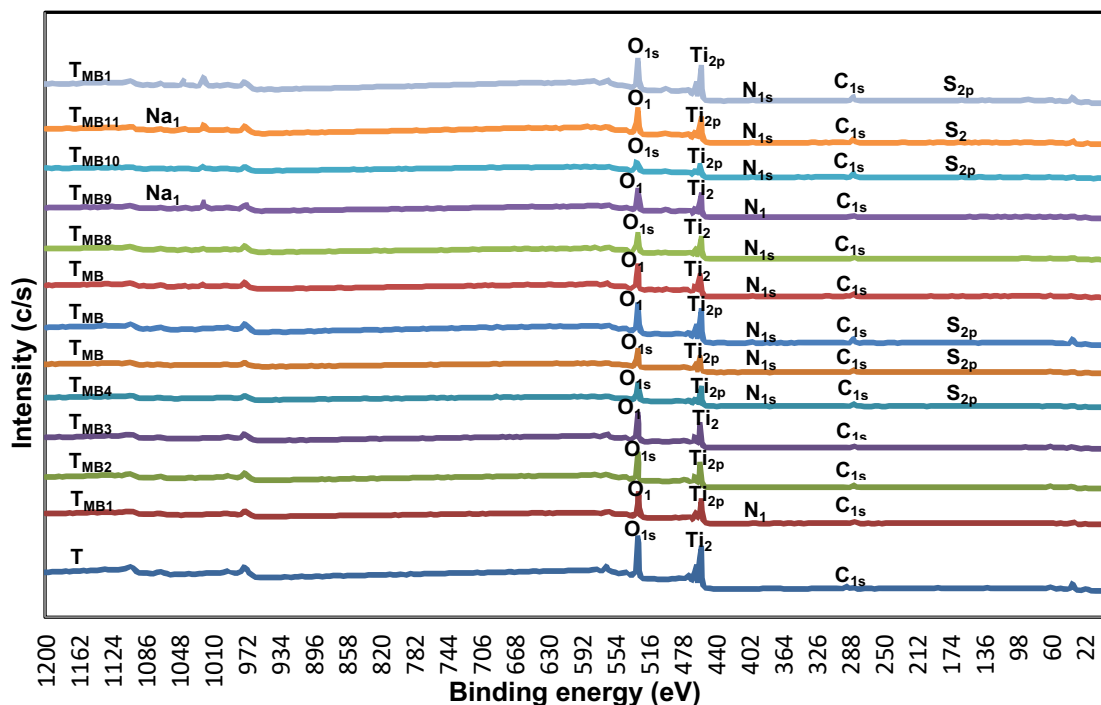


Figure 4.18: XPS survey spectra of samples T_F and T_{MB1} - T_{MB12} of MB

Figure 4.18 shows and compares the XPS survey spectra (SS) of T_F and the deactivated samples T_{MB1} - T_{MB12} while Fig. 4.19 shows and compare the XPS survey spectra of T_F and the deactivated samples T_{MO1} - T_{MO12} . Table 4.1 shows the SS PAC of the elements Ti, O, C, N, S and Na and the CPD of MB samples while Table 4.2 for MO samples. XPS high resolution spectra (HRS), would show detailed changes in the PAC of each element in the samples T_{MB1} - T_{MB12} for MB, and for MO and how they affect the CPD. These discussions were under different variables; UV effect, pH effect and NaCl effect, to present the effect of deactivation on reaction rate.

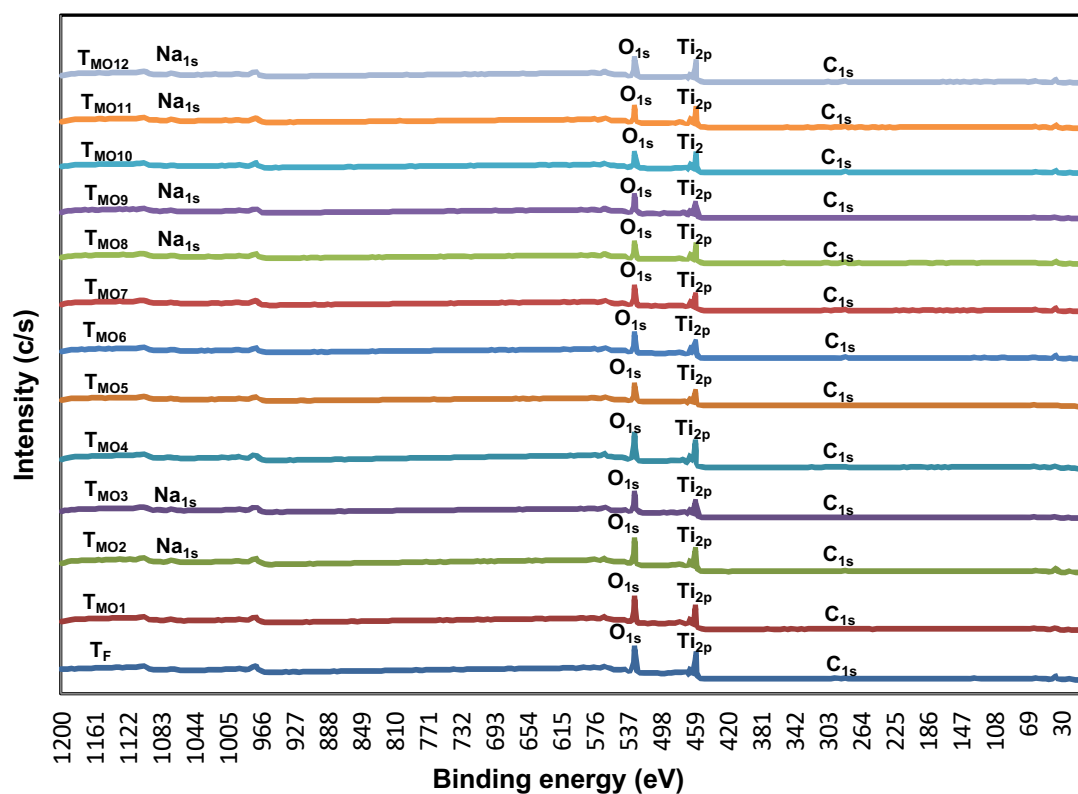


Figure 4.19: XPS survey spectra of samples T_F and T_{MO1}-T_{MO12} of MO

Table 4.1: XPS Survey Spectra of elemental composition and Percent Atomic concentration of T_F, T_{MB1}-T_{MB12} of MB

Sample	Ti%	O%	C%	N%	S%	Na%	K%	CPD
T _F	26.28	68.07	4.51	UD	UD	UD	1.14	NA
pH4								
T _{MB1} no salt, no UV	23.72	59.89	15.23	1.16	UD	UD	UD	15.16
T _{MB2} with NaCl, no UV	24.62	61.48	13.90	UD	UD	UD	UD	24.75
T _{MB3} with Na ₂ SO ₄ , no UV	25.21	67.58	7.21	UD	UD	UD	UD	29.72
T _{MB4} no salt, with UV	21.13	54.08	20.61	3.34	0.84	UD	UD	247.30
T _{MB5} with NaCl, with UV	20.40	53.36	21.35	3.17	1.72	UD	UD	236.91
T _{MB6} with Na ₂ SO ₄ , with UV	20.08	56.32	19.56	3.30	0.75	UD	UD	248.10
pH10								
T _{MB7} no salt, no UV	22.64	58.78	17.12	1.46	UD	UD	UD	47.48
T _{MB8} with NaCl, no UV	23.73	62.32	12.79	1.16	UD	UD	UD	46.85
T _{MB9} with Na ₂ SO ₄ , no UV	23.22	61.92	11.67	UD	UD	3.19	UD	51.17
T _{MB10} no salt, with UV	15.68	47.10	33.02	3.21	0.97	UD	UD	247.70
T _{MB11} with NaCl, with UV	19.59	52.13	21.13	3.02	1.11	3.02	UD	256.32
T _{MB12} with Na ₂ SO ₄ , with UV	20.71	57.03	17.88	3.29	1.09	UD	UD	294.59

UV: UV-irradiation, NA: Not Applicable

Table 4.2: XPS Survey Spectra of elemental composition and Percent Atomic concentration of T_F, T_{MO1}-T_{MO12} of MO

Sample	Ti%	O%	C%	N%	S%	Na%	K%	CPD
T _F	26.28	68.07	4.51	UD	UD	UD	1.14	NA
pH4								
T _{MO1} no salt, no UV	24.72	66.16	9.12	UD	UD	UD	UD	0.00
T _{MO2} with NaCl, no UV	25.31	59.23	5.50	UD	UD	9.96	UD	0.00
T _{MO3} with Na ₂ SO ₄ , no UV	22.95	62.94	6.89	UD	UD	7.22	UD	0.00
T _{MO4} no salt, with UV	25.61	65.67	8.72	UD	UD	UD	UD	349.61
T _{MO5} with NaCl, with UV	25.73	65.49	8.78	UD	UD	UD	UD	404.17
T _{MO6} with Na ₂ SO ₄ , with UV	24.94	66.41	8.65	UD	UD	UD	UD	431.96
pH10								
T _{MO7} no salt, no UV	25.34	67.44	7.22	UD	UD	UD	UD	0.00
T _{MO8} with NaCl, no UV	24.30	63.13	6.48	UD	UD	6.09	UD	0.00
T _{MO9} with Na ₂ SO ₄ , no UV	23.94	64.30	5.43	UD	UD	6.33	UD	0.00
T _{MO10} no salt, with UV	24.35	66.95	8.70	UD	UD	UD	UD	375.17
T _{MO11} with NaCl, with UV	25.22	62.75	7.76	UD	UD	4.27	UD	347.83
T _{MO12} with Na ₂ SO ₄ , with UV	23.99	62.73	7.91	UD	UD	5.37	UD	371.77

UD: Undetected, NA: Not applicable

4.4.2.1 *Percent atomic concentration changes in Titanium (Ti)*

The changes in the composition of fresh TiO₂ when compared with the deactivated sample of MB and MO in Table 4.3 and 4.4 respectively in terms of the Ti are presented, these changes are best expressed when the Ti region is resolved in high resolution spectra and analyzed in terms of the effects of variables UV, pH, added Na₂SO₄, NaCl and how MB cationic dye and MO anionic dye degradation affects nature of adsorbed elements.

UV effect

Methylene blue

In the SS of MB samples in Table 4.1, all samples with UV have obvious highest CPD and most consumed Ti. Generally, UV favors the consumption of Ti.

Methyl orange

In the SS of MO samples in Table 4.2, like in MB samples, all samples with UV have obvious highest CPD and most consumed Ti.

Table 4.3: High Resolution Spectra of Ti2p species on T_F, T_{MB1}-T_{MB12} of MB

Sample	Ti2p								Cumulative Percent Degradation (%)
	TiO ₂		TiO ₂		Ti+		Ti+		
	Atomic concentration (%)	Binding Energy (eV)	Atomic concentration (%)	Binding Energy (eV)	Atomic concentration (%)	Binding Energy (eV)	Atomic concentration (%)	Binding Energy (eV)	
T _F	66.97	458.46	33.03	464.16	UD	NA	UD	NA	NA
pH4									
T _{MB1}	66.83	458.73	33.17	464.42	UD	NA	UD	NA	15.16
T _{MB2}	66.84	458.67	32.66	464.37	UD	NA	UD	NA	24.75
T _{MB3}	66.67	458.67	33.33	464.37	UD	NA	UD	NA	29.72
T _{MB4}	31.74	458.76	15.87	464.76	34.92	458.35	17.47	463.75	247.30
T _{MB5}	67.92	458.55	32.01	464.27	UD	NA	UD	NA	236.91
T _{MB6}	66.67	458.40	33.33	464.12	UD	NA	UD	NA	248.10
pH10									
T _{MB7}	66.93	458.36	31.07	464.01	UD	NA	UD	NA	47.48
T _{MB8}	66.90	458.18	32.10	463.88	UD	NA	UD	NA	46.85
T _{MB9}	66.67	458.38	33.33	464.05	UD	NA	UD	NA	51.12
T _{MB10}	35.03	458.53	17.51	464.16	31.63	457.28	15.83	462.90	247.70
T _{MB11}	66.79	458.39	31.21	464.07	UD	NA	UD	NA	256.32
T _{MB12}	66.56	458.31	33.46	464.02	UD	NA	UD	NA	294.59

UV: Undetected, NA: Not Applicable

Table 4.4: High Resolution Spectra of Ti2p species on T_F, T_{MO1}-T_{MO12} of MO

Sample	Ti2p								Cumulative Percent Degradation (%)
	TiO ₂		TiO ₂		Ti+		Ti+		
	Atomic concentration (%)	Binding Energy (eV)	Atomic concentration (%)	Binding Energy (eV)	Atomic concentration (%)	Binding Energy (eV)	Atomic concentration (%)	Binding Energy (eV)	
T _F	66.97	458.46	33.03	464.16	UD	NA	UD	NA	NA
pH4									
T _{MO1}	66.67	458.67	33.33	464.42	UD	NA	UD	NA	0.00
T _{MO2}	66.66	458.50	33.34	464.25	UD	NA	UD	NA	0.00
T _{MO3}	66.67	458.55	33.33	464.25	UD	NA	UD	NA	0.00
T _{MO4}	66.67	458.65	33.33	464.39	UD	NA	UD	NA	349.61
T _{MO5}	66.66	458.55	33.34	464.36	UD	NA	UD	NA	404.17
T _{MO6}	66.66	458.71	33.34	464.36	UD	NA	UD	NA	431.96
pH10									
T _{MO7}	66.66	458.44	33.34	464.20	UD	NA	UD	NA	0.00
T _{MO8}	66.66	458.44	33.34	464.29	UD	NA	UD	NA	0.00
T _{MO9}	66.66	458.44	33.34	464.12	UD	NA	UD	NA	0.00
T _{MO10}	66.66	458.47	33.34	464.21	UD	NA	UD	NA	375.17
T _{MO11}	66.66	458.51	33.34	464.21	UD	NA	UD	NA	347.83
T _{MO12}	66.66	458.48	33.34	464.23	UD	NA	UD	NA	371.77

UD: Undetected, NA: Not applicable

Generally, the CPD of MO samples with UV were much higher than MB and have the least consumed Ti in SS Table 4.1 and 4.2. It was also observed that MB deactivates (adsorbed faster) the surface faster than MO. Unlike in MB samples, no activity was recorded in no UV samples of MO.

pH effect

It is an established fact that due to point of zero charge (PZC) phenomenon (Kirby, 2010), pH has an effect on the photodegradation efficiency of dyes. Any change in solution pH affects the surface charge of TiO₂ particles and reposition the potentials of the photocatalytic reactions, which will in turn, affect the reaction rate. In alkaline conditions, the surface of titania can be deprotonated (negatively charged) this will attract the mother molecule of a cationic dye (positively charged dye molecule), which is MB in this case, or in acidic conditions, the surface can be protonated (positively charged) and will attract more of the mother molecule of anionic dye (negatively charged dye molecule) in this case MO. This outcome was noticed in Table 4.1 where highest CPD in MB samples were recorded in basic medium, this high CPD was expected (Epling & Lin, 2002). Also, high consumption of Ti in MB (cationic dye) samples in pH10 was noticed. On the other hand, high CPD were recorded in MO samples (Table 4.2) in acidic medium, but the average consumption of Ti in basic and acidic medium were relatively similar. Another observation was that the differences in CPD values within the same dye MO or MB at pH10 and pH4 was not remarkable, as reported by Houas et al., (2001).

NaCl effect

Methylene blue

In XPS SS in Table 4.1, the effect of adding NaCl on Ti in samples in the dark and with UV irradiation at different pH can be compared. It was noticed that there was no

significant difference in the consumption of Ti and amount of CPD. However, in Table 4.3 the HRS of Ti2p in MB, in T_{MB4} (no NaCl, with UV) pH4, total initial two states of T_F, (TiO₂:66.97%) and (TiO₂:33.03%) were transformed into four states (TiO₂:31.74%), (TiO₂:15.87%), (Ti⁺:34.92%) and (Ti⁺:17.47%), similar effect was noted in T_{MB10} (no NaCl, with UV) pH10. The reduction of TiO₂ to Ti⁺ was probably due to coordinatively unsaturated Ti sites formed during reduction and surface reconstruction of anatase TiO₂ particles, when exposed to UV irradiation (Berger et al., 2005) at the terminal OH sites of the surface (Nosaka & Nosaka, 2016). Since charge recombination is dependent on the nature of the TiO₂ colloid (the environment where the surface was excited) (Berger et al., 2005), it is feasible that without NaCl in the TiO₂ colloid, the photogenerated electron reduces Ti⁴⁺ to Ti⁺ at much faster rate than the rate of charge recombination occurring on average of 10⁻¹⁰s (Colombo & Bowman, 1995; Colombo & Bowman, 1996; Serpone et al., 1995).

Methyl orange

In HRS of MO samples in Table 4.4 not much activity was observed on the samples as in MB, where in some samples of MB, TiO₂ was reduced to Ti⁺. This indicate that the addition of NaCl prevented the reduction of TiO₂ to T⁺. The addition of NaCl did not show any significant difference in amounts of Ti, but a reasonable difference in photocatalyst performance, where there was a CPD difference between T_{MO4} (CPD:349.61%) and T_{MO5} (CPD:404.17%), indicating that addition of NaCl may have been the cause of increased in CPD in T_{MO5}.

Na₂SO₄ effect

In samples of both MB and MO in Table 4.1 and Table 4.2 respectively, the presence of Na₂SO₄ in all the samples shows higher CPD in both pH4 and pH10. There was only

one exception in Table 4.2, where a sample in MO with Na₂SO₄, T_{MO12} (CPD:371.77%) has a slightly lower CPD than a sample with added NaCl, T_{MO10} (CPD:375.17%).

Methylene blue

In the SS of MB in Table 4.1, the presence of Na₂SO₄ in all the samples shows higher CPD (even though the difference is not substantial) than in samples with NaCl in both pH4 and pH10. This is because SO₄²⁻ is known to increase the rate of photocatalytic reactions (Anipsitakis & Dionysious, 2003; Lutze et al., 2015).

In Table 4.3 of MB, in the high-resolution spectra of Ti, it was noticed that in samples without salts but with UV (T_{MB4} and T_{MB10}), there was change in Ti oxidative state from TiO₂ to Ti⁺. Therefore, addition of the salts prevented the change in oxidation state in other samples.

Methyl orange

In the SS of MO in Table 4.2, the presence of Na₂SO₄ in sample T_{MO6} assisted in recording the highest CPD:431.96%, when compared to T_{MO4} (CPD: 349.61%), since they have the same condition differing only in presence or absence of Na₂SO₄.

4.4.2.2 Percent atomic concentration changes in Oxygen (O)

There were changes in oxygen from the values in T_F and deactivated TiO₂ samples in XPS survey spectra, as shown in Table 4.1 of MB and 4.2 of MO. The amount of O in all the deactivated samples in MB and MO were seen to decrease (regardless of the reaction conditions) from the initial amount of PAC 68.07% in T_F. This indicates that lower amounts of O in a sample signifies loss of activity at the survey spectra level.

In the XPS SS region of O1s peak is asymmetric, on deconvolution in Table 4.5 for MB and Table 4.6 for MO, the three peaks relate three different chemical states of oxygen

(Jensen et al., 2005), lattice oxygen (metal oxides) O^{2-} averaging around 529.58 eV, peak averaging at around 530.31 eV assigned to OH group and the oxygen-containing species averaged at 531.42 eV. In the HRS in Table 4.5 for MB and Table 4.6 for MO, the increased amount of OH group and oxygen-containing species in deactivated samples of MB and MO were likely due to the reaction products adsorbed onto the deactivated samples (T_{MB1} - T_{MB12}) and (T_{MO1} - T_{MO12}) (Shang et al., 2002).

Table 4.5: High Resolution Spectra of O1s species on T_F, T_{MB1}-T_{MB12} of MB

Sample	O1s								Cumulative Percent Degradation (%)
	TiO2		C-O		C=O		K3PO4		
	Atomic concentration (%)	Binding Energy (eV)	Atomic concentration (%)	Binding Energy (eV)	Atomic concentration (%)	Binding Energy (eV)	Atomic concentration (%)	Binding Energy (eV)	
T _F	77.96	529.62	3.18	531.48	UD	NA	18.85	530.57	NA
pH4									
T _{MB1}	51.45	529.81	39.27	530.21	9.27	531.49	UD	NA	15.16
T _{MB2}	56.74	529.76	34.57	530.23	8.69	531.49	UD	NA	24.75
T _{MB3}	53.07	529.89	37.09	530.25	9.83	531.81	UD	NA	29.72
T _{MB4}	39.55	529.51	51.46	530.04	8.99	531.26	UD	NA	247.30
T _{MB5}	66.63	529.63	25.25	530.28	8.12	531.26	UD	NA	236.91
T _{MB6}	36.14	529.47	53.06	529.81	10.80	531.30	UD	NA	248.10
pH10									
T _{MB7}	46.45	529.55	41.58	530.30	11.97	531.23	UD	NA	47.48
T _{MB8}	67.27	529.78	23.88	530.58	8.86	531.55	UD	NA	46.85
T _{MB9}	41.36	529.46	43.13	529.00	12.92	531.06	UD	NA	51.17
T _{MB10}	33.77	529.06	53.76	530.32	12.47	531.74	UD	NA	247.70
T _{MB11}	55.73	529.55	30.32	530.28	13.95	531.03	UD	NA	256.32
T _{MB12}	45.95	529.47	44.40	530.28	9.65	531.08	UD	NA	294.59

UD: Undetected, NA: Not Applicable

Table 4.6: High Resolution Spectra of O1s species on T_F, T_{MO1}-T_{MO12} of MO

Sample	O1s								Cumulative Percent Degradation (%)
	TiO2		C-O		C=O		K3PO4		
	Atomic concentration (%)	Binding Energy (eV)	Atomic concentration (%)	Binding Energy (eV)	Atomic concentration (%)	Binding Energy (eV)	Atomic concentration (%)	Binding Energy (eV)	
T _F	77.96	529.62	3.18	531.48	UD	NA	18.85	530.57	NA
pH4									
T _{MO1}	54.26	529.78	36.56	530.21	9.19	531.50	UD	NA	0.00
T _{MO2}	49.50	529.77	44.10	530.12	6.40	531.52	UD	NA	0.00
T _{MO3}	61.61	529.74	28.57	530.12	9.81	531.31	UD	NA	0.00
T _{MO4}	50.96	529.79	42.50	530.12	6.55	531.61	UD	NA	349.61
T _{MO5}	66.39	529.75	26.17	530.12	7.44	531.35	UD	NA	404.17
T _{MO6}	54.12	529.82	35.67	530.12	10.22	531.53	UD	NA	431.96
pH10									
T _{MO7}	72.17	529.68	18.15	530.12	9.67	531.19	UD	NA	0.00
T _{MO8}	73.74	529.69	17.52	530.12	8.74	531.20	UD	NA	0.00
T _{MO9}	85.42	529.63	5.42	530.93	9.16	531.04	UD	NA	0.00
T _{MO10}	86.89	529.68	6.94	530.70	6.17	531.52	UD	NA	375.17
T _{MO11}	88.60	529.72	6.74	530.86	4.65	531.62	UD	NA	347.83
T _{MO12}	87.16	529.75	8.87	531.03	3.97	531.87	UD	NA	371.77

UD: Undetected, NA: Not applicable

As metal oxides fall within the range of 529-530eV, a metal oxide impurity K₃PO₄ was seen in T_F due to original material, later displaced in the lattice of all the deactivated samples (T_{MB1}-T_{MB12}) and (T_{MO1}-T_{MO12}) by C-O averaging 530.31eV.

In T_F in Table 4.5 of MB and 4.6 of MO, no C=O only C-O was detected at relatively higher energy of 531.48eV, after degradation, the metal carbonates C=O were detected at average of 531.5eV in all samples (T_{MB1}-T_{MB12}) and (T_{MO1}-T_{MO12}). This indicates that new carbon species of C=O have been adsorbed.

UV effect

In the XPS SS in Table 4.1 of MB and Table 4.2 of MO, samples with UV irradiation in both pH4 and pH10 showed high CPD. This outcome is as expected because UV irradiation generates the needed •OH for the degradation reactions.

pH effect

Methylene blue

In HRS in Table 4.5 the contribution of O²⁻ in T_F was 77.96%. After deactivation, there was O²⁻ decrease in all the deactivated samples in both pH4 and pH10. This shows that regardless of pH difference, there was decrease in O²⁻.

Methyl orange

In HRS in Table 4.6, a different pattern was observed in MO. In all samples in pH4, O²⁻ was seen to reduce in all samples, but in some samples in pH10, T_{MO9} (O²⁻:85.42%), T_{MO10} (O²⁻:86.89%), T_{MO11} (O²⁻:88.60%) and T_{MO12} (O²⁻:87.16%), there was regeneration (increase) in O²⁻ including in T_{MO9} (a sample in the dark). The possibility of regeneration of O²⁻ on TiO₂ was reported in (Bharti et al., 2016; Lee & Falconer, 2000; Muggli & Falconer, 2000). It occurred when O₂ from the bulk diffuse into the TiO₂

surface to replenish the new surface oxygen vacancies created by formic acid. Unfortunately, the O^{2-} regeneration did not increase the CPD above values in other samples where O^{2-} regeneration was not observed. This outcome is not unexpected because regeneration have not been shown to enhance the performance of TiO_2 surface, only creation of defect sites either by lattice oxygen extraction (lattice oxygen extraction was reported delay TiO_2 deactivation (Muggli & Falconer, 2000)). There is a possibility that if the reactions were allowed to proceed longer than 60h, samples with O^{2-} regeneration might last longer than samples without regeneration. Also noticed a marked reduction in C-O in the samples with regenerated O^{2-} possibly due to displacement of earlier adsorbed CO_2 by O (Lee & Falconer, 2000).

NaCl effect

Methylene Blue

In the XPS HRS of Table 4.5 of MB, it was noted in samples with UV but no NaCl T_{MB4} and T_{MB10} the amount of O^{2-} has significantly decreased (up to 50% decrease) while the CPD was substantially high, averaged among the highest, this shows that the low amount of O^{2-} is not responsible for low CPD. On the other hand, one can conclude that the addition of NaCl both in UV (as UV seems to accelerate the consumption O^{2-}) and in the dark, minimizes the consumption of O^{2-} . In samples with NaCl the integrity (PAC) of lattice oxygen was maintained.

Methyl orange

The addition of NaCl did not show any significant influence on the PAC in XPS SS Tables 4.2 and 4.6 only that it is among the samples with high CPD.

Na₂SO₄ effect

Methylene Blue

In Table 4.1 of XPS SS, the addition of Na₂SO₄, did not demonstrate significant increase or decrease in PAC only that it is among the samples with the highest CPD in UV setup.

Methyl orange

In Table 4.2, the effect of Na₂SO₄ was responsible for highest CPD in UV irradiated sample in pH4 T_{MB6} (CPD:431.96%), but generally, the effect of Na₂SO₄ in both pH4 and pH10 was not very significant among the samples.

4.4.2.3 Percent atomic concentration changes in Carbon (C)

In this section, it is expected that the amount of adsorbed carbon will increase from the amounts available on T_F due to the deposit of new carbon species often associated with deactivation.

In Table 4.2 of MO in the XPS SS of C1s, there was increase in carbon species in all the deactivated samples (T_{MO1}-T_{MO12}) from initial value in T_F (C:4.51%), but the increase is not as much as the increase in MB samples in Table 4.1 (T_{MB1}-T_{MB12}). This indicates that generally, the low performance of the photocatalyst in MB is due to high amounts of adsorbed C in the shortest reaction time.

Table 4.7: High Resolution Spectra of C1s species on T_F, T_{MB1}-T_{MB12} of MB

Sample	C1s										Cumulative Percent Degradation (%)
	C-C		C-O		C-N, C-O		C=O		C=O, N-C		
	Atomic concentration (%)	Binding Energy (eV)	Atomic concentration (%)	Binding Energy (eV)	Atomic concentration (%)	Binding Energy (eV)	Atomic concentration (%)	Binding Energy (eV)	Atomic concentration (%)	Binding Energy (eV)	
T _F	74.97	284.69	25.02	285.84	UD	NA	UD	NA	UD	NA	NA
pH4											
T _{MB1}	82.84	284.88	UD	NA	13.74	286.17	UD	NA	3.42	289.09	15.16
T _{MB2}	76.45	284.80	18.17	286.27	UD	NA	5.38	289.05	UD	NA	24.75
T _{MB3}	82.47	284.82	11.96	286.31	UD	NA	5.57	288.80	UD	NA	29.72
T _{MB4}	55.56	284.49	UD	NA	39.45	285.56	UD	NA	5.00	288.07	247.30
T _{MB5}	78.89	284.76	UD	NA	16.27	285.99	UD	NA	4.84	287.92	236.91
T _{MB6}	58.89	284.76	UD	NA	32.94	285.99	UD	NA	8.17	287.47	248.10
pH10											
T _{MB7}	89.13	284.72	UD	NA	6.51	286.96	UD	NA	4.36	289.15	47.48
T _{MB8}	73.16	284.34	UD	NA	22.20	285.67	UD	NA	4.64	288.49	46.85
T _{MB9}	75.77	284.62	17.11	285.93	UD	NA	7.12	287.98	UD	NA	51.17
T _{MB10}	54.56	284.41	UD	NA	41.24	285.66	UD	NA	4.20	287.83	247.70
T _{MB11}	74.84	284.71	UD	NA	20.02	286.29	UD	NA	5.13	288.59	256.32
T _{MB12}	63.20	284.71	UD	NA	28.89	285.54	UD	NA	7.91	286.90	294.59

UD: Undetected, NA: Not applicable

Table 4.8: High Resolution Spectra of C1s species on T_F, T_{MO1}-T_{MO12} of MO

Sample	C1										
	C-C		C-O		C-N, C-O		C=O		C=O, N-C		Cumulative Percent Degradation (%)
	Atomic concentration (%)	Binding Energy (eV)	Atomic concentration (%)	Binding Energy (eV)	Atomic concentration (%)	Binding Energy (eV)	Atomic concentration (%)	Binding Energy (eV)	Atomic concentration (%)	Binding Energy (eV)	
T _F	74.97	284.69	25.02	285.84	UD	NA	UD	NA	UD	NA	NA
pH4											
T _{MO1}	83.09	284.74	11.19	286.31	UD	NA	5.72	288.99	UD	NA	0.00
T _{MO2}	65.01	284.53	27.14	285.69	UD	NA	7.85	288.78	UD	NA	0.00
T _{MO3}	75.75	284.62	19.20	285.86	UD	NA	5.05	288.83	UD	NA	0.00
T _{MO4}	78.75	284.71	13.99	286.15	UD	NA	7.26	288.85	UD	NA	349.61
T _{MO5}	74.36	284.69	17.50	286.01	UD	NA	8.14	288.90	UD	NA	404.17
T _{MO6}	76.16	284.78	16.45	286.23	UD	NA	7.39	288.95	UD	NA	431.96
pH10											
T _{MO7}	78.30	284.67	16.22	285.99	UD	NA	5.48	288.77	UD	NA	0.00
T _{MO8}	70.73	284.67	18.43	286.15	UD	NA	10.84	288.88	UD	NA	0.00
T _{MO9}	79.48	284.70	11.79	286.21	UD	NA	8.72	288.81	UD	NA	0.00
T _{MO10}	81.15	284.68	12.57	286.24	UD	NA	6.28	288.75	UD	NA	375.17
T _{MO11}	83.79	284.79	8.68	286.33	UD	NA	7.52	288.79	UD	NA	347.83
T _{MO12}	80.15	284.77	12.18	286.38	UD	NA	7.67	288.88	UD	NA	371.77

UD: Undetectable, NA: Not applicable

In the XPS HRS of C1s in MB, in Table 4.7, initially there was only C-C (atmospheric or adventitious carbon) and C-O in T_F, after degradation, there were shifts in the C-O as it bonded with N, emitting C-N and C-O signals from the C-O region. The initial amount of C-O (25.02%) in T_F were seen to have decreased in all MB samples except in samples with UV or both UV and Na₂SO₄, where an increase in C-O or its derivative C=O, C-N were seen. This shows that more of these carbon species were adsorbed because of UV and Na₂SO₄. On the other hand, C-O was seen to have reduced constantly in all the samples in MO except in T_{MO2} (C-O:27.14%). Additionally, there was formation of C=O or its derivative C=O, C-N (amides N-C=O) in all MB samples in Table 4.7. Similarly, in the XPS HRS of C1s in MO, in Table 4.8, C=O signal was detected in all samples (T_{MO1}-T_{MO12}) but no C-N. This has shown that each reaction products are unique to reaction conditions. It was also observed that the rate at which the intermediates and the possible end product like CO₂ get dissolve in solution and adsorbed on TiO₂ determines the rate of deactivation. The more the •OH is generated the faster it breaks the bonds in the intermediates (as they convert to CO₂) and other products and prevents their adsorption on the TiO₂ surface. As time progresses depending on the reaction conditions, the photogenerated holes become less in number and gradually the catalyst losses activity.

UV effect

Methylene Blue

In Table 4.1 of XPS SS of MB, samples with UV, with highest amount of absorbed C have the highest CPD. It was noticed that those with low amount of C, with lowest CPD lost their activity faster.

Methyl orange

In Table 4.2 of XPS SS of MO, samples with UV have relatively higher amount of adsorbed carbon except in T_{MO1} despite being without UV irradiation it records the highest amount of (C:9.12%). This could be due to physisorption of higher molecular weight carbon species.

pH effect

Methylene blue

In Table 4.1 of SS of MB, the highest CPD were recorded in pH10 agreeing with literature (Baran et al., 2008; Epling & Lin, 2002) that cationic dye solution degrades better in basic pH, because the TiO₂ surface is more negatively charged thereby the few positively charged mother dye molecules that are directly attracted to the surface, gets degraded and adds to the overall increase in degradation rate. The highest amount of C deposit was seen in T_{MB10} (C:33.02%) in pH10, this amount was considerably higher than the remaining samples, but CPD in this sample (CPD:247.70%) was found to be third highest. The high amount of C deposit was probably caused by absence of NaCl or Na₂SO₄.

Methyl orange

In Table 4.2 of XPS SS of MB, the highest CPD were recorded in pH4 agreeing with (Baran et al., 2008; Epling & Lin, 2002) that in pH4 anionic dyes are more degraded.

NaCl effect

Methylene blue

There was no distinct effect of NaCl in MB in both SS and HRS of C.

Methyl orange

In the XPS HRS of C in MO in Table 4.8, samples T_{MO2} (65.01%) pH4 no UV and T_{MO8} (70.73%) pH10 no UV both with NaCl showed the lowest amounts of C-C. In the same HRS Table 4.8, all the samples showed decrease in C-O except T_{MO2} (C-O:27.14%) with NaCl pH4 no UV, not only it shows increase in C-O, the C-O amount was unusually high, higher than in T_F (C-O:25.02%). This increase was attributed to the presence of NaCl since sample T_{MO1} with the same set up but no NaCl, no such effect was seen. Also, worth noting in Table 4.2 is the low amount of adsorbed carbon in samples with NaCl in the dark, T_{MO2} (C:5.50%) pH4 and T_{MO8} (C:6.48%) pH10 despite the zero degradation. This suggests predominantly physisorption of large molecules.

Na₂SO₄ effect

Methylene blue

In Table 4.1 of the XPS SS it was noted that in samples with no UV in both pH4 and pH10, those with Na₂SO₄ have shown relatively less amounts of adsorbed carbon in the samples. In same MB Table 4.1, in pH10 in samples with UV, the amount of C in T_{MB10} (C:33.02%) was seen to double T_{MB12} (17.88%), the less amount of C in T_{MB12} might have been the cause of higher CPD in T_{MB12} than T_{MB10}. Suggesting the earlier positive influence of SO₄²⁻ in the photodegradation (Anipsitakis & Dionysious, 2003). Additionally, in MB samples, samples with Na₂SO₄ had the highest C=O deposit or its derivative than in other samples.

Methyl orange

The XPS SS in Table 4.2 lowest absorbed C was recorded in T_{MO9} (C:5.43%) due to Na₂SO₄.

4.4.2.4 Percent atomic concentration changes in Nitrogen (N)

Houas et al., (2001) observed that in the photodegradation of MB, ammonium ions were the initial nitrogen-containing ions formed. NH_4^+ ions were then slowly oxidized to nitrate ions (maximum oxidation state of nitrogen (+5)) and they attribute this to the molecular structure of MB having all the three nitrogen atoms in the -3 oxidation state. They further observed that nitrogen retained its initial (-3) oxidation state because the amino groups were not involved in reactions at the initial step of MB and attribute the higher amount of ammonium and nitrate ions to the stoichiometric ratio $\text{N/S} = 3$ in the initial MB molecule.

While in the photodegradation of MO, from the LC-MS results, (Sheikh et al., 2016) a pathway beginning from the addition of a hydroxyl group to MO mainly in ortho positions to azo and $\text{N}(\text{CH}_3\text{CH}_3)$ groups (Baiocchi et al., 2002), further hydroxylation generates intermediates involving N that has been completely demethylated, possibly to minute quantities of nitrates (NO_3^-), principle reason N atom was not detected in the XPS or FTIR on the deactivated MO samples. Since the nature of the adsorbed species on the deactivated MO samples reflects the type of the intermediates and final products in MO photodegradation, possible products were free NO_2 , H_2O and CO_2 . The photodegradation pathway of both MB and MO provides an insight into what to expect on the surface of deactivated TiO_2 samples.

UV effect

Methylene blue

In Table 4.9 of XPS HRS, samples with UV in both pH4 and pH10 have shown relatively higher deposits of amides (N-C=O), methanamide, than those without UV irradiation. Indicating that UV irradiation favor the generation of more amides on the surface. But the N^+ (organic ammonium ion) have highest values in T_{MB1} (30.01%) T_{MB8}

(25.08%) non UV irradiated samples, while all the samples with UV also have available N^+ , the values are lower than in non UV irradiated samples.

Table 4.9: High Resolution Spectra of N1s species on T_F, T_{MB1}-T_{MB12} of MB

Sample	N1s				Cumulative Percent Degradation (%)
	N-C=O		N+		
	Atomic concentration (%)	Binding Energy (eV)	Atomic concentration (%)	Binding Energy (eV)	
T _F	UD	NA	UD	NA	NA
pH4					
T _{MB1}	69.99	399.66	30.01	402.30	15.16
T _{MB2}	UD	NA	UD	NA	24.75
T _{MB3}	UD	NA	UD	NA	29.72
T _{MB4}	80.78	399.34	19.22	401.28	247.30
T _{MB5}	79.77	399.36	20.23	401.65	236.91
T _{MB6}	80.57	399.18	19.43	401.08	248.10
pH10					
T _{MB7}	81.78	399.33	18.22	401.02	47.48
T _{MB8}	74.92	399.28	25.08	401.02	46.85
T _{MB9}	UD	NA	UD	NA	51.17
T _{MB10}	91.75	398.69	8.25	400.39	247.70
T _{MB11}	93.83	399.31	6.17	402.09	256.32
T _{MB12}	83.78	399.20	16.22	401.46	294.59

UD: Undetected, NA: Not applicable

Table 4.10: High Resolution Spectra of N1s species on T_F, T_{MO1}-T_{MO12} of MO

Sample	N1s				Cumulative Percent Degradation (%)
	N-C=O		N+		
	Atomic concentration (%)	Binding Energy (eV)	Atomic concentration (%)	Binding Energy (eV)	
T _F	UD	NA	UD	NA	NA
pH4					
T _{MO1}	UD	NA	UD	NA	0.00
T _{MO2}	UD	NA	UD	NA	0.00
T _{MO3}	UD	NA	UD	NA	0.00
T _{MO4}	UD	NA	UD	NA	349.61
T _{MO5}	UD	NA	UD	NA	404.17
T _{MO6}	UD	NA	UD	NA	431.96
pH10					
T _{MO7}	UD	NA	UD	NA	0.00
T _{MO8}	UD	NA	UD	NA	0.00
T _{MO9}	UD	NA	UD	NA	0.00
T _{MO10}	UD	NA	UD	NA	375.17
T _{MO11}	UD	NA	UD	NA	347.83
T _{MO12}	UD	NA	UD	NA	371.77

UD: Undetected, NA: Not applicable

Methyl orange

No N was absorbed on the samples, possibly the N products have vaporized as free NO₂.

pH effect

Methylene blue

pH10 was seen to favor the adsorption of N-C=O where all the values were higher than in pH4.

NaCl effect

Methylene blue

In the XPS SS of Table 4.1, if no volatile components containing S and N are assumed, the ratio of N/S adsorbed, should always be 3. However, the N/S ratio in the samples is not always 3, showing that the N/S of adsorbed N and S species is dependent on the experimental conditions. Also, the formation of ammonium and nitrate ions varies and does not strictly corresponds to the stoichiometric ratio. Additionally, does not significantly affect the overall performance as can be observed in the CPD values.

Methyl orange

Nitrogen was not detected on MO samples because it might have evaporated as NO₂.

Na₂SO₄ effect

Methylene blue

In Table 4.1 SS, T_{MB6} and T_{MB12} samples with added Na₂SO₄ have the highest CPD (294.59%). The addition of Na₂SO₄ was seen to increase the value of CPD. However, it was not seen to significantly affect the overall value of adsorbed N in the samples.

Methyl orange

No N was detected on deactivated samples.

4.4.2.5 Percent atomic concentration changes in Sulfur (S)

Houas et al., (2001) observed the evolution of sulfate ion were also among the initial products formed in photodegradation of MB. Heteroatom S goes through a direct oxidation from -2 to the highest final stable oxidation degree +6 in sulfate ions (SO₄²⁻). They also agreed with (Herman et al., 2003; Herrmann et al., 2002) that the amount of sulfate ions released is lower than expected from stoichiometry and reasoned that the most probable explanation for the low quantity of SO₄²⁻ is the partially irreversible adsorption of some SO₄²⁻ ions on TiO₂ surface. Unfortunately, in the deconvoluted HRS in this work, SO₄²⁻ was not detected only sulfite (SO₃), sulfur dioxide (SO₂), disulfur dinitride (S₂N₂) species were detected.

While in the photodegradation of MO, from the LC-MS results, (Sheikh et al., 2016) a pathway beginning from the addition of a hydroxyl group to MO mainly in ortho positions to azo and N(CH₃CH₃) groups, then the introduction of the second hydroxyl group in the ring containing the SO₃⁻ (Baiocchi et al., 2002) generates intermediates. The nature of the adsorbed species on the deactivated MO samples reflects the type of the intermediates and final products in the MO degradation. The generation of SO₃⁻ in its gaseous form will reduce its chances of being adsorbed, hence no S atom was detected in the XPS or FTIR analysis. Though other intermediates in minute amounts might be present in the solution after degradation (at the time of filtration of the colloid) none was

captured on XPS and FTIR analysis.

Table 4.11: High Resolution Spectra of S2p species on T_F, T_{MB1}-T_{MB12} of MB

Sample	S2p														Cumulative Percent Degradation (%)
	SO3 3/2		SO3 ½		SO2 3/3		SO2 1/2		SO2 3/2		S2N2 3/2		S2N2 1/2		
	Atomic conc. (%)	Binding Energy (eV)	Atomic conc. (%)	Binding Energy (eV)	Atomic conc. (%)	Binding Energy (eV)	Atomic conc. (%)	Binding Energy (eV)	Atomic conc. (%)	Binding Energy (eV)	Atomic conc. (%)	Binding Energy (eV)	Atomic conc. (%)	Binding Energy (eV)	
T _F	UD	NA	UD	NA	UD	NA	UD	NA	UD	NA	UD	NA	UD	NA	NA
pH4															
T _{MB1}	UD	NA	UD	NA	UD	NA	UD	NA	UD	NA	UD	NA	UD	NA	15.16
T _{MB2}	UD	NA	UD	NA	UD	NA	UD	NA	UD	NA	UD	NA	UD	NA	24.75
T _{MB3}	UD	NA	UD	NA	UD	NA	UD	NA	UD	NA	UD	NA	UD	NA	29.72
T _{MB4}	UD	NA	UD	NA	UD	NA	UD	NA	UD	NA	66.66	163.51	33.34	164.96	247.30
T _{MB5}	38.92	163.53	18.18	167.54	28.60	164.85	14.30	170.32	UD	NA	UD	NA	UD	NA	236.91
T _{MB6}	UD	NA	UD	NA	UD	NA	UD	NA	UD	NA	66.66	163.73	33.34	164.90	248.10
pH10															
T _{MB7}	UD	NA	UD	NA	UD	NA	UD	NA	UD	NA	UD	NA	UD	NA	47.48
T _{MB8}	UD	NA	UD	NA	UD	NA	UD	NA	UD	NA	UD	NA	UD	NA	46.85
T _{MB9}	UD	NA	UD	NA	UD	NA	UD	NA	UD	NA	UD	NA	UD	NA	51.17
T _{MB10}	UD	NA	UD	NA	UD	NA	UD	NA	UD	NA	64.59	163.13	35.41	164.55	247.70
T _{MB11}	51.08	163.73	24.56	164.60	UD	NA	8.55	169.23	15.81	167.39	UD	NA	UD	NA	256.32
T _{MB12}	UD	NA	UD	NA	UD	NA	UD	NA	UD	NA	66.69	163.68	33.31	164.83	294.59

UD: Undetected, NA: Not applicable

Table 4.12: High Resolution Spectra of S2p species on T_F, T_{MO1}-T_{MO12} of MO

Samples	S2p														Cumulative Percent Degradation (%)
	SO3 3/2		SO3 1/2		SO2 3/3		SO2 1/2		SO2 3/2		S2N2 3/2		S2N2 1/2		
	Atomic conc. (%)	Binding Energy (eV)	Atomic conc. (%)	Binding Energy (eV)	Atomic conc. (%)	Binding Energy (eV)	Atomic conc. (%)	Binding Energy (eV)	Atomic conc. (%)	Binding Energy (eV)	Atomic conc. (%)	Binding Energy (eV)	Atomic conc. (%)	Binding Energy (eV)	
T _F	UD	NA	UD	NA	UD	NA	UD	NA	UD	NA	UD	NA	UD	NA	NA
pH4															
T _{MO1}	UD	NA	UD	NA	UD	NA	UD	NA	UD	NA	UD	NA	UD	NA	0.00
T _{MO2}	UD	NA	UD	NA	UD	NA	UD	NA	UD	NA	UD	NA	UD	NA	0.00
T _{MO3}	UD	NA	UD	NA	UD	NA	UD	NA	UD	NA	UD	NA	UD	NA	0.00
T _{MO4}	UD	NA	UD	NA	UD	NA	UD	NA	UD	NA	UD	NA	UD	NA	349.61
T _{MO5}	UD	NA	UD	NA	UD	NA	UD	NA	UD	NA	UD	NA	UD	NA	404.17
T _{MO6}	UD	NA	UD	NA	UD	NA	UD	NA	UD	NA	UD	NA	UD	NA	431.96
pH10															
T _{MO7}	UD	NA	UD	NA	UD	NA	UD	NA	UD	NA	UD	NA	UD	NA	0.00
T _{MO8}	UD	NA	UD	NA	UD	NA	UD	NA	UD	NA	UD	NA	UD	NA	0.00
T _{MO9}	UD	NA	UD	NA	UD	NA	UD	NA	UD	NA	UD	NA	UD	NA	0.00
T _{MO10}	UD	NA	UD	NA	UD	NA	UD	NA	UD	NA	UD	NA	UD	NA	375.17
T _{MO11}	UD	NA	UD	NA	UD	NA	UD	NA	UD	NA	UD	NA	UD	NA	347.83
T _{MO12}	UD	NA	UD	NA	UD	NA	UD	NA	UD	NA	UD	NA	UD	NA	371.77

UD: Undetected, NA: Not applicable

UV effect

Methylene blue

In the XPS SS analysis carried out and calculated cumulative degradation in Table 4.1 for MB it was observed that there were amounts of S species in all the samples with UV in MB. In HRS of S2p in Table 4.11, some of the samples T_{MB4}, T_{MB6}, T_{MB10} and T_{MB12} adsorbed dinitrogen disulfide (S₂N₂), while T_{MB5} and T_{MB11} adsorbed sulfur trioxide and sulfur dioxide. These samples with adsorbed species have the highest CPD. Highest CPD was recorded at T_{MB12} a sample with added Na₂SO₄, indicating that presence of Na₂SO₄ favors the degradation reactions. Another observation was that, the CPD in MB is lower than CPD in MO this is possibly due to higher molecular mass of sulfate derivatives in the MB samples. The blockage of active sites of MB was not only by the carbon species, but was made more profound due to S derivatives, whose combine effect will be higher than the carbon species in MO samples.

Methyl orange

There was no S detected in the MO samples possibly due to generation of free SO₃⁻.

pH effect

pH has effect on the type and amount of adsorbed species in Table 4.11 and can be seen at HRS, where T_{MB11} pH10 has higher amount of SO_{33/2} (51.08%) than T_{MB5} pH4 (38.92%) and T_{MB11} SO_{3 1/2} (24.56%) higher than T_{MB5} (18.18%) but SO_{21/2} (14.30%) was higher in T_{MB5} than in T_{MB11} (8.55%). It is important to note that in T_{MB5} no SO_{23/2} was detected and in T_{MB11} no SO_{2 3/3} was detected showing that considering the differential pH the amount of species can differ.

NaCl effect

It can also be reasoned that the absence of NaCl lead to the adsorption of dinitrogen disulfide in T_{MB4} and T_{MB10} while in T_{MB5} and T_{MB11} there was adsorption of sulfur oxide compounds and no dinitrogen disulfides, indicating that NaCl can alter the type of S species adsorbed on the photocatalyst surface.

Na₂SO₄ effect

Methylene blue

The presence of Na₂SO₄ lead to the adsorption of dinitrogen disulfide in T_{MB6} and T_{MB12}. Na₂SO₄ can alter the type of S species adsorbed on the photocatalyst surface. Additionally, samples with Na₂SO₄ have highest CPD.

Methyl orange

Unlike in MB Table 4.11, where different species were adsorbed due to added salt NaCl; in T_{MB4} lead to the adsorption of only dinitrogen disulfide, and in T_{MB5} sulfite and sulfur dioxide were adsorbed. In Table 4.12, both T_{MO4} and T_{MO5} have identical adsorbed products despite the addition of Na₂SO₄ in T_{MO5}. Showing that Na₂SO₄ does not seem to have any effect in the nature of the adsorbed species in MO, except having the highest CPD in T_{MO12} (CPD:371.77%%) (samples with both UV irradiation and Na₂SO₄).

4.4.2.6 Percent atomic concentration changes in Sodium (Na)

The presence of Na on some of deactivated samples was expected due to added Na⁺ salts in the reacting mixture. In the SS of Table 4.1 of MB Na1s was detected in only two samples with added salts (NaCl or Na₂SO₄) T_{MO9} (Na: 3.19%) and T_{MO11} (Na:3.02%). But no Na was detected in other samples with added salts.

Contrary to the low adsorption of Na in MB samples, in Table 4.14 of MO, the amount of adsorbed Na was available in all samples with added salts except T_{MO5} and T_{MO6}. Also, MO samples have much higher amounts of adsorbed Na than the amounts in MB. It can be inferred that the higher amounts of Na in MO were not only due to the added Na⁺ from the added salts, it was also from the Na⁺ from the structural formula of MO. It was evident that the Na ions in the colloid can get absorbed on the photocatalyst surface but did not seem to have unique effect on the CPD.

Table 4.13: High Resolution Spectra of Na1s species on T_F, T_{MB1}-T_{MB12} of MB

Samples	Na1s						Cumulative Percent Degradation (%)
	Na1s		TiLMM		TiLMM		
	Atomic concentration (%)	Binding Energy (eV)	Atomic concentration (%)	Binding Energy (eV)	Atomic concentration (%)	Binding Energy (eV)	
T _F	UD	NA	UD	NA	UD	NA	NA
pH4							
T _{MB1}	UD	NA	UD	NA	UD	NA	15.16
T _{MB2}	UD	NA	UD	NA	UD	NA	24.75
T _{MB3}	UD	NA	UD	NA	UD	NA	29.72
T _{MB4}	UD	NA	UD	NA	UD	NA	247.30
T _{MB5}	UD	NA	UD	NA	UD	NA	236.91
T _{MB6}	UD	NA	UD	NA	UD	NA	248.10
pH10							
T _{MB7}	UD	NA	UD	NA	UD	NA	47.48
T _{MB8}	UD	NA	UD	NA	UD	NA	46.85
T _{MB9}	51.36	1071.67	27.32	1066.86	21.32	1074.78	51.17
T _{MB10}	UD	NA	UD	NA	UD	NA	247.70
T _{MB11}	100	1071.98	UD	NA	UD	NA	256.32
T _{MB12}	UD	NA	UD	NA	UD	NA	294.59

UD: Undetected, NA: Not applicable

Table 4.14: High Resolution Spectra of Na1s species on T_F, T_{MO1}-T_{MO12} of MO

Samples	Nals						Cumulative Percent Degradation (%)
	Nals		TiLMM		TiLMM		
	Atomic concentration (%)	Binding Energy (eV)	Atomic concentration (%)	Binding Energy (eV)	Atomic concentration (%)	Binding Energy (eV)	
T _F	UD	UD	UD	UD	UD	UD	NA
pH4							
T _{MO1}	UD	NA	UD	NA	UD	NA	0.00
T _{MO2}	41.77	1071.77	34.07	1067.15	24.16	1075.33	0.00
T _{MO3}	41.77	1071.77	34.07	1067.15	24.16	1075.33	0.00
T _{MO4}	UD	NA	UD	NA	UD	NA	349.61
T _{MO5}	UD	NA	UD	NA	UD	NA	404.17
T _{MO6}	UD	NA	UD	NA	UD	NA	431.96
pH10							
T _{MO7}	UD	NA	UD	NA	UD	NA	0.00
T _{MO8}	51.27	1071.66	29.51	1068.24	19.22	1074.26	0.00
T _{MO9}	49.03	1071.57	30.07	1067.77	20.90	1074.26	0.00
T _{MO10}	UD	NA	UD	NA	UD	NA	375.17
T _{MO11}	43.97	1071.61	35.92	1068.04	20.11	1074.24	347.83
T _{MO12}	41.43	1071.61	38.39	1067.99	20.18	1074.24	371.77

UD: Undetected, NA: Not applicable

Considering the HRS of Na, even though there was no high concentration of Ti in the colloid, in HRS of Table 4.13 of MB, Na1s and overlapping regions Ti LMM auger peaks were detected in sample T_{MB9}. But more overlaps were detected in Table 4.14 of MO, (detected in T_{MO2}, T_{MO3}, T_{MO8}, T_{MO9}, T_{MO11} and T_{MO12}). Curiously, identical amounts of Na1s and Ti LMM were detected in T_{MO2} and T_{MO3}.

UV effect

Methylene blue

Na was detected only in sample T_{MB9} and T_{MB11}, UV irradiation was not seen to have significant effect on Na adsorption.

Methyl orange

Na was adsorbed in T_{MO2}, T_{MO3}, T_{MO8}, T_{MO9}, T_{MO11} and T_{MO12} (both samples with UV and no UV irradiation) implying Na adsorption was not only unique to UV irradiated samples.

pH effect

Methylene blue

In the SS of Na1s in Table 4.1, it was obvious that pH10 generates environment with the highest range of different and unique depositions like Na1s including high CPD, that the highest degradation was at pH10 and was partly responsible for making the adsorption of Na on the surface. Guillard et al., (2005) inferred that the photoactivity inhibition of different salts including NaCl, was the same if maintained within the basic pH range but differs in acidic pH by increasing with increase in acidity.

Methyl orange

In the SS of NaI in Table 4.2, there were four samples with adsorbed Na in pH10 T_{MO8}, T_{MO9}, T_{MO11} and T_{MO12} unlike in pH4 with only two samples T_{MO2} and T_{MO3}, the pH can determine the adsorption of Na. pH10 allows for more adsorbed species.

NaCl effect

Methylene blue

In the observed XPS SS Table 4.1, the unique effect of NaCl was to cause adsorption of Na in sample T_{MB11}.

Methyl orange

In the SS Table 4.2, all samples with NaCl regardless of whether there is UV or no UV irradiation, pH4 or pH10 induced adsorption of Na except in T_{MO5}.

Na₂SO₄ effect

Methylene blue

In Table 4.1, T_{MB9} though in the dark, showed adsorption (physisorption) of Na which was perhaps due to the effect of addition of Na₂SO₄.

Methyl orange

In Table 4.2, all samples with Na₂SO₄ T_{MO3} and T_{MO9} (both in the dark) and T_{MO12} though with UV irradiation, except T_{MO6}, show the adsorption of Na, which was perhaps due to the effect of addition of Na₂SO₄.

4.4.2.7 Percent atomic concentration changes in Potassium (K)

More often than not, impurities are encountered in the original samples. In T_F there was presence of potassium as an impurity, but its percentage (K:1.14%), in the fresh TiO₂ was not enough to cause any effect on the overall outcome of the reactions.

Table 4.15: High Resolution Spectra of K2p species on T_F, T_{MO1}-T_{MO12} of MB

Samples	K2p				Cumulative Percent Degradation (%)
	K3PO4		K3PO4		
	Atomic concentration (%)	Binding Energy (eV)	Atomic concentration (%)	Binding Energy (eV)	
T _F	66.37	293.12	33.63	295.86	NA
pH4					
T _{MB1}	UD	NA	UD	NA	15.16
T _{MB2}	UD	NA	UD	NA	24.75
T _{MB3}	UD	NA	UD	NA	29.72
T _{MB4}	UD	NA	UD	NA	247.30
T _{MB5}	UD	NA	UD	NA	236.91
T _{MB6}	UD	NA	UD	NA	248.10
pH10					
T _{MB7}	UD	NA	UD	NA	47.48
T _{MB8}	UD	NA	UD	NA	46.85
T _{MB9}	UD	NA	UD	NA	51.17
T _{MB10}	UD	NA	UD	NA	247.70
T _{MB11}	UD	NA	UD	NA	256.32
T _{MB12}	UD	NA	UD	NA	294.59

UD: Undetected, NA: Not applicable

Table 4.16: High Resolution Spectra of K2p species on T_F, T_{MO1}-T_{MO12} of MO

Samples	K2p				Cumulative Percent Degradation (%)
	K3PO4		K3PO4		
	Atomic concentration (%)	Binding Energy (eV)	Atomic concentration (%)	Binding Energy (eV)	
T _F	66.37	293.12	33.63	295.86	NA
pH4					
T _{MO1}	UD	NA	UD	NA	0.00
T _{MO2}	UD	NA	UD	NA	0.00
T _{MO3}	UD	NA	UD	NA	0.00
T _{MO4}	UD	NA	UD	NA	349.61
T _{MO5}	UD	NA	UD	NA	404.17
T _{MO6}	UD	NA	UD	NA	431.96
pH10					
T _{MO7}	UD	NA	UD	NA	0.00
T _{MO8}	UD	NA	UD	NA	0.00
T _{MO9}	UD	NA	UD	NA	0.00
T _{MO10}	UD	NA	UD	NA	375.17
T _{MO11}	UD	NA	UD	NA	347.83
T _{MO12}	UD	NA	UD	NA	371.77

UD: Undetected, NA: Not applicable

Additionally, in Table 4.15 of MB and 4.16 of MO, the K₃PO₄ detected in the original material (T_F) was not detected in deactivated samples (T_{MB1}-T_{MB12}) and (T_{MO1}-T_{MO12}).

4.4.2.8 *Effect of Cl⁻ and SO₄²⁻ on scavenging active holes and competitive adsorption*

TiO₂ photocatalyst might lose its activity because of active site deactivation, which was suggested to worsen in textile wastewater due to Cl⁻ and SO₄²⁻ competing for active sites meant for ⁻OH conversion to [•]OH on TiO₂ surface (Abdullah et al., 1990; Ghaly et al., 2007; Selvam et al., 2007; Y. Wang et al., 2013). As reviewed by (Farouk et al., 2016), owing to their charges, Cl⁻ and SO₄²⁻ are most likely to compete with ⁻OH depending on their affinity for the sites, thereby blocking the active sites. Unfortunately, Cl or its derivatives were never captured on MO or MB samples in the analysis in this work (not detected at 200eV and ~198.5–199eV for organic Cl and metal chloride respectively). On the other hand, sulfur ions were detected in some of the MB degradation activities perhaps due to the presence of S in some of the MB intermediates or from the SO₄²⁻, but none of S derivatives were detected in MO samples. The adsorbed S derivatives (SO₃ 3/2, SO₃ 1/2, SO₂ 3/3, SO₂ 1/2, SO₂ 3/2, S₂N₂ 3/2, S₂N₂ 1/2) did not appear to shorten the life of TiO₂ photocatalyst, because high CPD was recorded in these samples T_{MB4} (CPD:247.30%), T_{MB5} (CPD:236.91%) T_{MB6} (CPD:248.10%), T_{MB10} (CPD:247.70%), T_{MB11} (CPD:256.32%) and T_{MB12} (CPD:294.59%) and the high or low CPD did not correspond to low or high amounts of the S derivatives in Table 4.1. But can still be argued that the S derivatives due their higher molecular mass than other carbon species without S, might have contributed to low TiO₂ performance (lower CPD) in MB when compared to higher performance in MO (higher CPD).

This assertion can further be observed considering Fig. 4.12 showing 10hourly performance of each sample and CPD in MB and Fig. 4.13 showing 10hourly

performance of each sample and CPD in MO. The CPD at 60th hour in all MO samples was higher than in MB. The pattern in the 10hour decline (Fig. 4.12 and 4.13) with time, determines how long the TiO₂ will continue to degrade the wastewater. MO TiO₂ samples have a higher probability to continue to degrade longer than the MB samples. Furthermore, it is almost certain that most of the traces of S derivatives were not from the Na₂SO₄ salt because other samples without the salt were found to have adsorbed S derivatives. The S derivatives were most probably from the S heteroatom from the MB parent structure. Though MO also has such S heteroatom in the parent structure, the intermediates formed did not seem to get adsorbed on the deactivated TiO₂ surface. However, the likely scenario causing the high CPD (in samples with added NaCl and Na₂SO₄ salts) is the conversion of Cl⁻ and SO₄²⁻ to Cl[•] and SO₄^{•-} radicals respectively and assist in degrading the MB and MO molecules, and the likely intermediates. Thereby lengthening the time before deactivation because of the high reactivity of SO₄^{•-} and Cl[•]. Even though the reactivity of sulfate radical was found to be higher than hydroxyl radical and both are higher than chloride radical (SO₄^{•-} > •OH > Cl[•]) (Anipsitakis & Dionysious, 2003; W. Li et al., 2017; Lutze et al., 2015). The model is similar to H₂O splitting reactions only that unlike in H₂O dissociating into OH then reacting with the hole to form •OH, it is the Cl or SO₄ that transform into the radical anion specie Cl[•] and SO₄^{•-} thereby engaging in degrading the organic solute.

The effect of Na⁺ could be highlighted because by introducing Cl⁻ and SO₄²⁻ due to adding NaCl or Na₂SO₄, Na⁺ have been introduced automatically. This was from the outcome of the XPS SS analysis in Table 4.1, it makes it unlikely that a double layer of salt covers the TiO₂ surface causing the decrease in adsorption of dyes at both neutral or basic pH (Guillard et al., 2005). If the competitive adsorption between the cationic molecule of MB and Na⁺ were to occur and Na⁺ got adsorbed instead of MB mother

molecule, as suggested by (Guillard et al., 2005), it is expected to take place in all samples with NaCl, but instead, the adsorption of Na^+ was only detected in samples T_{MB9} and T_{MB11} . In MO in Table 4.2, Na1s was detected in all samples with added salts (NaCl or Na_2SO_4) except T_{MO5} and T_{MO6} . The competitive adsorption of ions on the TiO_2 surface, can only occur when the ions have nearly the same energy but as was seen from the XPS SS no matter how abundant the number of molecule/ions in the colloid, it has to be captured at bridging O, before affecting the CPD, only compounds/atoms/molecules that have energies similar to C species can compete for the active site and have influence on the performance of TiO_2 . Also, the available Na ions in the colloid can get absorbed on the photocatalyst surface but did not seem to have unique effect on the CPD.

4.5 Recommended practice for deactivation analysis in photocatalysis

The studies on deactivation in photocatalysis was mostly postulated by the authors without references to any standard criteria. As the need for more water recycle and reuse plants arises due to urbanization, photoreactors have to be studied systematically. Some authors (Sauer & Ollis, 1996) while presenting their deactivation work, recommended using the photocatalyst in photodegradation experiments many times without washing and observe the level of deactivation. Though it was in gaseous media, this idea was widely accepted. Other studies in photocatalyst deactivation in gaseous media recommended use of XPS and FTIR for surface analysis and the presentation of the result was useful (Shang et al., 2002). The investigations in deactivation and surface coverage in gaseous media, could be attributed to earlier works done in temperature programmed desorption (TPD) and Brunauer-Emmett-Teller (BET) analysis base on Langmuir-Hinshelwood mechanism. On the contrary, deactivation in aqueous media differ from gaseous media because of the water splitting reactions, where majority of the degradation pathway starts with the attack on the mother molecule by the generated $\bullet\text{OH}$ radical. This reaction mechanism (generation of $\bullet\text{OH}$ radical) in aqueous media, warrant a modified

approach from the photodegradation in gaseous media deactivation analysis. Thus, a need for a unified approach becomes imminent as presented in this work.

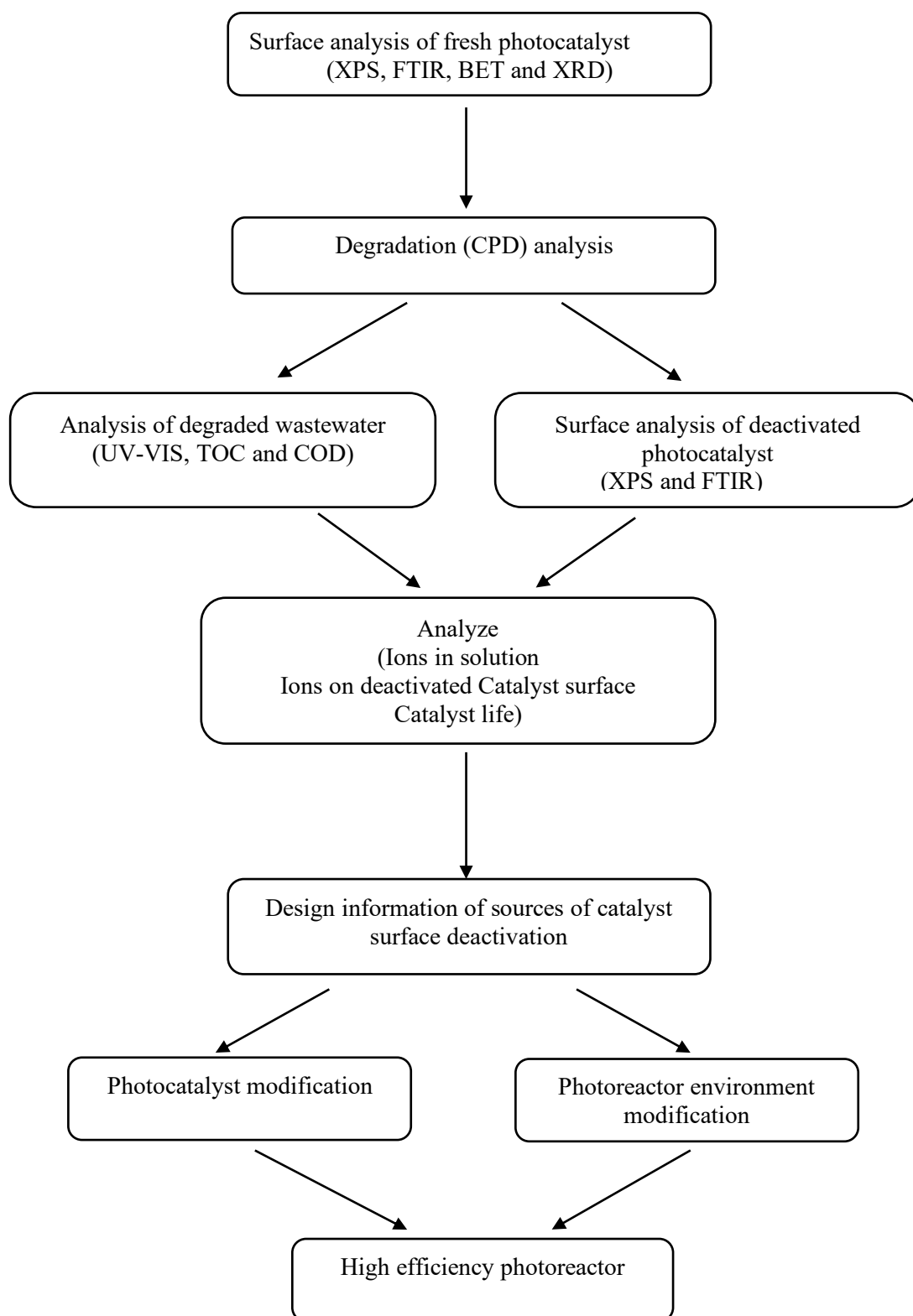


Figure 4.20 Schematic diagram for the proposed practice of photocatalyst performance analysis

The methodology introduced in this work, notably the cumulative percent degradation (CPD) and how reaction factors are considered, including variation in dye wastewater composition, was able to provide a built-in control and test experiment, to ensure proper representation of the reaction products available and how they affect photocatalyst performance. This stratification has been shown to play a great role on the studies of photocatalyst surface changes as reaction conditions change. Fig. 4.20 is a flowchart of the recommended practice.

CHAPTER 5: CONCLUSION AND RECOMMENDATION

5.1 Conclusion

Researches on the surface properties of photocatalysts are in the forefront in recent publications in photocatalysis, providing foundations in proper understanding of surface behavior in various reaction conditions. Moreover, the nature of reaction environment (type and number of ions) affects the life of photocatalyst differently. The aim of this work is to identify main cause of surface deactivation of anatase TiO_2 photocatalyst for enhanced treatment of recalcitrant dye wastewaters. The investigation was designed such that, the reaction conditions reflect the nature of industrial wastewater, while the reactor is to represent accessible components. The outcome matches the objectives of this investigation and the study concludes the following:

1. The characterization of the chosen fresh TiO_2 was to confirm it as anatase, suitable for photocatalysis surface analysis due to its potentiality as preferred photocatalyst.
2. The reaction kinetics for both MB and MO obeyed the Langmuir-Hinshelwood mechanism as a first order kinetic equation, consistently the rate r was found to be proportional to surface coverage (θ) depending on the reaction conditions.
3. The characterization of deactivated TiO_2 revealed the nature of adsorbed species differ at different reaction conditions. The XPS and FTIR revealed that reaction conditions have an influence on the rate of deactivation of the TiO_2 surface. The increased amount of C was consistently seen as part of source of reduced activity of TiO_2 and the low CPD values in the samples, while the relatively reduced PAC of O was seen as an indicator of low CPD. The CPD of MO being higher than the CPD of MB samples was as a result of combine effect S derivatives due to their high molecular mass and the C species. Traces of other chemical species on the TiO_2 surface N and Na do not appear to have an influence on the CPD. The rate

at which $\bullet\text{OH}$ is generated in photocatalysis in aqueous media largely determines the overall reaction and how the catalyst gets deactivated. The deactivation of TiO_2 surface can be linked to the way the C compounds/molecules in the TiO_2 colloid, get attached to the region of bridged O, being the plausible source of $\bullet\text{OH}$ radical generation. Once the bridged O does not immediately generate $\bullet\text{OH}$, it gets occluded by the C specie and degradation rate begin to decline. That is why samples with UV irradiation showed a high value of CPD, due to continues $\bullet\text{OH}$ generation over a longer period than in the dark, where generation of $\bullet\text{OH}$ was not effectively achieved. Cl^- was reported to block active sites and reduce the rate of degradation of TiO_2 surface, Cl^- ought to be detected at $\sim 198.5\text{--}199\text{eV}$ if it is to have any influence on the anatase surface, most importantly to have attached with the bridging O and cause shifts in binding energy at some point, in the absence of such observations it is safe to theorize that Cl^- and SO_4^{2-} has no detrimental effect on the active sites of TiO_2 surface. Moreover, the Cl^- and SO_4^{2-} ions reported to scavenge on $\bullet\text{OH}$ radicals and reduce degradation on the surface, findings revealed that the effect of Cl^- and SO_4^{2-} in the presence UV irradiation were positive, synergistic and promote degradation. Considering the nature of the dye as cationic or anionic, pH does not seem to have a significant effect to warrant a marked difference in the general CPD values. There was regeneration of lattice oxygen O^{2-} in some of the MO samples in pH10 which did not appear to increase the CPD in short term, therefore have no noticeable effect at the end of 60h run.

4. The relation between CPD and adsorbed species was found to be useful and served its purpose by providing a measure of photocatalyst performance over time. The repeated usage of the photocatalyst allow the investigation to determine the extent of its activity in different reaction.

5. Introducing a practice is critical at this stage of surge of studies in surface analysis of photocatalysts. The flowchart of the recommended practice provides a guide to photocatalyst surface analysis which was unavailable. It can easily be used to investigate any variable in photocatalysis.

5.2 Recommendation for future work

There are numerous proposed photodegradation activities of dyes on the anatase TiO_2 surface, these studies need to investigate different reaction conditions with different dyes and salts to determine the principle reaction path, as $\cdot\text{OH}$ attacked a parent dye. The following are recommendations to improve the base knowledge of adsorption mechanism of species in photocatalysis:

1. Synthesis of new photocatalysts should be carried out to investigate ways to reduce their adsorption potential leading to deactivation (physisorption and chemisorption).
2. Synthesis of photocatalysts for degradation in aqueous media should focus on photocatalysts that can generate $\cdot\text{OH}$.
3. Rate of degradation of more dyes need to be investigated using the procedure recommended in this work.
4. Quantum chemical calculations are to combine with experimental analysis to predict the reactivity and stability of reactants/intermediates in TiO_2 colloid at different set parameters.

REFERENCES

- Abdullah, M., Low, G. K., & Matthews, R. W. (1990). Effects of Common Inorganic Anions on Rates of Photocatalytic Oxidation of Organic Carbon over Illuminated Titanium Dioxide. *J. Phys. Chem.*, 94(17), 6820-6825.
- Alahiane, S., Qourzal, S., El Ouardi, M., Abaamrane, A., & Assabbane, A. (2014). Factors Influencing the Photocatalytic Degradation of Reactive Yellow 145 by TiO₂-Coated Non-Woven Fibers. *American Journal of Analytical Chemistry*, 05(08), 445-454.
- Alberici, R. M., Canela, M. C., Eberlin, M. N., & Jardim, W. F. (2001). Catalyst deactivation in the gas phase destruction of nitrogen-containing organic compounds using TiO₂/UV-VIS. *Applied Catalysis B: Environmental*, 30(3-4), 389-397.
- Alinsafi, A., Evenou, F., Abdulkarim, E. M., Pons, M. N., Zahraa, O., Benhammou, A., Nejmeddine, A. (2007). Treatment of textile industry wastewater by supported photocatalysis. *Dyes and Pigments*, 74, 439-445.
- Ameen, M. M., & Raupp, G. B. (1999). Reversible Catalyst Deactivation in the Photocatalytic Oxidation of Diluteo-Xylene in Air. *Journal of Catalysis*, 184(1), 112-122.
- Anipsitakis, G., & Dionysious, D. D. (2003). Degradation of organic contaminants in water with sulfate radicals generated by the conjunction of peroximonosulfate with cobalt. *Environmental science and technology*(37), 4790-4790.
- Arami-Niya, A., Wan Daud, W. M. A. S., Mjalli, F., Abnisa, F., & Shafeeyan, M. S. (2012). Production of microporous palm shell based activated carbon for methane adsorption: Modelling and optimisation using response surface methodology. *Engineering research and design*, 90(6), 776-784.
- Auvinen, S. (2013). *Computational modeling of the properties of TiO₂ nanoparticles*. *Acta Universitatis Lappeenrantaensis*. (Doctor of Science), Lappeenranta University of Technology, Lappeenranta, Finland, Acta universitatis Lappeenrantaensis.
- Baiocchi, C., Brussino, M. C., Pramauro, E., Prevot, A. B., Palmisano, L., & Marci, G. (2002). Characterization of methyl orange and its photocatalytic degradation products by HPLC/UV-VIS diode array and atmospheric pressure ionization quadrupole ion trap mass spectrometry. *International Journal of Mass Spectrometry*, 214, 247-256.
- Baran, W., Makowski, A., & Wardas, W. (2008). The effect of UV radiation absorption of cationic and anionic dye solutions on their photocatalytic degradation in the presence TiO₂ *Dyes and Pigments*, 76, 226-230.
- Baroutian, S., Aroua, M. K., Raman, A. A. A., & Sulaiman, N. M. N. (2011). A packed bed membrane reactor for production of biodiesel using activated carbon supported catalyst. *Bioresource Technology*, 102(2), 1095-1102.

- Berger, H., Tang, H., & Levy, F. (2005). Growth and Raman spectroscopic characterization of TiO₂ anatase single crystals. *Journal of Crystal Growth*, 130(1-2), 108-112.
- Borker, P., & Salker, A. V. (2006). Photocatalytic degradation of textile azo dye over Ce_{1-x}Sn_xO₂ series. *Materials Science and Engineering: B*, 133(1-3), 55-60.
- Brandi, R. J., Rintoul, G., Alfano, O. M., & Cassano, A. E. (2002). Photocatalytic reactors. *Catalysis Today*, 76(2-4), 161-175.
- Buthiyappan, A., Abdul Raman, A., & Daud, W. M. A. W. (2016). Development of Advanced Chemical Oxidation Wastewater Treatment System for the Batik Industry in Malaysia. *RSC Advances*, 6, 25222-25241.
- Cao, L., Gao, Z., Suib, S. L., Obee, T. N., Hay, S. O., & Freihaut, J. D. (2000). Photocatalytic Oxidation of Toluene on Nanoscale TiO₂ Catalysts: Studies of Deactivation and Regeneration. *Journal of Catalysis*, 196(2), 253-261.
- Carmen, Z., & Daniela, S. (2012). Textile Organic Dyes – Characteristics, Polluting Effects and Separation/Elimination Procedures from Industrial Effluents – A Critical Overview. In T. Puzyn (Ed.), *Organic Pollutants Ten Years After the Stockholm Convention - Environmental and Analytical Update* (pp. 54-86). Croatia: InTech Europe.
- Cinar, Z. (2017). The Role of Molecular Modelling in TiO₂ Photocatalysis. *Molecules*, 22(556).
- d'Hennezel, O., Pichat, P., & Ollis, D. F. (1998). Benzene and toluene gas-phase photocatalytic degradation over H₂O and HCL pretreated TiO₂: by-products and mechanisms. *Journal of Photochemistry and Photobiology A: Chemistry*, 118(3), 197-204.
- Daimon, T., Hirakawa, T., Kitazawa, M., Suetake, J., & Nosaka, Y. (2008). Formation of singlet molecular oxygen associated with the formation of superoxide radicals in aqueous suspensions of TiO₂ photocatalysts. *Applied Catalysis A: General*, 340, 169-175.
- Diebold, U. (2003). The surface science of titanium dioxide. *Surface Science Reports*, 48, 53-229.
- Eckert, H., Bobeth, M., Teixeira, S., Kühn, K., & Cuniberti, G. (2015). Modeling of photocatalytic degradation of organic components in water by nanoparticle suspension. *Chemical Engineering Journal*, 261, 67-75.
- Einaga, H. (2002). Heterogeneous photocatalytic oxidation of benzene, toluene, cyclohexene and cyclohexane in humidified air: comparison of decomposition behavior on photoirradiated TiO₂ catalyst. *Applied Catalysis B: Environmental*, 38(3), 215-225.
- Epling, G. A., & Lin, C. (2002). Photoassisted bleaching of dyes utilizing TiO₂ and visible light *Chemosphere*, 46, 561-570.

- Fan, H.-Y., Shi, C., Li, X.-S., Zhang, S., Liu, J.-L., & Zhu, A.-M. (2012). In-situ plasma regeneration of deactivated Au/TiO₂ nanocatalysts during CO oxidation and effect of N₂ content. *Applied Catalysis B: Environmental*, 119-120, 49-55.
- Farouk, H. U., Raman, A. A. A., & Daud, W. M. A. W. (2016). TiO₂ catalyst deactivation in textile wastewater treatment: Current challenges and future advances. *Journal of Industrial and Engineering Chemistry*, 33, 11-21.
- Ganduglia-Pirovano, M. V., Hofmann, A., & Sauer, J. (2007). Oxygen vacancies in transition metal and rare earth oxides: Current state of understanding and remaining challenges. *Surface Science Reports*, 62(6), 219-270.
- Gerven, T. V., Mul, G., Moulijn, J., & Stankiewicz, A. (2007). A review of intensification of photocatalytic processes. *Chemical Engineering and Processing*, 46.
- Ghaly, M. Y., Farah, J. Y., & Fathy, A. M. (2007). Enhancement of decolorization rate and COD removal from dyes containing wastewater by the addition of hydrogen peroxide under solar photocatalytic oxidation. *Desalination*, 217, 74-84.
- Gong, X. Q., Selloni, A., Batzill, M., & Diebold, U. (2006). Steps on anatase TiO₂(101). *Nat Mater*, 5(8), 665-670.
- Guillard, C., Lachheb, H., Houas, A., Ksibi, M., Elaloui, E., & Herrmann, J. M. (2003). Influence of chemical structure of dyes, of pH and of inorganic salts on their photocatalytic degradation by TiO₂ comparison of the efficiency of powder and supported TiO₂. *J. Photochem. Photobiol. A: Chem.*, 158, 27.
- Guillard, C., Puzenat, E., Lachheb, H., Houas, A., & Herrmann, J.-M. (2005). Why inorganic salts decrease the TiO₂ photocatalytic efficiency. *International Journal of Photoenergy*, 7.
- Gurylev, V., Su, C.-Y., & Perng, T.-P. (2015). Surface reconstruction, oxygen vacancy distribution and photocatalytic activity of hydrogenated titanium oxide thin film. *Journal of Catalysis*, 330, 177-186.
- Habibi, M. H., Hassanzadeh, A., & Mahdavi, S. (2005). The effect of operational parameters on the photocatalytic degradation of three textile azo dyes in aqueous TiO₂ suspensions *Journal of Photochem Photobiol A: Chem*, 172, 89-96.
- He, Y., Tilocca, A., Dulub, O., Selloni, A., & Diebold, U. (2009). Local ordering and electronic signatures of submonolayer water on anatase TiO₂(101). *Nat Mater*, 8(7), 585-589.
- Henderson, M. A. (2002). The interaction of water with solid surfaces: fundamental aspects revisited. *Surface Science Reports*, 46, 1-308.
- Henderson, M. A. (2011). A surface science perspective on TiO₂ photocatalysis. *Surface Science Reports*, 66, 185-297.
- Herman, G. S., Dohnalek, Z., & Ruzycki, N. D., U. (2003). Experimental Investigation of the Interaction of Water and Methanol with Anatase-TiO₂(101). *J. Phys. Chem. B*, 107, 2788-2795.

- Herrmann, J. M., Guillard, C., Disdier, J., Lehaut, C., Malato, S., & Blanco, J. (2002). New industrial titania photocatalysts for the solar detoxification of water containing various pollutants. *Appl. Catal. B: Environ.*, 35, 281-294.
- Hirakawa, T., & Nosaka, Y. (2002a). Properties of O^{2-} and OH. formed in TiO_2 aqueous suspensions by photocatalytic reaction and the influence of H_2O_2 and some ions. *Langmuir*, 18, 3247–3254.
- Hirakawa, T., & Nosaka, Y. (2002b). Properties of O^{2-} and OH. formed in TiO_2 aqueous suspensions by photocatalytic reaction and the influence of H_2O_2 and some ions. *Langmuir*, 18, 3247–3254.
- Hong, C.-S., Wang, Y., & Bush, B. (1998). Kinetics and products of the TiO_2 , photocatalytic degradation of 2-chlorobiphenyl in water. *Chemosphere*, 36(7), 1653-1667.
- Houas, A., Lachheb, H., Ksibi, M., Elaloui, E., Guillard, C., & Herman, J. M. (2001). Photocatalytic degradation pathway of methylene blue in water. *Applied Catalysis B: Environmental*, 31(2), 145-157.
- Hu, C., Yu, J. C., Hao, Z., & Wong, P. K. (2003). Photocatalytic degradation of triazine-containing azo dyes in aqueous TiO_2 suspensions. *Applied Catalysis B: Environmental*, 42(1), 47-55.
- Ishibashi, K., Fujishima, A., Watanabe, I., & Hashimoto, K. (2000). Generation and deactivation processes of superoxide formed on TiO_2 films illuminated by weak UV light in air or water. *J Phys Chem B*, 104, 4934-4938.
- Izadifard, M., Achari, G., & Langford, C. H. (2013). Application of Photocatalysts and LED Light Sources in Drinking Water Treatment. *Catalysis*, 3, 726-743.
- Jawad, A. H., Alkarkhi, A. F. M., & Mubarak, N. S. A. (2014). Photocatalytic decolorization of methylene blue by an immobilized TiO_2 film under visible light irradiation: optimization using response surface methodology (RSM). *Desalination and Water Treatment*, 1-12.
- Jensen, H., Soloviev, A., Li, Z., & Sogaard, E. G. (2005). XPS and FTIR investigation of the surface properties of different prepared titania nano-powders. *Applied Surface Science*, 246(1-3), 239-249.
- Kaariainen, M. L., Kaariainen, T. O., & Cameron, D. C. (2009). Titanium dioxide thin films, their structure and its effect on their photoactivity and photocatalytic properties. *Thin Solid Films*, 517(24), 6666-6670.
- Kafizas, A., Wang, X., Pendlebury, S. R., Barnes, P., Ling, M., Sotelo-Vazquez, C., Durrant, J. R. (2016). Where Do Photogenerated Holes Go in Anatase:Rutile TiO_2 ? A Transient Absorption Spectroscopy Study of Charge Transfer and Lifetime. *J Phys Chem A*, 120(5), 715-723.
- Kavitha, S. K., & Palanisamy, P. N. (2010). Photocatalytic Degradation of Vat Yellow 4 Using UV/ TiO_2 . *Modern Applied Science*, 4, 130-142.

- Kirby, B. J. (2010). *Micro- and Nanscale Fluid Mechanics: Transport in Microfluidic Devices*: Cambridge University Press.
- Konstantinou, I. K., & Albanis, T. A. (2004). TiO₂-assisted photocatalytic degradation of azo dyes in aqueous solution: kinetic and mechanistic investigations: A review. *Applied Catalysis B: Environmental*, 49, 1-14.
- Kozlov, D. V., Vorontsov, A. V., Smirniotis, P. G., & Savinov, E. N. (2003). Gas-phase photocatalytic oxidation of diethyl sulfide over TiO₂: kinetic investigations and catalyst deactivation. *Applied Catalysis B: Environmental*, 42(1), 77-87.
- Krishnan, P., Liu, M., Itty, P. A., Liu, Z., Rheinheimer, V., Zhang, M.-H., Yu, L. E. (2017). Characterization of photocatalytic TiO₂ powder under varied environments using near ambient pressure X-ray photoelectron spectroscopy. *Scientific Reports*.
- Lachheb, H., Puzenat, E., Houas, A., Ksibi, M., Elaloui, E., Guillard, C., & Herrmann, J.-M. (2002). Photocatalytic degradation of various types of dyes (Alizarin S, Crocein Orange G, Methyl Red, Congo Red, Methylene Blue) in water by UV-irradiated titania. *Applied Catalysis B: Environmental*, 39(1), 75-90.
- Larson, S. A., & Falconer, J. L. (1994). Characterization of TiO₂ photocatalysts used in trichloroethene oxidation. *Applied Catalysis B: Environmental*, 4(4), 325-342.
- Lee, G. D., & Falconer, J. L. (2000). Transient measurement of lattice oxygen in photocatalytic decomposition of formic acid on TiO₂. *Catalysis letters*, 70, 145-148.
- Lee, Y.-S., Kim, S. J., Venkateswaran, P., Jang, J.-S., Kim, H., & Kim, J.-G. (2008). Anion co-doped Titania for Solar Photocatalytic Degradation of Dyes. *Carbon Letters*, 9(2), 131-136.
- Li, H., Yin, S., & Sato, T. (2010). Persistent deNO_x Ability of CaAl₂O₄:(Eu, Nd)/TiO₂-xNy Luminescent Photocatalyst. *Nanoscale Res Lett*, 6(1), 5.
- Li, J.-y., Ma, W.-h., Lei, P.-x., & Zhao, J.-c. (2007). Detection of intermediates in the TiO₂-assisted photodegradation of Rhodamine B under visible light irradiation. *Journal of Environmental Sciences*, 19(7), 892-896.
- Li, W., Jain, T., Ishida, K., & Liu, H. (2017). A mechanistic understanding of the degradation of trace organic contaminants by UV/hydrogen peroxide, UV/persulfate and UV/free chlorine for water reuse. *Environ. Sci. Water Res. Technol.*, 3, 128-138.
- Li, Z., Xie, Z., Zhang, Y., Wu, L., Wang, X., & Fu, X. (2007). Wide Band Gap p-Block Metal Oxyhydroxide InOOH: A New Durable Photocatalyst for Benzene Degradation. *Journal of Physical Chemistry C*, 111(49), 18348-18352.
- Linsebigler, A. L., Lu, G., & Yates, J. T. (1995). Photocatalysis on TiO₂ Surfaces--Principles, Mechanism, and Selected Results. *Chem. Rev.*, 95, 735-758.

- Liu, C., Hsieh, Y., Lai, P., Li, C., & Kao, C. (2006). Photodegradation treatment of azo dye wastewater by UV/TiO process. *Dyes and Pigments*, 68(2-3), 191-195.
- Liu, Y., Chen, X., Li, J., & Burda, C. (2005). Photocatalytic degradation of azo dyes by nitrogen-doped TiO₂ nanocatalysts. *Chemosphere*, 61(1), 11-18.
- Lutze, V. H., Bircher, S., Rapp, I., Kerlin, N., Bakkour, R., Geisler, M., Schmidt, T. C. (2015). Degradation of chlortriazine pesticide by sulfate radicals and the influence of organic matter. *Environ. Sci. Technol.*, 49(3), 1673-1680.
- Madhavan, J., Maruthamuthu, P., Murugesan, S., & Anandan, S. (2008). Kinetic studies on visible light-assisted degradation of acid red 88 in presence of metal-ion coupled oxone reagent. *Applied Catalysis B: Environmental*, 83(1-2), 8-14.
- MeenaKumari, M., & Philip, D. (2015). Degradation of environment pollutant dyes using phytosynthesized metal nanocatalysts. *Spectrochim Acta A Mol Biomol Spectrosc*, 135, 632-638.
- Mendez-Roman, R., & Cardona-Martinez, N. (1998). Relationship between the formation of surface species and catalyst deactivation during the gas-phase photocatalytic oxidation of toluene. *Catalysis Today*, 40(4), 353-365.
- Mills, A., & Le Hunte, S. (1997). An overview of semiconductor photocatalysis. *Journal of Photochemistry and Photobiology A: Chemistry*, 108(1), 1-35.
- Muggli, D. S., & Falconer, J. L. (2000). Role of Lattice Oxygen in Photocatalytic Oxidation on TiO₂. *Journal of Catalysis*, 191, 318-325.
- Nitoi, I., Oncescu, T., & Oancea, P. (2013). Mechanism and kinetic study for the degradation of lindane by photo-Fenton process. *Journal of Industrial and Engineering Chemistry*, 19(1), 305-309.
- Nosaka, Y., & Nosaka, A. (2016). Understanding Hydroxyl Radical ([•]OH) Generation Processes in Photocatalysis. *ACS Energy Letters*, 1 (2), 356-359.
- Ohko, Y., Ando, I., Niwa, C., Tatsuma, T., Yamamura, T., Nakashima, T., Fujishima, A. (2001). Degradation of Bisphenol A in Water by TiO₂ Photocatalyst. *Environmental Science & Technology*, 35(11), 2365-2368.
- Ozkan, A., Ozkan, M. H., Gurkan, R., Akcay, M., & Sokmen, M. (2004). Photocatalytic degradation of a textile azo dye, Sirius Gelb GC on TiO₂ or Ag-TiO₂ particles in the absence and presence of UV irradiation: the effects of some inorganic anions on the photocatalysis. *Journal of Photochem Photobiol A: Chem*, 163, 29-35.
- Penn, R. L., & Banfield, J. F. (1999). Morphology development and crystal growth in nanocrystalline aggregates under hydrothermal conditions: insights from titania. *Geochimica et Cosmochimica Acta*, 63(10), 1549-1557.
- Peral, J., & Ollis, D. F. (1997). TiO₂ photocatalyst deactivation by gas-phase oxidation of heteroatom organics. *Journal of Molecular Catalysis a-Chemical*, 115(2), 347-354.

- Prado, A. G. S., Bolzon, L. B., Pedroso, C. P., Moura, A. O., & Costa, L. L. (2008). Nb₂O₅ as efficient and recyclable photocatalyst for indigo carmine degradation. *Applied Catalysis B: Environmental*, 82(3-4), 219-224.
- Rajeshwar, K., Osugib, M. E., Chanmanee, W., Chenthamarakshana, C. R., Zanonib, M. V. B., Kajitvichyanukul, P., & Krishnan-Ayer, R. (2008). Heterogeneous photocatalytic treatment of organic dyes in air and aqueous media. *Journal of Photochemistry and Photobiology C: Photochemistry Reviews*, 9, 171-192.
- Ramamoorthy, M., Vanderbilt, D., & King-Smith, R. D. (1994). First-principles calculations of the energetics of stoichiometric TiO₂ surfaces. *Physical Review B, Condensed Matter*, 49(23), 16721-16727.
- Rochkind, M., Pasternak, S., & Paz, Y. (2015). Using dyes for evaluating photocatalytic properties: a critical review. *Molecules*, 20(1), 88-110.
- Sacco, O., Stoller, M., Vaiano, V., Ciambelli, P., Chianese, A., & Sannino, D. (2012). Photocatalytic Degradation of Organic Dyes under Visible Light on N-Doped TiO₂ Photocatalysts. *International Journal of Photoenergy*, 2012, 1-8.
- Sacco, O., Vaiano, V., Hana, C., Sannino, D., & Dionysiou, D. D. (2015). Photocatalytic removal of atrazine using N-doped TiO₂ supported on phosphors. *Applied Catalysis B: Environmental*, 164, 462-474.
- Sauer, M. L., & Ollis, D. F. (1996). Catalyst Deactivation in Gas-Solid Photocatalysis. *Journal of Catalysis*, 163(1), 215-217.
- Selli, D., Fazio, G., & Di Valentin, C. (2017). Using Density Functional Theory to Model Realistic TiO₂ Nanoparticles, Their Photoactivation and Interaction with Water *Catalysts*, 7, 357.
- Selvam, K., Muruganandham, M., Muthuvel, I., & Swaminathan, M. (2007). The influence of inorganic oxidants and metal ions on semiconductor sensitized photodegradation of 4-fluorophenol. *Chemical Engineering Journal*, 128, 51-57.
- Senthilkumar, S., & Porkodi, K. (2005). Heterogeneous photocatalytic decomposition of Crystal Violet in UV-illuminated sol-gel derived nanocrystalline TiO₂ suspensions. *J Colloid Interface Sci*, 288(1), 184-189.
- Shang, J., Zhu, Y., Du, Y., & Xu, Z. (2002). Comparative Studies on the Deactivation and Regeneration of TiO₂ Nanoparticles in Three Photocatalytic Oxidation Systems: C₇H₁₆, SO₂, and C₇H₁₆-SO₂. *Journal of Solid State Chemistry*, 166, 395-399.
- Sheikh, M. U. D., Naikoo, G. A., Thomas, M., Bano, M., & Khan, F. (2016). Solar-assisted photocatalytic reduction of methyl orange dye over porous TiO₂ nanostructures. *New J. Chem.*, 40, 5483-5494.
- Sie, S. T. (2001). Consequences of catalyst deactivation for process design and operation. *Applied Catalysis A: General*, 212, 129-151.

- Spadaro, J. T., Isabelle, L., & Renganathan, V. (1994). Hydroxyl radical mediated degradation of azo dyes: evidence for benzene generation. *Environ Sci Technol*, 28(7), 1389-1393.
- Stapleton, D. R., Konstantinou, I. K., Mantzavinos, D., Hela, D., & Papadaki, M. (2010). On the kinetics and mechanisms of photolytic/TiO₂-photocatalytic degradation of substituted pyridines in aqueous solutions. *Applied Catalysis B: Environmental*, 95, 100-109.
- Sun, R.-D., Nakajima, A., Watanabe, T., & Hashimoto, K. (2003). Decomposition of gas-phase octamethyltrisiloxane on TiO₂ thin film photocatalysts—catalytic activity, deactivation, and regeneration. *Journal of Photochemistry and Photobiology A: Chemistry*, 154(2-3), 203-209.
- Tanaka, K., Padermpole, K., & Hisanaga, T. (2000). Photocatalytic Degradation of Commercial Azo Dyes. *Wat. Res.*, 34, 327-333.
- Vaiano, V., Sacco, O., Pisano, D., Sannino, D., & Ciambelli, P. (2015). From the design to the development of a continuous fixed bed photoreactor for photocatalytic degradation of organic pollutants in wastewater. *Chemical Engineering Science*, 137, 152-160.
- Vaiano, V., Sacco, O., Sannino, D., & Ciambelli, P. (2015). Process intensification in the removal of organic pollutants from wastewater using innovative photocatalysts obtained coupling Zinc Sulfide based phosphors with nitrogen doped semiconductors. *Journal of Cleaner Production*, 100, 208-211.
- Vaiano, V., Sacco, O., Stoller, M., Chianese, A., Ciambelli, P., & Sannino, D. (2014). Influence of the Photoreactor Configuration and of Different Light Sources in the Photocatalytic Treatment of Highly Polluted Wastewater. *International Journal of Chemical Reactor Engineering*, 12(1).
- Valdes, A., Qu, Z.-W., Kroes, G.-J., Rossmeisl, J., & Norskov, J. K. (2008). Oxidation and Photo-Oxidation of Water on TiO₂ Surface. *J. Phys. Chem. C*, 112, 9872-9879.
- Vittadini, A., Selloni, A., Rotzinger, F. P., & Grätzel, M. (1998). Structure and Energetics of Water Adsorbed at TiO₂ Anatase (101) and (001) Surfaces. *Physical Review Letters*, 81(14), 2954-2957.
- Wang, J., Wen, F.-Y., Zhang, Z.-H., Zhang, X.-D., Pan, Z.-J., Zhang, P., Xu, L. (2006). Investigation on degradation of dyestuff wastewater using visible light in the presence of a novel nano TiO₂ catalyst doped with upconversion luminescence agent. *Journal of Photochemistry and Photobiology A: Chemistry*, 180(1-2), 189-195.
- Wang, L. K., Hung, Y.-T., Lo, H. H., & Yapijakis, C. (2004). *Handbook of Industrial and Hazardous Wastes Treatment* (Second Edition ed.): CRC Press.
- Wang, R., Hashimoto, K., Fujishima, A., Chikuni, M., Kojima, E., Kitamura, A., Watanabe, T. (1998). Photogeneration of Highly Amphiphilic TiO₂ Surfaces. *Advanced Materials*, 10(2), 135-138.

- Wang, Y., Lu, K., & Feng, C. (2013). Influence of inorganic anions and organic additives on photocatalytic degradation of methyl orange with supported polyoxometalates as photocatalyst. *Journal of Rare Earths*, 31, 360.
- Wendt, S., Matthiesen, J., Schaub, R., Vestergaard, E. K., Laegsgaard, E., Besenbacher, F., & Hammer, B. (2006). Formation and splitting of paired hydroxyl groups on reduced TiO₂(110). *Phys Rev Lett*, 96(6), 066107.
- Wu, X., Yin, S., Dong, Q., & Sato, T. (2014). Blue/green/red colour emitting up-conversion phosphors coupled C-TiO₂ composites with UV, visible and NIR responsive photocatalytic performance. *Applied Catalysis B: Environmental*, 156-157, 257-264.
- Xie, T. H., & Lin, J. (2007). Origin of Photocatalytic Deactivation of TiO₂ Film Coated on Ceramic Substrate. *Journal of Physical Chemistry C*, 111(27), 9968-9974.
- Yates, J. T. (2009). Photochemistry on TiO₂: Mechanisms behind the surface chemistry. *Surface Science*, 603(10-12), 1605-1612.
- Ye, L., Yang, M., Xu, L., Guo, C., Li, L., & Wang, D. (2014). Optimization of inductive angle sensor using response surface methodology and finite element method. *Measurement*, 48, 252-262.
- Yu, J., Zhao, X., & Zhao, Q. (2000). Effect of surface structure on photocatalytic activity of TiO₂ thin films prepared by sol-gel method. *Thin Solid Films*, 379(1-2), 7-14.
- Yu, P., & Cardona, M. (2010). *Fundamentals and Materials Properties*. Germany: Springer Berlin Heidelberg.
- Zhang, H., & Banfield, J. F. (1998). Thermodynamic analysis of phase stability of nanocrystalline titania. *Journal of Materials Chemistry*, 8(9), 2073-2076.
- Zhang, Q., Li, C., & Li, T. (2012). Rapid Photocatalytic Degradation of Methylene Blue under High Photon Flux UV Irradiation: Characteristics and Comparison with Routine Low Photon Flux. *International Journal of Photoenergy*, 2012, 1-7.
- Zhang, W., Xiao, X., Zheng, L., & Wan, C. (2015). Fabrication of TiO₂/MoS₂@zeolite photocatalyst and its photocatalytic activity for degradation of methyl orange under visible light. *Applied Surface Science*.
- Zhao, W.-N., & Liu, Z.-P. (2014). Mechanism and active site of photocatalytic water splitting on titania in aqueous surroundings. *Chemical Science*, 5(6), 2256.

LIST OF PUBLICATIONS AND PAPERS PRESENTED

Academic articles

Hamisu Umar Farouk, Abdul Aziz Abdul Raman, Wan Mohd Ashri Wan Daud (2015):
TiO₂ catalyst deactivation in textile wastewater treatment: Current challenges and future
advances. Journal of Industrial and Engineering Chemistry 33 (2016) 11–21.
Doi:10.1016/j.jiec.2015.10.022.

Hamisu Umar Farouk, Abdul Aziz Abdul Raman, Wan Mohd Ashri Wan Daud (2017):
Surface transformations of TiO₂ anatase deactivated in methylene blue solution with Cl⁻
ions in the colloid. Journal of the Taiwan Institute of Chemical Engineers 80 (2017) 203-
214. Doi: 10.1016/j.jtice.2017.06.051.

Conference Proceeding

Hamisu Umar Farouk, Abdul Aziz Abdul Raman and Wan Mohd Ashri Wan Daud (2015): Commercial viability of photoreactors in textile wastewater treatment hindered by titanium dioxide (TiO_2) deactivation. Asia Pacific Confederation of Chemical Engineering Congress 2015: APCCChE 2015, incorporating CHEMECA 2015, Engineers Australia.